Small lightweight aircraft navigation in the presence of wind

Cornel-Alexandru Brezoescu

Par **Cornel-Alexandru BREZOESCU**

Navigation d'un avion miniature de surveillance aérienne en présence de vent

Thèse présentée
pour l'obtention du grade
de Docteur de l'UTC

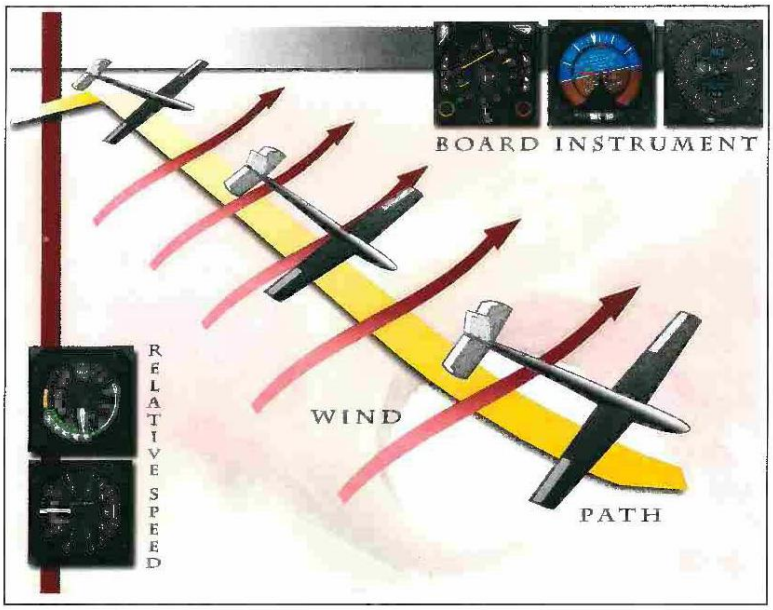

Soutenue le 28 octobre 2013
Spécialité : Laboratoire HEUDIASYC

D2105

Navigation d'un avion miniature de surveillance aérienne en présence de vent

Student: BREZOESCU Cornel Alexandru

PHD advisors : LOZANO Rogelio
CASTILLO Pedro

Contents

Chapter 1

Introduction

Performance improvement is a requirement for all physical systems including Unmanned Aerial Vehicles (UAVs) whose applications are steadily increasing. They offer a smooth transition of autonomous flight control design from theory to practice in addition to providing a proper solution in environments inaccessible or dangerous to human life. However, the lack of a human pilot on board implies that the UAVs rely on automation to navigate or to avoid obstacles. Thus, given the complex dynamics of a flying vehicle, a flight controller capable to provide, maintain and improve the aircraft performance is required in order to guarantee the stability of the system despite uncertainties in the model or some external perturbing forces like wind.

1.1 Motivation and objectives

This work is motivated by commonly encountered situations which are dangerous to human life such as extreme manifestations of force or hostage crisis, among others. The number of casualties would be significantly reduced if information on the site were available before the procedure of the emergency services. This information could be obtained by the use of a drone which must be able to navigate a safe distance to the place of intervention and back to the ground station in an unobtrusive way. However, the relatively low operating speed of small UAVs makes them particularly affected by wind field which is any movement of the air mass with respect to the surface of the

Earth. Therefore, the drone in question must also be able to overcome the effect of such perturbation in order to safely meet the mission objectives.

Miniature drones seem to be best suited to solve this kind of problems due to their discretion and portability. Nevertheless, it is necessary to increase their flight time and make them more tolerant to wind. Note that the wind may be of the order of the drone speed, which makes the problem very difficult.

Based on these considerations, the aim of this thesis is to develop a navigation strategy for a model aircraft of conventional configuration in order to accomplish different missions in presence of wind. If it is possible to obtain the path that minimizes the time of flight, the energy consumption or the forces acting on the structure of the vehicle, then the flight controller must be able to steer the vehicle along this path. As for what concerns the direction and intensity of the wind, the information provided by a ground station can be taken into account to define the trajectory of the mission.

Since the aircraft is considered small, wind has a significant influence on its flight performance. Note that the wind measured by the ground station may be different from the one actually encountered at higher altitudes or at any location away from the initial point of measurement. To improve the performance of flight, a method for estimating the intensity and the direction of the wind will be explored and the navigation strategy will be adapted accordingly. To this end, the measures provided by the ground station and the changes in the aircraft trajectory due to the wind must be considered. To simplify the study, a first assumption will be to consider that the wind gusts are isolated. Thus, the wind field is relatively constant or varies slowly over time. Finally, the proposed navigation strategies need to be validated in real flight tests using an experimental prototype which also must be developed.

1.2 Challenges

The large flight envelope of the aerial devices posses several challenges to the successful achievement of the proposed objectives. First, the choice of a robust airframe possessing reliable flight characteristics is essential for real flight tests. Long duration

flight and sufficient payload capacity to carry the weight of sensors and batteries are two features of great interest. Then, the appropriate avionics equipment meeting the requirements of the application being treated in this work needs to be integrated. Onboard sensors are required, on the one hand, to provide measurements of the quantities needed to determine the relevant parameters of the nonlinear dynamic model of the airplane. For this purpose, the use of parameter identification techniques is mandatory. On the other hand, the avionics system must provide the parameters of any integrated or developed flight controller.

This emphasizes the second main challenge that must be faced when dealing with UAVs, which is the development of a control law capable of governing the airplane during the flight. The motion of an airplane through the air is modeled as a coupled nonlinear system with complex dynamics. Its performance depends on the operating altitude, speed, atmosphere or the geometric characteristics of the airplane. That involves an increased complexity in the implementation of flight controllers which should provide both the internal stability of the aircraft and the achievement of the commanded attitude and velocity. In addition, the controller must be able to remove the adverse effects of external disturbances or model uncertainties in order to maintain good performance.

Last but not least, developing autonomous aerial devices requires a good understanding of the principles of aircraft operation. With this stock of knowledge, the influence of wind on aircraft performance can be incorporated into the equations of motion and, then, compensated with appropriate control input.

1.3 Approach

In order to achieve these objectives, the following research areas have been addressed. First, a literature review on the subject is necessary in order to obtain the aerodynamic model of the miniature aircraft in the presence of wind. Secondly, the development of navigation strategies is required in order to allow the airplane to perform various tasks in the presence of wind. To improve the performance of flight, the nav-

igation strategies need to take into account the wind measured by a ground station or estimated by an online estimator based on the aerodynamic model.

The third axis is the design and implementation of an experimental setup which consists of a ground station used for visualization and control purposes and an embedded autopilot architecture containing the airframe platform equipped with appropriate avionics such as inertial measurement unit, global positioning system, communication devices, air sensors and a control processing unit to manage the control law and the sensors data.

1.4 Thesis outline

The manuscript is divided in two main sections which are: modeling of the aircraft dynamics and designing flight controllers in order to achieve autonomous flight in presence of wind. The first section focuses on deriving complete and reduced-order mathematical models for a fixed-wing UAV and it is represented by Chapter 2. In the first part of the section, a description of the physical principles of flight is presented with the aim of deriving the dynamic model of an airplane. The additional forces acting on the aircraft subjected to wind, which is modeled as a stochastic process, have been incorporated into the equations of motion. Further, this section presents a reduced-order model of the airplane which is appropriate for control design.

On the other hand, the second aspect addressed in this report, i.e., achieving autonomous flight in presence of wind, is described in chapters 3 and 4. The control design developed in these chapters relies on the simplified model introduced in the previous section of the thesis. Furthermore, chapter 5 describes the practical implementation of a test platform with the purpose of obtaining flight test results. Finally, general conclusions are presented in chapter 6.

Chapter 2

Modeling for control

To address the problem of designing an autonomous flight controller for a small fixed-wing UAV, first an accurate nonlinear dynamic model of the vehicle needs to be derived. Unlike ground transportation systems, whose motion is primarily governed by propulsive inputs, airplanes rely on aerodynamic forces which are difficult to model since they depend on many varying operating conditions. As a consequence, the development of autonomous operating aerial devices is a challenging problem which requires significant attention.

The present chapter begins by introducing the basic principles of flight and the common parts of an airframe. Then, the derivation of the airplane equations of motion is described in order to formulate the problem from an automatic control perspective. Finally, the effect of a moving atmosphere on the aircraft performance is discussed and the wind is incorporated into the mathematical model of the vehicle.

2.1 Basic principles of flight

The design of an effective flight controller for an autonomous UAV starts with a good understanding of the principles of flight theory. A lack of knowledge about basic aerodynamics may cause inappropriate input commands when the aircraft operates at the limit of its performance capabilities. For this reason, the objective of this section is to provide a basic insight into the mechanics of flight.

2.1.1 The forces of flight

Fundamental aerodynamic principles involve the interaction between a solid object and the air which flows around the body of the object maintaining contact at all points. Considering the case of an aircraft in flight, the pressure variations along its component parts, caused by the physical contact with the air, generate an aerodynamic force which act through the center of pressure[1]. This force can be resolved into a component normal to the airflow direction which is called lift, L, and a component along the airflow direction which is called drag, D.

L is always an upward force perpendicular to the flight direction and it depends on several variables. Likewise, D is a backward force highly sensitive to many factors and its main source is the skin friction between the air and the surface of the aircraft [36]. However, the theory explaining the generation of lift is more complex than the one justifying the drag and this difficulty has led to several incorrect descriptions which will be presented further in this chapter. There are two other forces acting on the airplane: thrust which is generated by the engines and which makes the aircraft to move forward and the gravitational force which is due to the weight of the airplane and is always directed downward the center of the Earth.

Consequently, the lift force is what holds the airplane in the air overcoming its weight while the thrust force is what moves the airplane forward overcoming drag. When the airplane flies straight and level without accelerating, the four forces are in balance, thrust equalling drag and lift equalling weight. This particular case is represented in Figure $2-1$.

The four forces affecting the flight of an airplane are vector quantities which means that they have both magnitude and direction. The motion of flight depends exclusively on the parameters of these vectors and on how they are related. In order for a pilot to manoeuvre the aircraft, the four forces have to be precisely manipulated. Therefore, understanding their nature and possessing means to adjust their direction and magnitude is required in order to achieve precise control of the airplane.

[1]The center of pressure is the average location of all the pressure forces acting on the aircraft [31]. Similarly, the center of gravity is the average location of the weight of the airplane.

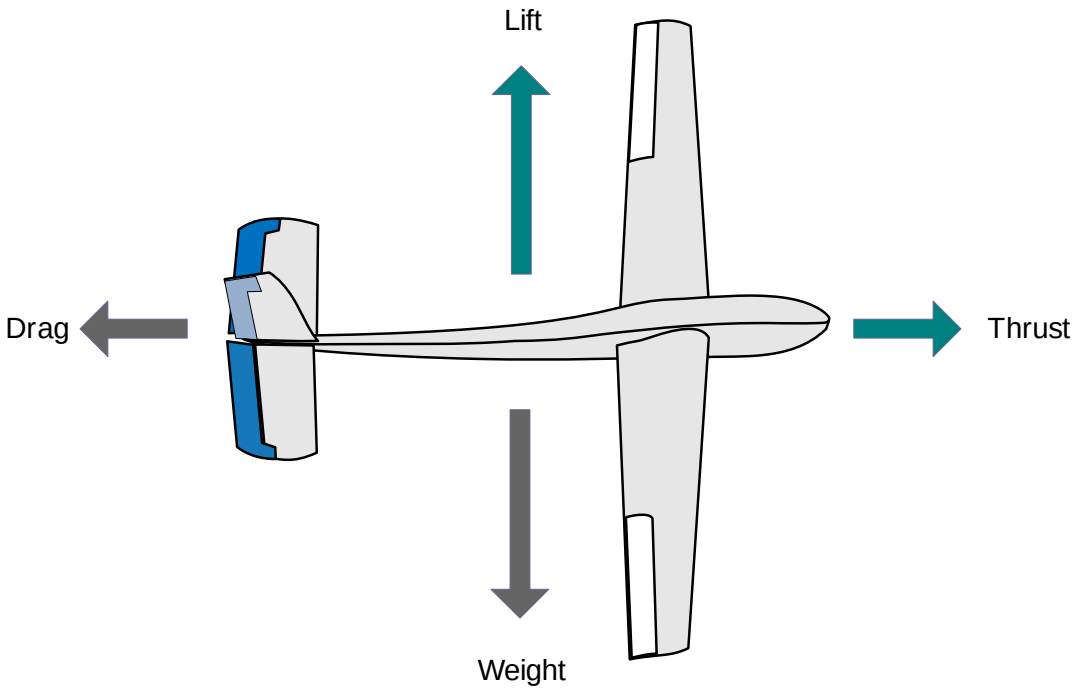

Figure 2-1: The forces of flight

2.1.2 Parts of an airplane

Aircrafts may come in several configurations and sizes but they all work on the same principle, namely manipulating the for forces of flight. Therefore, any vehicle which is capable to provide these forces is said to be an aircraft, regardless its shape. But, since the subject of this thesis is fixed-wing UAVs, let us introduce the component parts of an aircraft of conventional shape.

An airplane consists of a propulsion system and many aerodynamic shapes which can be fixed or variable. The propulsion system or the engine is used to power the vehicle. The fixed aerodynamic shapes provide the lift force and the stability of the airplane and they are represented by: fuselage, wings and tail stabilizers. With respect to the variable aerodynamic shapes, they are commonly known as control surfaces and they are divided in elevator, ailerons and rudder, see Figure $2-2$. In some aircrafts there are additional parts to vary the aerodynamics of the wing, most of them being high lift devices such as flaps and slats. In addition, spoilers can be employed to break the airflow over the wing or winglets to reduce drag.

The fixed component parts of an airplane are listed below:

1. The **propulsion system** is the component which generates the thrust force required to move the airplane forwards. Both propeller and jet engines produce thrust by throwing the air backwards. By manipulating the power of the engine, one can control the magnitude of the resulting force while its direction is fixed along the longitudinal axis of the airplane.

2. The **fuselage** is the airplane component which connects all the parts together. It has an aerodynamic shape in order to reduce the resulting drag force. Besides, a small proportion of produced lift comes from the fuselage.

3. The **wings** produce the most significant amount of lift which is the force that makes the flight of heavier-than-air vehicles possible.

4. **Horizontal stabilizer** is a small horizontal wing located at the tail of the airplane used to avoid up and down undesirable motion.

5. **Vertical stabilizer** - is a small vertical wing located at the tail of the airplane used to avoid side to side motion.

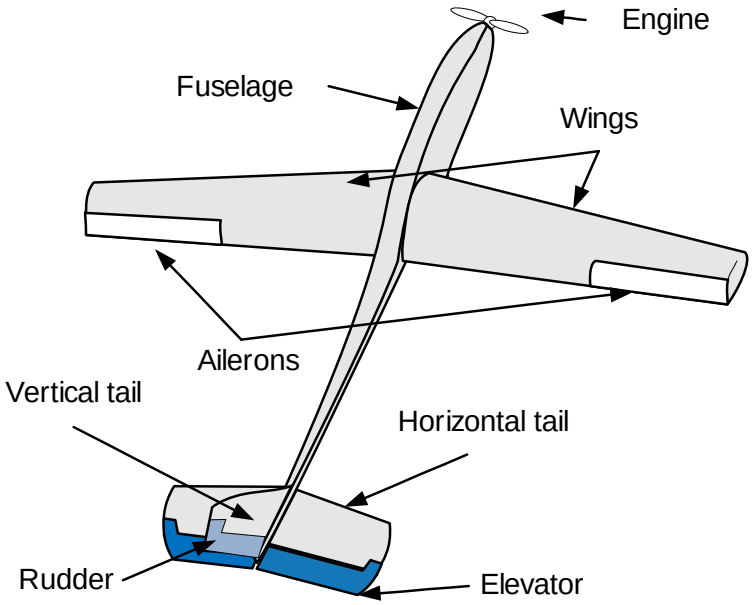

Figure 2-2: Component parts of an airplane

The aerodynamic control surfaces are moving parts of the wings (including the tail stabilizers) that can change the airflow over these particular locations of the aircraft in very specific ways. Actually, they act by modifying the shapes of the wings and, thus, their cambers. This results in a desired pressure difference producing a controlled force. The common control surfaces of a fixed-wing aircraft are:

1. The **elevator** is a hinged-surface connected to the horizontal stabilizer which is used to control the vertical motion of the airplane. When the elevator is deflected downwards, the horizontal tail wing produces an increased lift force which makes the tail of the airplane to rise relative to the nose and, thereby, the airplane to descend[2]. An upward deflection of the elevator creates an opposite effect, making the aircraft to climb. Hence, the elevator controls the motion of the airplane around the lateral axis that is known as pitching motion.

2. The **ailerons** are movable sections placed outboard toward the wing tips which work usually in opposition: one deflected upward and one deflected downward. They work in the same way as the elevator. As they are deflected, the airfoils chambers vary resulting an increased lift on one wing and a decreased lift on the other. The resulting motion of the airplane is a rotation around its longitudinal axis known as rolling.

3. The **rudder** is a variable part placed at the rear of the vertical stabilizer which causes the airplane to move from side to side. Deflecting the rudder, one can manipulate the amount of force produced by the vertical tail wing and, thereby, the motion of the aircraft around the vertical axis known as yawing.

Unlike pitching motion, rolling and yawing motions are not pure, that is rudder and ailerons deflections excite both yawing and rolling displacements. When rolling an airplane, the lowered aileron has more drag than the up-going aileron and this causes an adverse yaw. Therefore, the rudder is mainly used is to maintain the nose of the aircraft into the direction of flight, thus to obtain a coordinated flight.

[2]The aircraft descends when the elevator is deflected downward as a result of changing the angle of attack and the direction of the thrust vector.

2.1.3 Misleading lift theories

At this point we can make a legit answer to the question "How the airplanes fly?" by saying that there is a lift force produced by the wings which keeps the aircraft into the air. Such a general explanation satisfies just the curious but those ones really passionate about the flight of an airplane need a more detailed description of how this force is created. This is, for that matter, a much more difficult question which has been answered throughout time in several ways, but many concepts describing the basic principles of lift have been shown to be misleading and incorrect [32], such as "the equal transit times" or "the skipping stone" principles. Unfortunately, such misconceptions about flight have been taught for many years in most flight training manuals and they still create passionate debates between physicists and aeronautical engineers [38]. This subsection stars by examining the components of a wing in order to explain further some classical descriptions of lift.

Wing section

Let us first illustrate a wing section, usually called airfoil, as shown in Figure 2-3. Notice from this figure that wings have generally a rounded leading edge and a pointed trailing edge. The line joining the center of the leading edge to the point of the trailing edge is called the chord line. When the wing has a curvature we speak about the camber of the airfoil. The airflow striking the aircraft and its component parts is called the relative wind and its direction is always opposite to and parallel with the flight path of the airplane.

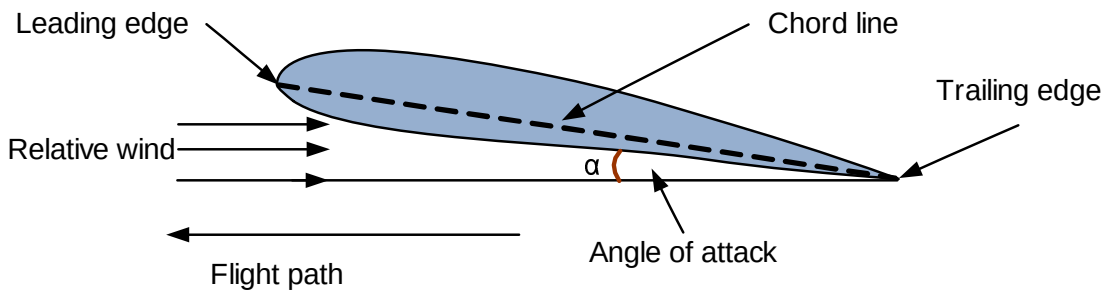

Figure 2-3: Parts of a wing

The relative wind and the flight path are horizontal and parallel in level flight. However, the chord line of the airfoil forms a small angle, called the angle of attack α, with the flight path even in level flight. As it will be later discussed, α is an important variable in the flight dynamics since even small variations affect the amount of lift.

The equal transit theory

This subsection discusses one of the most popular incorrect explanations of the lift force. Although the theory is correct in principle, it fails to provide a satisfactory explanation in detail. The theory starts from a basic principle of aerodynamics proposed by the Swiss scientist Daniel Bernoulli who claims that the faster the air moves, the less pressure it exerts. In order to invoke this principle, the proponents of the theory state that the molecules of the air on the upper surface of the airfoil have to reach the trailing edge at the same time as the molecules on the lower surface [33]. Then, claiming that the top of the wing is shaped in order to provide a longer surface than the bottom, it follows that the air molecules have to generate higher velocities over the wing than underneath it. This difference in velocity is balanced by an increased air pressure under the wing which lifts the airplane into the air.

Figure 2−4 illustrates the "equal transit time" theory. In this figure, the airfoil has a particular shape with the upper surface longer than the bottom. The air molecules split apart at the leading edge of the wing (point A) and they have to move faster over the top of the airfoil in order to meet at the trailing edge (point C). This difference in velocity produces a higher pressure underneath the wing and, thereby, lift.

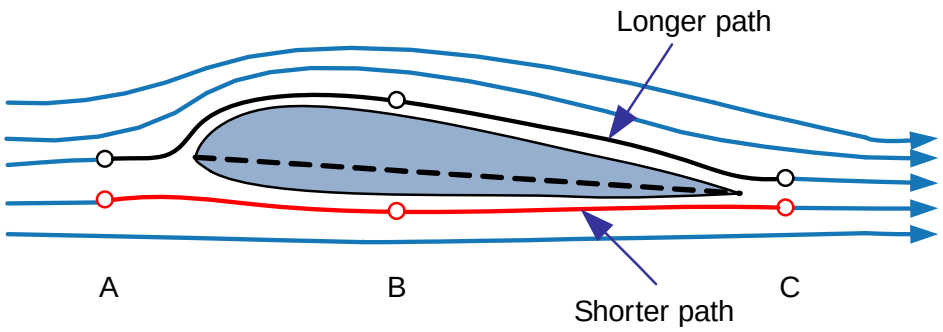

Figure 2-4: The "equal transit time" lift theory.

According to this theory, wings possessing a symmetrical airfoil have equal pressure on the both sides of the airfoil when flying in level flight, thus they do not produce any lift. But how do paper airplanes with perfectly flat wings fly? Or how can airplanes fly upside down since, using the same explanation based on Bernoulli principle, would show that the aircraft is pushed down. Moreover, how do the air particles know to speed up over the wing since they do not have any information about the geometry of the object with which they will interact? In reality, the air molecules on the upper surface of a wing travels at much higher velocity than the one required by the equal transit time theory. What goes wrong with this explanation is the fact that it uses the Bernoulli's equation for the wrong assumption that the air molecules have to meet at the end of the wing. In addition, this theory fails to explain why the air moves faster over the wing than beneath it. Therefore, although Bernoulli's argument is correct, the complete explanation is misleading.

The skipping stone theory

This theory uses the Newton's laws of motion to explain the generation of lift. For this purpose, the wing is described as a surface which forces the air to go down. Then, by Newton's third law which states that "for every action there is an equal and opposite reaction", the lift is considered to be the reaction force of the airfoil to the air molecules striking the bottom surface of the wing. The name of the theory comes from the similarity with skipping a flat rock across a body of water when thrown at a small angle and its principle is shown in Figure $2-5$.

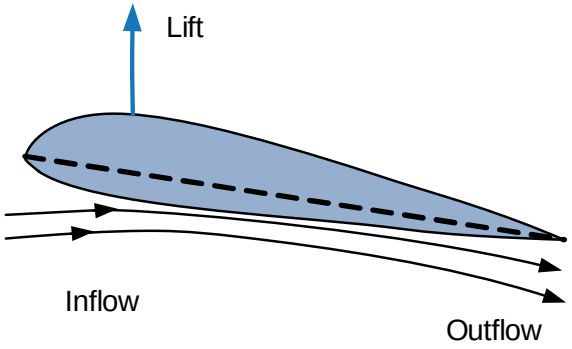

Figure 2-5: The "skipping stone" lift theory.

The deficiency of this theory is that it does not consider the upper surface of the wing assuming that the downwash is all produced by the lower surface. Following this idea, it results that two airfoils having identical lower surfaces but different upper surfaces give the same amount of lift. In reality this is not the case, and this is due to the fact that the upper surface of the airfoil contributes more to the downwash than the lower surface.

2.1.4 Lift generated by airflow deflection

Lift is a mechanical force generated the by the airfoil of the airplane as it interacts with the air [35]. Indeed, the airfoil has an aerodynamic shape which produces a net deflection of the incoming flow since the molecules of the air stay in contact with the body of the wing. Hence, the airflow velocity vector is changed producing an acceleration. Finally, from Newton's second law of motion, when a mass is accelerated then a force is produced.

Therefore, the wing creates lift as a reaction force from redirecting air downwards with the major part coming from the upper wing surface pushing air down [39]. Figure $2-6$ shows the streamlines over a wing with lift generated by using the FoilSim III Java Applet provided by NASA. Notice from this figure that both the flow above and below the wing are bent down. In addition, the air passing above the wing travels faster than the air on the lower surface.

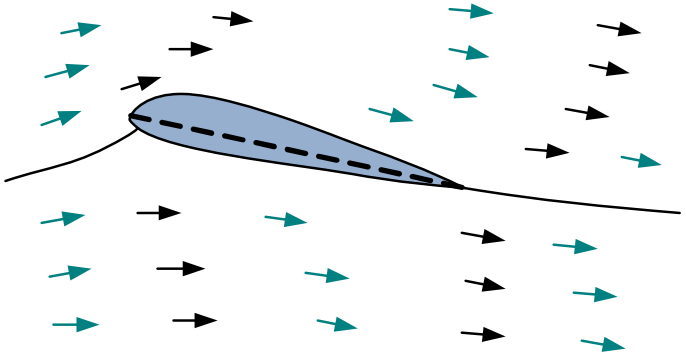

Figure 2-6: Lift generated by the airflow deflection.

2.2 Coordinate frames

When analyzing the dynamics of an aircraft it is necessary to express its position and orientation relative to a suitable coordinate system in which the Newton's laws of motion can be applied. In addition, several frames of reference need to be used in order to define relative positions and velocities, the choice of the frame to be employed being a matter of convenience. For example, sensors such as GPS measure the aircraft velocity relative to the Earth, thus a coordinate system fixed on Earth surface is preferable to write the velocity equations. On the other hand, sensors such as rate gyros give information with respect to the body of the vehicle where they are installed. Accordingly, the airplane angular rates are most easily described in a vehicle-fixed reference frame.

Based on these considerations, this section discusses the commonly used coordinate frames for the problem of the airplane flight dynamics and introduces the required transformations to bring vectors from one frame to another. The presentation in this section is mainly based on textbooks by B. Etkin [17] and Randal W. Beard & Timothy W. McLain [40].

2.2.1 Inertial and Earth-fixed reference frames $\mathcal{F}^I$, $\mathcal{F}^E$

Solving a dynamic problem requires an inertial reference frame, $\mathcal{F}^I$, which is fixed or in uniform rectilinear translation relative to the distant stars. Meeting this requirement leads to the possibility of using the Newton's second law for the motion of a particle, which relates the external forces acting on the particle to its mass and acceleration relative to $\mathcal{F}^I$. Generally, the rotation of the Earth relative to such an inertial frame is neglected in the analysis of the flight dynamics. Therefore, any coordinate frame with the origin at a defined location on the Earth can be used as an inertial frame.

Let $\mathcal{F}^E$ denote an Earth-fixed frame having the origin close to the vehicle body and its axes directed North, East and vertically down as shown in Figure $2-7$. This coordinate system will be used in further analysis to describe aircraft position and orientation since many sensors measure these quantities with respect to the Earth.

In addition, most mission are defined in this frame, such as waypoint guidance, flight trajectories etc.

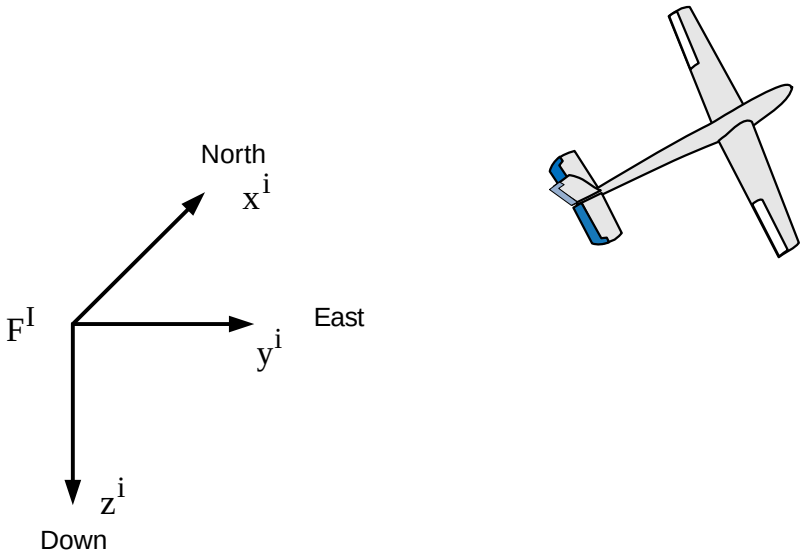

Figure 2-7: Illustration of the inertial coordinate frame.

2.2.2 Body-fixed coordinate system $\mathcal{F}^B$

The origin of the body-fixed frame, $\mathcal{F}^B$, is identical to the vehicle center of gravity and the axes point out the nose of the airframe, out the right wing and downward, as shown in Figure $2-8$. $\mathcal{F}^B$ has angular velocity relative to $\mathcal{F}^I$ denoted by $\omega = [p,\ q,\ r]^T$. It is employed since the aerodynamic and propulsive forces act on the aircraft body and they are easily defined in this reference system. Moreover, on-board sensors generally measure information with respect to the body frame.

The orientation of $\mathcal{F}^B$ relative to $\mathcal{F}^I$ can be given by the Euler angles $(\psi,\ \theta,\ \phi)$ which are three consecutive rotations about the axes z, y and x. The angles represent the yaw, pitch and roll and they rotate the body of the airplane about the vertical, lateral and longitudinal inertial axes. The transformations associated with each single rotation are given by

$$R_1(\phi) = \begin{bmatrix} 1 & 0 & 0 \\ 0 & \cos\phi & \sin\phi \\ 0 & -\sin\phi & \cos\phi \end{bmatrix}$$

$$R_2(\theta) = \begin{bmatrix} \cos\theta & 0 & -\sin\theta \\ 0 & 1 & 0 \\ \sin\theta & 0 & \cos\theta \end{bmatrix}$$

$$R_3(\psi) = \begin{bmatrix} \cos\psi & \sin\psi & 0 \\ -\sin\psi & \cos\psi & 0 \\ 0 & 0 & 1 \end{bmatrix}$$

The complete transformation from $\mathcal{F}^I$ to $\mathcal{F}^B$ reads

$$R_{BI} = R_1(\phi)R_2(\theta)R_3(\psi)$$

$$= \begin{bmatrix} \cos\theta\cos\psi & \cos\theta\sin\psi & -\sin\theta \\ \sin\phi\sin\theta\cos\psi & \sin\phi\sin\theta\sin\psi & \sin\phi\cos\theta \\ -\cos\phi\sin\psi & +\cos\phi\cos\psi & \\ \cos\phi\sin\theta\cos\psi & \cos\phi\sin\theta\sin\psi & \cos\phi\cos\theta \\ +\sin\phi\sin\psi & -\sin\phi\cos\psi & \end{bmatrix} \tag{2.1}$$

2.2.3 Wind axes coordinate frame $\mathcal{F}^W$

The wind axes frame, $\mathcal{F}^W$, has the origin at the aircraft center of gravity and the x-axis is directed along the velocity vector of the vehicle relative to the atmosphere as depicted in Figure $2-8$. In calm conditions, i.e. atmosphere at rest, the origin of $\mathcal{F}^W$ will trace out the trajectory of the aircraft relative to the Earth.

The wind frame is of interest since the lift, drag and side forces are directly measured in the direction of its axes. It has angular velocity relative to $\mathcal{F}^I$ and its components are denoted by $\omega_w = [p_w,\ q_w,\ r_w]^T$. The orientation of $\mathcal{F}^W$ relative to the body-fixed frame is determined by the aerodynamic angles α and β which stand for angle of attack and sideslip, respectively. This implies that some trigonometry is required in order to bring the measured vectors from $\mathcal{F}^W$ into $\mathcal{F}^B$ or vice versa.

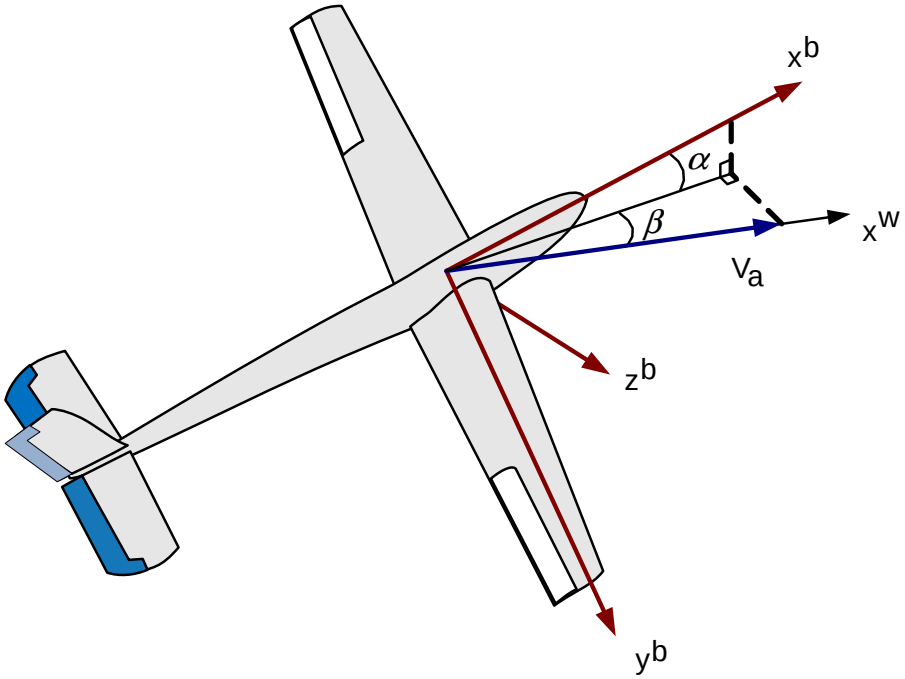

Figure 2-8: Illustration of the body and wind axes reference frames.

In order to obtain the total transformation from wind to body frame, one may follow the same steps as for R_{BI} considering the sequence of rotations given by $(-\beta,\ \alpha,\ 0)$, where

$$R_2(\alpha) = \begin{bmatrix} \cos\alpha & 0 & -\sin\alpha \\ 0 & 1 & 0 \\ \sin\alpha & 0 & \cos\alpha \end{bmatrix}$$

$$R_3(-\beta) = \begin{bmatrix} \cos\beta & -\sin\beta & 0 \\ \sin\beta & \cos\beta & 0 \\ 0 & 0 & 1 \end{bmatrix}$$

Thus

$$\begin{aligned} R_{BW} &= R_1(0)R_2(\alpha)R_3(-\beta) \\ &= \begin{bmatrix} \cos\alpha\cos\beta & -\cos\alpha\sin\beta & -\sin\alpha \\ \sin\beta & \cos\beta & 0 \\ \sin\alpha\cos\beta & -\sin\alpha\sin\beta & \cos\alpha \end{bmatrix} \end{aligned} \tag{2.2}$$

2.3 Aircraft nonlinear model

The present section focuses on the derivation of the mathematical model of a fixed-wing UAV which is considered as a rigid body having 6 degrees of freedom. In addition, the Earth is considered as flat and stationary for the purpose of simplicity and that makes $\mathcal{F}^E$ a Newtonian frame of reference. Note that this is a valid approximation for most problems of aircraft flight. The equations of motion are derived considering that the atmosphere is at rest relative to the Earth and making an appropriate adjustment at the end in order to include the effect of the wind into the model. The presentation in this section is mainly based on the textbooks by [49, 17, 1].

2.3.1 State variables

The Earth relative aircraft motion can be described by position, orientation, velocity, and angular velocity over time. The position of the aircraft center of gravity in the inertial coordinate frame will be denoted by the vector p_E, whose components are

$$p_E = [p_n \quad p_e \quad -p_h]^T$$

with p_n being the inertial position along the North axis in $\mathcal{F}^E$, p_e representing the inertial position along the East axis in $\mathcal{F}^E$ and p_h denoting the inertial altitude along the vertical axis in $\mathcal{F}^E$.

The Earth related aircraft orientation is represented by the Euler angles from the attitude vector Φ

$$\Phi = [\phi \quad \theta \quad \psi]^T$$

where ϕ is the roll angle, θ defines the pitch angle, and ψ represents the yaw angle.

The aircraft inertial velocity vector V_E is commonly represented in several coordinate systems. Its components are given by

$$V_E = R_{EW} V_W = R_{EB} V_B \tag{2.3}$$

where

$$V_E = \begin{bmatrix} v_n \\ v_e \\ v_h \end{bmatrix}; \quad V_W = \begin{bmatrix} V_a \\ 0 \\ 0 \end{bmatrix}; \quad V_B = \begin{bmatrix} v_u \\ v_v \\ v_w \end{bmatrix};$$

and R_{EW} is the transformation from $\mathcal{F}^W$ to $\mathcal{F}^E$ and it is obtained from the sequence of rotations given by the angles (ϕ_w, θ_w, ψ_w) which provide the orientation of the wind axes, V_W represents the inertial velocity vector measured in the direction of the wind axes reference frame, V_a denotes the magnitude of the aircraft velocity relative to the air mass known as airspeed, R_{EB} describes the rotation from $\mathcal{F}^B$ to $\mathcal{F}^E$ and $R_{EB} = R_{IB} = R_{BI}^T$ while V_B represents the inertial velocity vector of the aircraft in the body coordinate system having components along the longitudinal, lateral and normal axes denoted by(v_u, v_v, v_w).

The velocity vector of the aircraft relative to surrounding air is denoted by $\mathcal{V}_a$ having the components $\mathcal{V}_a = [u\ v\ w]^T$ in the body frame of reference. If the atmosphere is at rest, the air-relative aircraft velocity equals the velocity of the vehicle with respect to the Earth. Writing the equation describing this relationship for both body and wind axes, it follows

$$\mathcal{V}_a = V_B = R_{BW} V_W$$

and using equation (2.2), it yields

$$\begin{bmatrix} u \\ v \\ w \end{bmatrix} = V_a \begin{bmatrix} \cos\alpha\cos\beta \\ \sin\beta \\ \sin\alpha\cos\beta \end{bmatrix}$$

which implies that

$$\begin{aligned} V_a &= \sqrt{u^2 + v^2 + w^2} \\ \alpha &= \arctan\frac{w}{u} \\ \beta &= \arcsin\frac{v}{V_a} \end{aligned}$$

The angular velocity vector is also represented in the body-fixed and in the wind-axes coordinate frames having the components

$$\omega = \begin{bmatrix} p \\ q \\ r \end{bmatrix}; \quad \omega_w = R_{WB}\omega = \begin{bmatrix} p_w \\ q_w \\ r_w \end{bmatrix}$$

where ω is the angular velocity vector of $\mathcal{F}^B$ relative to $\mathcal{F}^E$, p denotes the roll rate, q the pitch rate and r the yaw rate while ω_w represents the angular velocity vector of $\mathcal{F}^W$ relative to $\mathcal{F}^E$.

Based on the above notations typically employed in the aeronautics literature, the state vector is given by

$$\begin{aligned} x^T &= \begin{bmatrix} V_B^T & \omega^T & \Phi^T & p_E^T \end{bmatrix}^T \\ &= \begin{bmatrix} u & v & w & p & q & r & \phi & \theta & \psi & p_n & p_e & p_h \end{bmatrix}^T \end{aligned} \tag{2.4}$$

Then, the equations of motion of a rigid body aircraft when considering a stationary flat-Earth and the atmosphere at rest ar given in [49] and they have the form

$$\dot{p}_E = R_{BE}^T \mathcal{V}_a \tag{2.5a}$$

$$\dot{\Phi} = \mathcal{G}(\Phi)\omega \tag{2.5b}$$

$$\dot{V}_B = -\Omega_B V_B + R_{BE} g_0 + \frac{F_B}{m} \tag{2.5c}$$

$$\dot{\omega} = -J^{-1}\Omega_B J\omega + J^{-1}T_B \tag{2.5d}$$

where Ω_B is the cross-product matrix of the body axes angular rates, g denotes the gravitational acceleration, F_B is the net applied force on the aircraft center of gravity, m is the vehicle mass, J represents the inertia matrix of the rigid aircraft, T_B is the net torque acting about the aircraft center of gravity. The complete mathematical model given in (2.5) can be separated into translational and rotational equations as it will be further shown.

2.3.2 The navigation equations

Equation (2.5a) provides the coordinates of the flight path in the inertial frame and it is known as the navigation equation. Introducing (2.1) in (2.5a) and using the above notations in order to extend the equation in terms of the vector components introduced in subsection 2.3.1, the rate of change of the translational position reads

$$\begin{aligned}
\dot{p}_n &= u\cos\theta\cos\psi + v\left(-\cos\phi\sin\psi + \sin\phi\sin\theta\cos\psi\right) \\
&\quad +w\ \left(\sin\phi\sin\psi + \cos\phi\sin\theta\cos\psi\right) && \text{(2.6a)} \\
\dot{p}_e &= u\cos\theta\sin\psi + v\left(\cos\phi\cos\psi + \sin\phi\sin\theta\sin\psi\right) \\
&\quad +w\ \left(-sin\phi\cos\psi + \cos\phi\sin\theta\sin\psi\right) && \text{(2.6b)} \\
\dot{p}_h &= u\sin\theta - v\sin\phi\cos\theta - w\cos\phi\cos\theta && \text{(2.6c)}
\end{aligned}$$

A more convenient form of the inertial position coordinates can be obtained from equation (2.3) when employing the velocity vector in the wind axes reference frame. The differential equations governing the translational position are given by

$$\begin{aligned}
\dot{p}_n &= V_a\cos\theta_w\cos\psi_w && \text{(2.7a)} \\
\dot{p}_e &= V_a\cos\theta_w\sin\psi_w && \text{(2.7b)} \\
\dot{p}_h &= -V_a\sin\theta_w && \text{(2.7c)}
\end{aligned}$$

2.3.3 The attitude equations

The attitude equation is represented by (2.5b) which provide the orientation of the airplane in the inertial frame. Note from this equation that the angular velocity vector of the aircraft in the body-fixed reference frame is related to the angular velocity vector in the inertial frame through a transformation matrix $\mathcal{G}(\Phi)$ defined as

$$\mathcal{G}(\Phi) = \begin{bmatrix} 1 & \sin\phi\tan\theta & \cos\phi\tan\theta \\ 0 & \cos\phi & -\sin\phi \\ 0 & \sin\phi\sec\theta & \cos\phi\sec\theta \end{bmatrix}$$

Thus, the rate of change of angular position reads

$$\dot{\phi} = p + \tan\theta\,(q\sin\phi + r\cos\phi) \tag{2.8a}$$

$$\dot{\theta} = q\cos\phi - r\sin\phi \tag{2.8b}$$

$$\dot{\psi} = \frac{q\sin\phi + r\cos\phi}{\cos\theta} \tag{2.8c}$$

2.3.4 The force and moment equations

The last two equations derived in (2.5) are driven by the forces and moments acting on the aircraft center of gravity. They have both components due to several factors with main sources being the propulsive and aerodynamic effects. In order to extend the dynamic equations in terms of vector components and forces and moments acting on the aircraft, let us first examine how F_B and T_B can be expressed.

The force vector from equation (2.5c) can be represented in terms of the propulsive and aerodynamic components, F_p and F_a respectively. Thus

$$F_B = F_p + F_a$$

The propulsive force is produced by the engine thrust denoted by T. Generally, the engines are placed along the longitudinal body axis of the aircraft so that the produced force has just a component pointing in the direction of this axis, that is

$$F_p = \begin{bmatrix} T \\ 0 \\ 0 \end{bmatrix}$$

Regarding the aerodynamic force, it can be expressed in both body or wind axes; whether one frame or another is employed, the components are related by the rotation matrix given in equation (2.2). Actually, the aerodynamic force may be naturally

defined in the wind axes as lift L, drag D and sideforce Y. Hence

$$F_a^W = \begin{bmatrix} -D \\ Y \\ -L \end{bmatrix} = \begin{bmatrix} \bar{q}SC_D \\ \bar{q}SC_Y \\ \bar{q}SC_L \end{bmatrix}$$

where $\bar{q} = \frac{1}{2}\rho(h)V_a^2$ is the free-stream dynamic pressure, S is the wing area and C_D, C_L, C_Y are dimensionless aerodynamic coefficients which are primarily dependent on aerodynamic angles, the geometry of the aircraft, the deflections of the control surfaces, etc.

Denoting the components of the aerodynamic force in the body axes by (X_a, Y_a, Z_a), they can be expressed in terms of body-axes dimensionless aerodynamic coefficients C_x, C_y, C_z

$$F_a = \begin{bmatrix} X_a \\ Y_a \\ Z_a \end{bmatrix} = \begin{bmatrix} \bar{q}SC_x \\ \bar{q}SC_y \\ \bar{q}SC_z \end{bmatrix}$$

or in terms of the wind axes components of the aerodynamic force

$$\begin{aligned} X_a &= -D\cos\alpha\cos\beta - Y\cos\alpha\sin\beta + L\sin\alpha \\ Y_a &= -D\sin\beta + Y\cos\beta \\ Z_a &= -D\sin\alpha\cos\beta - Y\sin\alpha\sin\beta - L\cos\alpha \end{aligned}$$

Extending the force equation (2.5c) and introducing the above notations, it yields

$$\dot{u} = rv - qw - g_0\sin\theta + \frac{X_a + T}{m} \tag{2.9a}$$

$$\dot{v} = -ru + pw + g_0\sin\phi\cos\theta + \frac{Y_a}{m} \tag{2.9b}$$

$$\dot{w} = qu - pv + g_0\cos\phi\cos\theta + \frac{Z_a}{m} \tag{2.9c}$$

In some particular cases, e.g. derivation of a linear small-perturbation model or estimation of the aerodynamic derivatives values, it is more convenient to express the force equations of motion in the wind axes in which the aerodynamic coefficients are naturally measured. In the following, we will provide the final form of these equations, the reader being referred to [17] for a detailed description of how the equations were obtained.

The scalar expansion of the wind axes equations reads

$$
\begin{aligned}
m\dot{V}_a &= T_{xw} - D - mg\sin\theta_w && \text{(2.10a)}\\
\dot{\alpha} &= q - q_w\sec\beta - p\cos\alpha\tan\beta - r\sin\alpha\tan\beta && \text{(2.10b)}\\
\dot{\beta} &= r_w + p\sin\alpha - r\cos\alpha && \text{(2.10c)}
\end{aligned}
$$

where T_{xw} represents the thrust component along the x-axis of the wind frame and $[p_w \; q_w \; r_w]$ are the angular velocities of the wind frame relative to the inertial frame of reference.

A similar procedure applied to the moment equation $(2.5d)$, in which T_B is defined in terms of aerodynamic and propulsive components, leads to

$$
T_B = T_p + T_a = \begin{bmatrix} 0 \\ dT \\ 0 \end{bmatrix} + \begin{bmatrix} \bar{L}_a \\ M_a \\ N_a \end{bmatrix} = \begin{bmatrix} \bar{q}SbC_l \\ dT + \bar{q}S\bar{c}C_m \\ \bar{q}SbC_n \end{bmatrix}
$$

where d is the offset of the engine from the aircraft center of gravity along the z-axis of the body frame, T_a^B is the moment due to aerodynamic effects having components $(\bar{L}_a \;\; M_a \;\; N_a)$ in the direction of the body axes, b represents the wing span, $\bar{c}$ defines the mean geometric chord of the wing and $(C_l,\, C_m,\, C_n)$ are dimensionless coefficients primarily dependent on the aerodynamic angles.

Denoting the body axes moment components by $T_B = \begin{bmatrix} \bar{L} & M & N \end{bmatrix}^T$ in accordance

with traditional usage, the expended set of the moment equation reads

$$\dot{p} = (c_1 r + c_2 p)\, q + c_3 \bar{L} + c_4 N \tag{2.11a}$$

$$\dot{q} = c_5 pr - c_6 \left(p^2 - r^2\right) + c_7 M \tag{2.11b}$$

$$\dot{r} = (c_8 p - c_2 r)\, q + c_4 \bar{L} + c_9 n \tag{2.11c}$$

where the constants $c_i, i = \overline{1,9}$ are given by

$$\begin{aligned}
\Gamma c_1 &= (J_y - J_z)\, J_z - J_{xz}^2, & \Gamma c_2 &= (J_x - J_y + J_z)\, J_{xz} \\
\Gamma c_3 &= J_z, & \Gamma c_4 &= J_{xz} \\
c_5 &= \tfrac{J_z - J_x}{J_y}, & c_6 &= \tfrac{J_{xz}}{J_y} \\
c_7 &= \tfrac{1}{J_y}, & \Gamma c_8 &= J_x\,(J_x - J_y) + J_{xz}^2 \\
\Gamma c_9 &= J_x, & \Gamma &= J_x J_z - J_{xz}^2
\end{aligned}$$

Remark: Writing the wind-axes moment equations offers no advantages for use in a nonlinear model. In reality, these equations are more complex than the previously derived body-axes equations. Therefore, typical nonlinear models combine force equations in either body or wind axes with body-axes moment equations [49].

2.3.5 Discussion of the equations

The complete state model of the airplane consists of 12 coupled nonlinear ordinary differential equations obtained from (2.6), (2.8), (2.9) and (2.11). Note that two alternatives have been presented for both navigation and force equations given in (2.7) and (2.10). The control vector, although it is not directly observable in these equations, determines the thrust force and the deflections of the movable surfaces managing the aerodynamic forces (D, L, Y) and moments ($\bar{L}$, M, N). The mathematical model established by collecting these equations is subject to some general assumptions such as: (i) the airplane is a rigid body having a plane of symmetry, (ii) the Earth is flat and stationary and (iii) the atmosphere is at rest relative to the Earth.

2.4 Flying in a moving atmosphere

It has been shown in the previous section that airplane dynamics offer challenging control problems since they are nonlinear, require transformations between several reference frames and depend on uncertain forces and moments. In addition, in real conditions airplanes are subjected to environmental disturbances such as wind which is the movement of the surrounding air that disturbs the stability of the vehicle and its inertial track. Hence, an analysis of how these perturbations affect the dynamics of flight is required to obtain improved flight capabilities.

Accordingly, the aim of this section is to extend the mathematical model previously derived by including the effects of the wind on the aircraft performance. For this reason, the section begins by describing a model of low altitude wind which is adequate for analysis purposes. Further, the vulnerability of airplanes to wind is analyzed and incorporated into the equations of motion.

2.4.1 Wind description

To understand and analyze how the air motion impacts the modeling of an aircraft, we need first to describe the wind itself as part of the velocity field in which the aircraft flies. The air mass is in a continuous state of motion due to the solar heating, Earth rotation or various thermodynamic and electromagnetic processes. The velocity vector of the atmosphere is generally variable in both space and time and it can be decomposed into a mean value and variations from it [17]. The steady-state velocity at a given position is known as mean wind while the remaining fluctuating part is defined as atmospheric turbulence or gust. The wind occurs primarily in navigation and guidance applications while the turbulence affects mainly the airplane stability.

The conventional notation for the velocity vector of the air mass relative to the Earth is W. Based on the above considerations, the total velocity field within the atmosphere is defined as

$$\mathrm{W} = \mathrm{W}_M + \mathrm{W}_F$$

where W_M is the mean wind vector and W_F is the atmospheric turbulence.

Local wind is naturally measured in the direction of the Earth-fixed reference frame having north, east and down velocity components denoted by W_n, W_e and W_h, respectively. For convenience, it may be represented in other coordinate systems using the transformation matrices derived in the previous section. Thus

$$\mathrm{W} = \begin{bmatrix} \mathrm{w}_n \\ \mathrm{w}_e \\ \mathrm{w}_h \end{bmatrix} = \begin{bmatrix} \mathrm{w}_{n_M} + \mathrm{w}_{n_F} \\ \mathrm{w}_{e_M} + \mathrm{w}_{e_F} \\ \mathrm{w}_{h_M} + \mathrm{w}_{h_F} \end{bmatrix} = R_{IB} \begin{bmatrix} u_w \\ v_w \\ w_w \end{bmatrix}$$

where (u_w, v_w, w_w) represent the wind components in the body-fixed reference frame and R_{IB} is given by equation (2.1) with $R_{IB} = R_{BI}^T$.

The investigation of the wind vector effect on the flying qualities of an aircraft requires a mathematical model of such perturbation. In principle, a deterministic description of complete wind is not possible; in other words, it can not be described by analytical expressions. Rather, the wind field can be modeled as a stochastic process for which statistical properties can be described [1, 17, 50]. The derivation of a wind gust model relies heavily on the random-process theory, the reader being referred to [17, 1] for a detailed discussion on the subject.

There are two spectral forms of random continuous turbulence used to model atmospheric turbulence which were provided by the scientists von Karman and Dryden. To generate the fluctuating wind vector with the correct characteristics, the Von Karman velocity spectra are used to filter a unit variance, band-limited white noise signal. The transfer functions of a Von Karman model are further listed [41].

$$\begin{aligned}
H_u(s) &= \frac{\sigma_u \sqrt{\frac{2}{\pi}\frac{L_u}{V}\left(1 + 0.25\frac{L_u}{V}s\right)}}{1 + 1.357\frac{L_u}{V}s + 0.1987\left(\frac{L_u}{V}\right)^2 s^2} \\
H_v(s) &= \frac{\sigma_v \sqrt{\frac{1}{\pi}\frac{L_v}{V}\left(1 + 2.7478\frac{L_v}{V}s + 0.3398\left(\frac{L_v}{V}\right)^2 s^2\right)}}{1 + 2.9958\frac{L_v}{V}s + 1.9754\left(\frac{L_v}{V}\right)^2 s^2 + 0.1539\left(\frac{L_v}{V}\right)^3 s^3} \\
H_w(s) &= \frac{\sigma_w \sqrt{\frac{1}{\pi}\frac{L_w}{V}\left(1 + 2.7478\frac{L_w}{V}s + 0.3398\left(\frac{L_w}{V}\right)^2 s^2\right)}}{1 + 2.9958\frac{L_w}{V}s + 1.9754\left(\frac{L_w}{V}\right)^2 s^2 + 0.1539\left(\frac{L_w}{V}\right)^3 s^3}
\end{aligned}$$

where L_u, L_v, L_w represent the turbulence scale lengths, σ_u, σ_v, σ_w represent the turbulence intensities and V is the speed of the vehicle.

In terms of Dryden models, the forming filters are derived from the spectral square roots of the spectrum equations and the transfer functions are given by [41]

$$\begin{aligned} H_u(s) &= \sigma_u \sqrt{\frac{2L_u}{\pi V}} \frac{1}{1+\frac{L_u}{V}s} \\ H_v(s) &= \sigma_v \sqrt{\frac{L_v}{\pi V}} \frac{1+\frac{\sqrt{3}L_v}{V}s}{\left(1+\frac{L_v}{V}s\right)^2} \\ H_w(s) &= \sigma_w \sqrt{\frac{L_w}{\pi V}} \frac{1+\frac{\sqrt{3}L_w}{V}s}{\left(1+\frac{L_w}{V}s\right)^2} \end{aligned}$$

The parameters of a Dryden gust model are summarized in Table 2.1 for different conditions of flight and an example of a low altitude low turbulence Dryden gust model is illustrated in Figure $2-9$ having the mean values equal to $\mathrm{w}_{n_M} = 4$ m/s, $\mathrm{w}_{e_M} = 1.7$ m/s and $\mathrm{w}_{h_M} = 0.4$ m/s. In real conditions, the parameters of the mean wind change along the flight path due to the movement of air masses relative to one another. A significant variation over a relatively short distance in either the speed or direction of the wind is called wind shear and it is of special interest during the take-off and landing approaches [42].

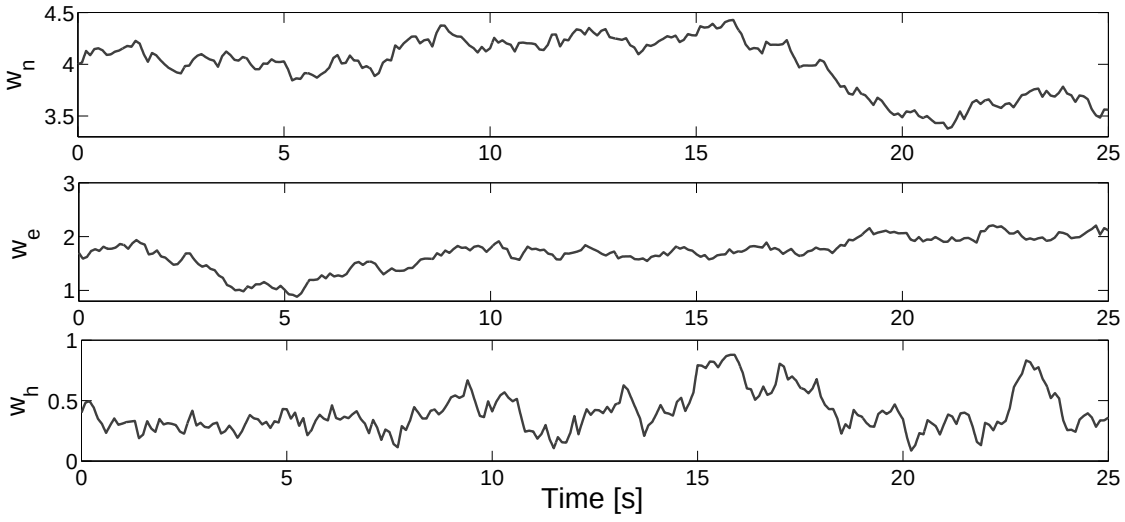

Figure 2-9: Illustration of a low altitude low turbulence Dryden gust model.

Gust description	Altitude (m)	$L_u = L_v$ (m)	L_w (m)	$\sigma_u = \sigma_v$ (m/s)	σ_w (m/s)
Low altitude, light turbulence	50	200	50	1.06	0.7
Low altitude, moderate turbulence	50	200	50	2.12	1.4
Medium altitude, light turbulence	600	533	533	1.5	1.5
Medium altitude, moderate turb.	600	533	533	3.0	3.0

Table 2.1: Dryden gust model parameters.

We distinguish vertical wind shear, in which the wind parameters vary with changing altitude, and horizontal wind shear which refers to variations in the wind field along horizontal distances [1]. Figure $(2-10)$ shows a horizontal wind shear affecting an aircraft during the landing approach. Note from this figure that the magnitude of the wind shear is a function of height above the ground. Therefore, the aircraft control system must account for variations in the lift force as the airplane descends since the amount of the air mass around the wing diminishes as a result of the decreasing wind velocity. An exponential variation of the mean wind with altitude can be computed based on the wind measured at a reference height of 10 meters from [44]

$$\mathrm{W}(h) = \mathrm{W}_{10} \left(\frac{h}{h_{10}} \right)^{a}$$

where $\mathrm{W}(h)$ is the velocity of the wind at height h, W_{10} represents represents the velocity of the wind at height $h_{10} = 10$ m and a is the Hellman exponent which depends on the shape and the coastal location of the terrain.

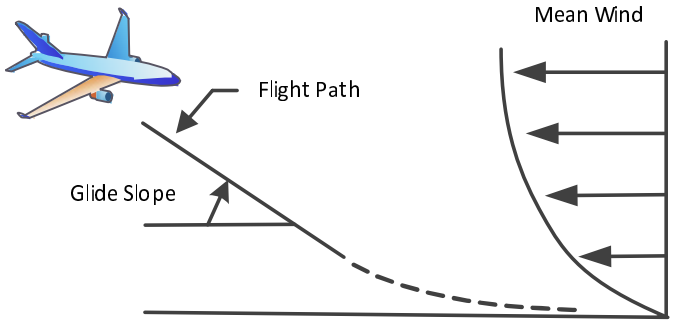

Figure 2-10: Aircraft descending into a horizontal wind shear.

The wind shear is influenced by the contours of the terrain and by its aerodynamic 'roughness'. For example, the velocity profile of a wind shear over a large urban area will be much different than over a woods or flat grassy area since they are characterized by completely different roughnesses. Furthermore, a sloping ground produces different wind profiles at the bottom and at the top of the slop [43].

2.4.2 The vulnerability of airplanes to wind

Whether we refer to the movement of the aircraft relative to the surrounding atmosphere or to the movement of the latter relative to the aircraft, the flight is possible due to the velocity difference of the airflow over the upper and the lower surface of the aircraft wing. The direction and the magnitude of the airflow experienced by the aircraft is affected when the air mass itself is in motion relative to the Earth. The wind affects both the longitudinal and the lateral variables of the airplane contributing to its nonlinear, coupled and complex dynamics.

When an aircraft flies in windy conditions, it is subjected to unknown external forces which can endanger its structural integrity but also the internal stability of the flight controller. The additional forces can degrade the overall performance of the vehicle causing, in certain situations, aircraft accidents. In order to avoid such undesirable situations, the control system must provide additional control effort to perform particular flight maneuvers such as crosswind takeoff or landing.

There are two standard techniques to handle steady crosswinds. The first one is called "crab" and it balances the crosswind component by engine thrust pointing the nose of the airplane into the wind. The second one, known as "sideslip", consists in maintaining the aircraft heading aligned with the inertial track and correcting for wind drift with a slight bank angle. Typically, both rudder and aileron inputs are required during crosswind maneuvers. Some critical flight conditions may require maximum control power to account for heavy crosswinds during the landing approach. In order to obtain augmented rudder control, structural improvements in the aircraft conceptual design phase may be considered. For example, the "Boeing $B-52$ Stratofortress" airplane model has been designed with a "yaw-adjustable cross-

wind landing gear" which points down the runway while the airplane is yawed into the relative wind [45]. Furthermore, turbulent winds may roll the airplane during the takeoff or landing approaches and additional aileron control is required to counter this motion. Upper surface wing spoilers can be used to augment aileron effectiveness in order to hold the upwind wing down in heavy crosswinds [51].

The Earth relative motion of the air affects the groundspeed/airspeed relationship but also the inertial course with respect to the aircraft heading. In extreme conditions, turbulent wind may affect the vehicle to fly outside the flight envelope. In order to provide some insight into the influence of environmental wind on aircraft response, we shall examine the landing approach of an airplane that encounters aggressive wind shear caused by thunderstorms, as illustrated in Figure $2-11$. As the aircraft enters the wind shear, it flies into a headwind created by the outflow which increases the airspeed. This leads to a reduction of the engine power in order to bring the airspeed at nominal value. Since the wind shear acts over short distances, the airplane will pass through the other side of the outflow flying in a tailwind which reduces substantially the lift and increases the sink rate. Aggressive control input is required since the aircraft is in a low-power, low-speed descent and it may be close to the ground.

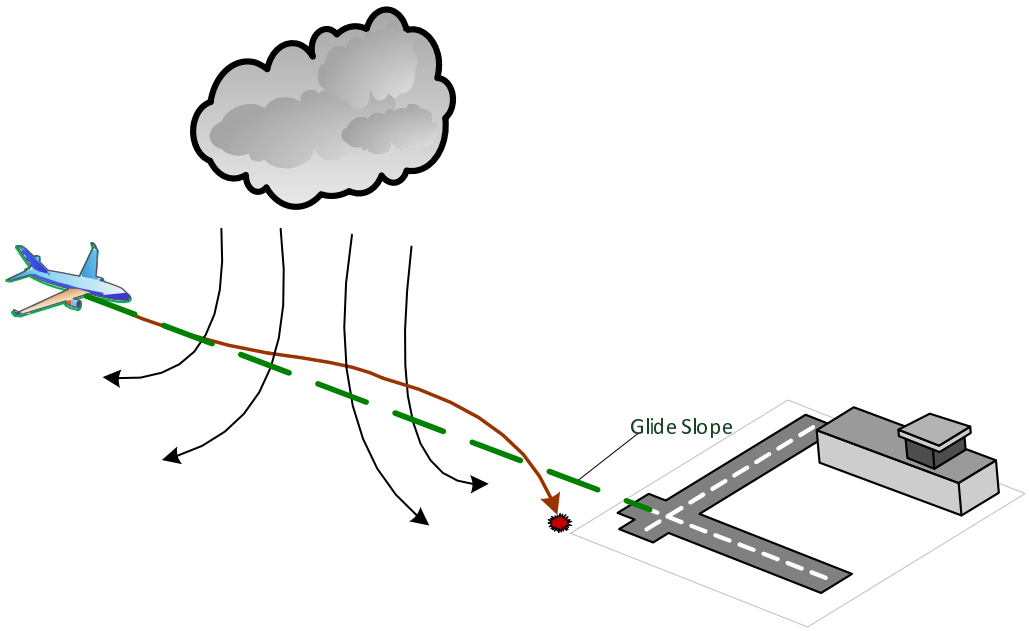

Figure 2-11: Effect of wind shear on aircraft trajectory.

The relatively low operating speed of small fixed-wing airplanes, such as those explored in our work, makes them particularly affected by the wind field in all phases of flight. The aerodynamic forces produced by their wings are strongly dependent on relative wind, based on the aerodynamic knowledge gained in the previous section. The latter varies with the moving atmosphere resulting in an imbalance between the forces of flight and, thereby, an uncontrolled airplane behavior. Moreover, if lift decreases abruptly due to adverse wind, drag becomes the principal component of the aerodynamic force and stall may occur.

2.4.3 Incorporating the wind in the equations of motion

The previous subsection has provided intuitive aspects of the effect of a moving atmosphere on the aircraft performance. In order to continue to describe accurately the behavior of the vehicle when flying in such conditions, the mathematical model needs to be modified so that the wind will be incorporated in the equations of motion. This requirement is due to the fact that the relative motion of the aircraft with respect to the air mass is affected by wind and, thereby, the aerodynamic forces and moments acting on the vehicle. It is therefore necessary to determine how the velocity of the atmosphere results in aerodynamic forces and moments.

To begin with, note that both longitudinal and lateral airplane dynamics are sensitive to wind perturbations. Mainly, the surrounding wind provides variations in the lift force but, given its predominantly horizontal movement relative to the Earth, it may produce as well a lateral force which tends to affect the directional stability of the airplane. Therefore, the wind velocities along the three axis of the body-fixed reference frame must be considered.

The mean component of the wind vector affects the navigation of an aircraft by differentiating the velocity of the vehicle with respect to the air from its velocity with respect to the ground. The relation of the velocities can be expressed as

$$\mathrm{V}_g = \mathrm{V}_a + \mathrm{W} \tag{2.12}$$

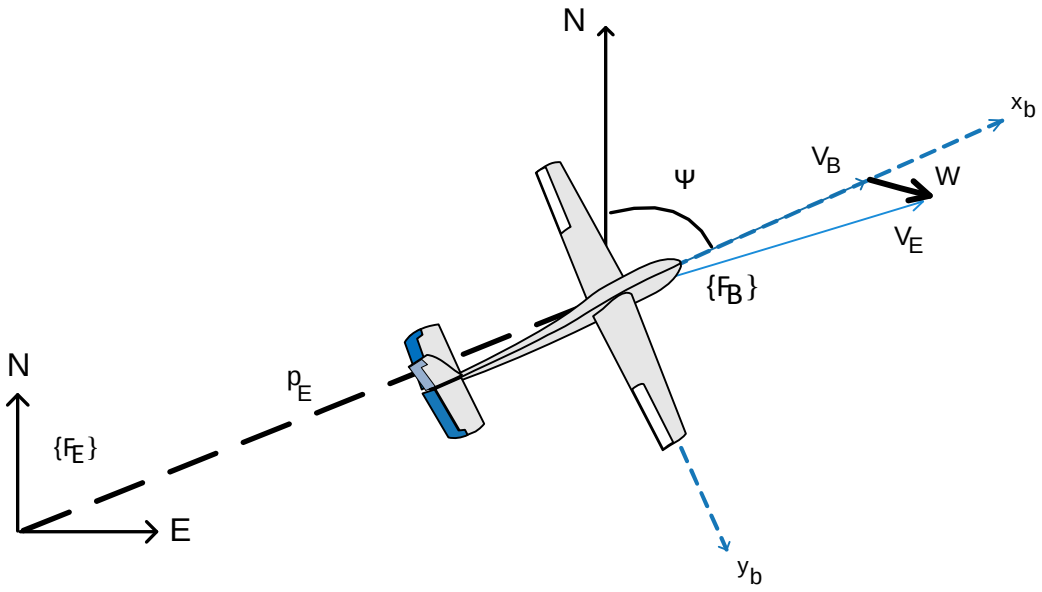

Figure 2-12: The velocities affecting the navigation of an airplane.

where V_g is the aircraft velocity relative to the ground, V_a represents the air-relative aircraft velocity and W is the velocity of the wind with respect to the ground.

For convenience, V_g and W from the above expression are expressed in the inertial reference frame. In terms of V_a, there is no direct measurement of the airspeed from a ground position and this is computed by using sensors placed on board. Consequently, its components are expressed in the direction of the body-fixed reference frame axes, F_B. Thus, it yields

$$\mathrm{V}_g^e = R_{EB}\mathrm{V}_a^b + \mathrm{W}^e$$

where the superscript refers to the frame of reference in which the vector is expressed with e denoting the inertial frame and b representing the body frame.

Therefore, the rate of change of the airplane translational position when the atmosphere is moving relative to the Earth is expressed in the Earth-fixed coordinate system, F_E, as

$$\dot{p}_E^e = \mathrm{V}_g^e = R_{EB}\mathrm{V}_a^b + \mathrm{W}^e$$

where p_E^e is the position of the vehicle in F_E. Figure $2-12$ show a geometrical representation of the velocities affecting the inertial track of the airplane.

Remember that $p_E^e = [p_n\ p_e\ p_h]^T$, $\mathrm{V}_a^b = [u\ v\ w]^T$ and $\mathrm{W}^e = [\mathrm{w}_n\ \mathrm{w}_e\ \mathrm{w}_h]^T$. With the latter, the position of the aircraft relative to inertial space is computed from

$$\begin{aligned}
\dot{p}_n &= u\cos\theta\cos\psi + v\left(\sin\phi\sin\theta\cos\psi - \cos\phi\sin\psi\right) \\
&\quad + w\left(\cos\phi\sin\theta\cos\psi + \sin\phi\sin\psi\right) + \mathrm{w}_n \\
\dot{p}_e &= u\cos\theta\sin\psi + v\left(\sin\phi\sin\theta\sin\psi + \cos\phi\cos\psi\right) \\
&\quad + w\left(\cos\phi\sin\theta\sin\psi - \sin\phi\cos\psi\right) + \mathrm{w}_e \\
\dot{p}_h &= -u\sin\theta + v\sin\psi\cos\theta + w\cos\psi\cos\theta + \mathrm{w}_h
\end{aligned}$$

Note also that V_g, rather than V_B, must be used in the force equation (2.5c). Let us denote the components of the ground velocity vector in the body frame by $\mathrm{V}_g^b = [u_g\ v_g\ w_g]^T$. From (2.12), we get

$$\begin{aligned}
u_g &= u + u_w \\
v_g &= v + v_w \\
w_g &= w + w_w
\end{aligned}$$

where $(u_w,\, v_w,\, w_w)$ represent the wind components in the body-fixed reference frame. The force equations of motion described in (2.9) become

$$\begin{aligned}
\frac{X_a + T}{m} &= \dot{u}_g + qw_g - rv_g + g_0\sin\theta \\
\frac{Y_a}{m} &= \dot{v}_g + ru_g - pw_g - g_0\cos\theta\sin\phi \\
\frac{Z_a}{m} &= \dot{w}_g + pv_g - qu_g - g_0\cos\theta\cos\phi
\end{aligned}$$

Using the fact that $\dot{\mathrm{V}}_g^b = \dot{\mathrm{V}}_a^b + \dot{\mathrm{W}}^b$ in the above equations, it yields

$$\dot{u} = \frac{X_a + T}{m} - qw_g + rv_g - g_0\sin\theta - \dot{u}_w \tag{2.13a}$$

$$\dot{v} = \frac{Y_a}{m} - ru_g + pw_g + g_0\cos\theta\sin\phi - \dot{v}_w \tag{2.13b}$$

$$\dot{w} = \frac{Z_a}{m} - pv_g + qu_g + g_0\cos\theta\cos\phi - \dot{w}_w \tag{2.13c}$$

The aerodynamic forces and moments acting on the vehicle are dependent mainly on V_a, α and β. The values of these quantities are computed based on u, v and w from (2.13) affected by the wind vector through $\dot{u}_w$, $\dot{v}_w$ and $\dot{w}_w$. Note that the vector of wind accelerations in this equation is given in the body-fixed axes while the wind velocities in (2.12) are given in the inertial coordinate system.

2.5 Reduced-order aircraft nonlinear models

This section focuses on deriving simplified airplane models which are appropriate for control design, so that autonomous flight can be easier achieved, while capturing the essential behavior of the system. The models derived here will be the basis for analysis, simulation, and control design that will be discussed in chapters 3 and 4. The material in this section addresses the flight in both horizontal and vertical plane. For this reason, this section discusses first the equations decoupling problem. Then, the dynamics of a coordinated flight are introduced.

2.5.1 Decoupling the equations

The equations of motion can be separated into a longitudinal and a lateral-directional set which, under certain assumptions, become independent solutions of the airplane dynamics. The longitudinal variables are represented by the position, velocity, angle, and angular rate in the vertical plane and they are denoted by p_n, p_h, u, w, θ and q. The lateral directional vector is also composed of six variables representing the position, velocity, angle, and angular rate out of the vertical plane and they are denoted by p_e, v, ϕ, ψ, p and r.

Generally, the two sets of equations are coupled. However, variations of the longitudinal variables do not induce lateral-directional motions for the case of a symmetric aircraft [52]. On the other hand, lateral-directional perturbations do induce longitudinal motions. For example, as the aircraft begins to roll, it starts to lose lift and, thereby, altitude.

Longitudinal variables

Restricting the flight path to the vertical plane by setting the lateral-directional motions to zero ($X_{lat} = 0; \dot{X}_{lat} = 0$), the longitudinal equations reduce to

$$\begin{aligned}
\dot{p}_n &= u\cos\theta + w\sin\theta \\
\dot{p}_e &= -u\sin\theta + w\cos\theta \\
\dot{\theta} &= q \\
\dot{u} &= \frac{X_b}{m} - g\sin\theta - qw \\
\dot{w} &= \frac{Z_b}{m} + g\cos\theta + qu \\
\dot{q} &= \frac{M}{I_{yy}}
\end{aligned}$$

The above equations can be further transformed by replacing the body components of the velocity (u, w) by polar inertial components (V, γ) and by expressing the forces in the wind axes direction, (T, D, L) instead of (X_b, Z_b). In addition, neglecting the range and the altitude and replacing the pitch angle by the angle of attack from the relationship $\alpha = \theta - \gamma$, it yields

$$\begin{aligned}
\dot{V} &= \frac{1}{m}\left[T\cos\alpha - D - mg\sin\gamma\right] \\
\dot{\gamma} &= \frac{1}{mV}\left[T\sin\alpha + L - mg\cos\gamma\right] \\
\dot{q} &= \frac{M}{I_{yy}} \\
\dot{\alpha} &= \dot{\theta} - \dot{\gamma} = q - \frac{1}{mV}\left[T\sin\alpha + L - mg\cos\gamma\right]
\end{aligned}$$

Lateral-directional variables

Also, we can restrict the flight path to steady, level longitudinal flight by specifying nominal airspeed (V_{a_N}), altitude (p_{h_N}) and constant longitudinal variables ($q_N = 0$, $\gamma_N = 0$, $\theta_N = \alpha_N \simeq 0$, $w_N = 0$).

Therefore, we get the reduced lateral-directional equations

$$\begin{aligned}
\dot{p}_e &= u_N \sin\psi + v\cos\phi\cos\psi \\
\dot{\psi} &= r\cos\phi \\
\dot{\phi} &= p \\
\dot{v} &= \frac{Y_b}{m} + g\sin\phi - ru_N \\
\dot{p} &= \frac{I_{zz}\bar{L} + I_{xz}N}{I_{xx}I_{zz} - I_{xz}^2} \\
\dot{r} &= \frac{I_{xz}\bar{L} + I_{xx}N}{I_{xx}I_{zz} - I_{xz}^2}
\end{aligned}$$

It is evident that the equations will be considerably simplified if the bank angle is zero since it leads to decoupling the equations of motion and the aircraft model can be approximated by two independent lower order systems. If $\phi \simeq 0$ then there is no lateral force in the body axes and no roll rate or moment. Moreover, considering a symmetrical airplane with the propulsion system placed in the direction of its body, it can then be considered, without loss of generality, that V is acting only in the x-axis. Hence, the following expressions can be stated

$$\begin{aligned}
v &\ll 1 \\
u &\simeq V
\end{aligned}$$

and, introducing the wind wind parameters, it yields

$$\begin{aligned}
\dot{p}_e &= V\sin\psi + W\sin\psi_w \\
\dot{\psi} &= r \\
\dot{r} &= N
\end{aligned}$$

There are two lateral steady states that are of interest, namely the steady sideslip and the steady turn. In steady sideslip, the flight path is rectilinear and this motion is used to correct for cross-wind on landing approaches. During a steady turn the

vehicle angular velocity vector ω is constant and vertical and the resultant of gravity and centrifugal force at the mass center lies in the plane of symmetry [17]. The equation describing a steady turn is

$$\dot{\psi} = \frac{g}{V} \tan \phi$$

2.6 Chapter summary

This chapter presents the theoretical aspects of a nonlinear model derivation for a fixed-wing aircraft flying in a moving atmosphere. Developing autonomous operating aerial devices requires first a good understanding of the principles of flight theory. For this reason, the component parts of an aircraft of conventional shape have been presented and the forces that act on an aircraft in flight have been briefly introduced. Nevertheless, since the lift is the force that makes the flight possible, a more detailed explanation of how this force is created has been provided, along with two misleading theories which have been taught for many years in most flight training manuals.

Moreover, airplane dynamics require transformations between several frames of reference. In order to describe the relative orientation of the vehicle, three coordinate systems have been presented and the rotation matrices, used to transform coordinates from one frame to another, have been derived in terms of Euler angles or angles of attack and sideslip. Based on all information gathered, the equations of motion of a rigid body aircraft have been extended in terms of vector components and two alternatives have been presented for both navigation and force equations, the choice being a matter of convenience.

Further, an analysis of how a moving atmosphere affects the dynamics of flight has been provided and two models of wind and atmospheric turbulence have been presented. Finally, the mathematical model of the airplane has been extended so that the effects of the wind on the aircraft performance were incorporated. Simplified airplane models capturing the essential behavior of the system have been presented in order to achieve autonomous flight.

Chapter 3

Lyapunov-based flight guidance control

In this chapter we address the guidance problem of autonomous air vehicles in order to follow an inertial trajectory when flying in other than calm conditions. An application of light fixed-wing Unmanned Aerial Vehicles (UAVs) that consists in following straight-line paths between geo-referenced waypoints is first formulated and the dynamic of the cross track error with respect to such trajectory is further obtained from the lateral airplane equations of motion. The control strategy is designed in the framework of Lyapunov theory in order to minimize the error position of the airplane relative to the desired path.

3.1 Problem statement

A crucial requirement for the autonomous flight control system of the aerial vehicles is the ability to fly in a commanded fashion so that the UAV to be in a particular location at a prespecified time. This capability requires the simultaneous solving of two basic issues in aerial navigation: path planning and trajectory tracking. While the first concern refers to generating a reference path, the second deals with guiding the vehicle towards a constantly moving position with a specified progression rate. In addition, in order to increase their usefulness, small fixed-wing UAVs also need

to account for wind since they fly constantly at low speed and they are significantly sensitive to the surrounding air.

3.1.1 General description of the problem

Flying in complex environments, i.e. in presence of wind as considered in our analysis, makes the trajectory tracking a challenging problem [1, 2] since this perturbation directly affects some important variables of airplane navigation: airspeed and course. Therefore, rather than tracking the trajectory, this work addresses the problem of steering the airplane along a geometric path without any temporal requirement. Moreover, the main purpose of this study is to offer path following capabilities in windy conditions, therefore a reasonable flight path is considered available and just the problem of path following will be addressed. A simplified geometrical description of the problem is shown in Figure 3-1.

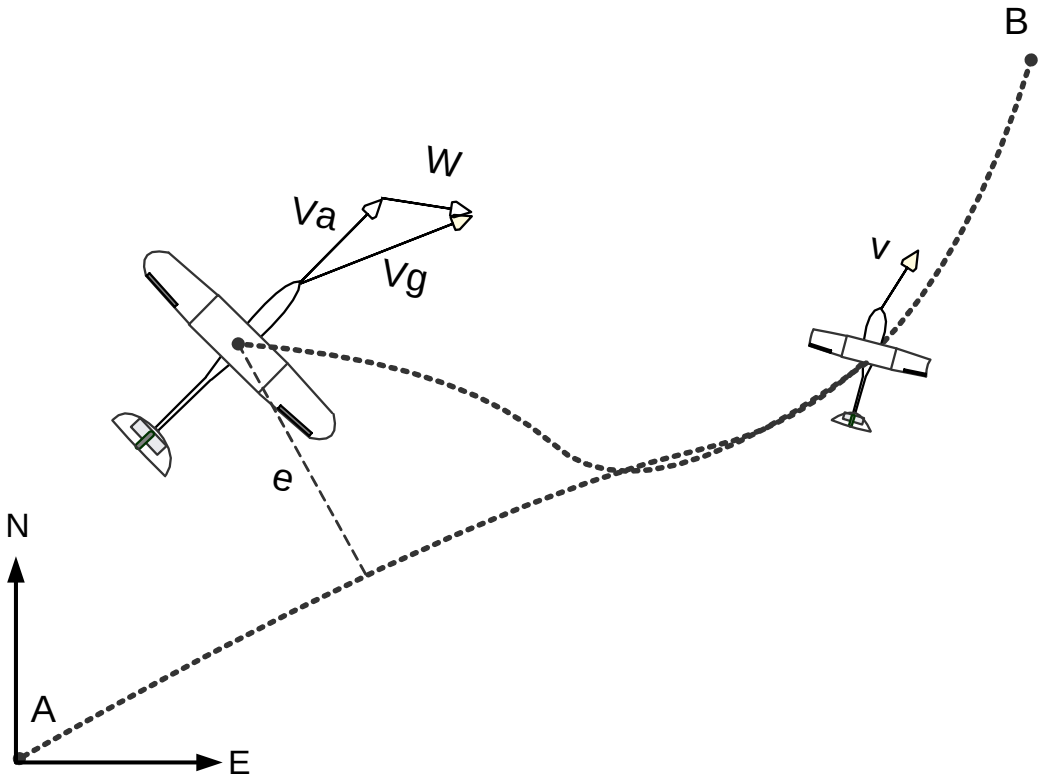

Figure 3-1: Path following formulation problem

If there is a difference, d, between the real position of the airplane and the reference position generated by the path planner controller, then a corrective action, u_d, is required in order to compensate for d. The feedback control is enabled until the airplane position and the reference path overlap.

3.1.2 Previous work on path following

Traditionally, the problem of path following has been addressed by considering two approaches. First design involves the complete dynamics of the vehicle which is stabilized by means of well established control strategies. A typical example of this methodology is the use of the linear control theory by employing approximate linearized models to describe the aircraft dynamics. Further, Proportional and Derivative (PD) controllers are usually developed to generate the lateral acceleration required to follow a desired path. Nevertheless, in real conditions the wind may affect the plant to fly outside the set of the operating points, making the system to describe the behavior of the airplane inaccurately.

A solution to this problem is the interpolation between several operating regions and local stabilizing controllers in the framework of gain scheduling control theory. General features of gain scheduling design do not restrict the system to remain close to a single equilibrium but the controller performs well for slowly varying signals [5, 6]. An example of gain scheduling based trajectory tracking controller for an autonomous underwater vehicle is presented in [7]. In terms of applications in flight control, the airspeed and the altitude are the prevailing scheduling variables used to parameterize the operating points. Consequently, gain scheduled controllers usually guarantee the stability only for low angular rates and low angles of attack [8, 9].

In certain situations the aerial vehicles are required to perform aggressive maneuvers outside of the linear region of the flight dynamics, thus, the need for nonlinear control tools arises. The drawback of a nonlinear flight controller over a linear one is that it involves high on-line computational complexity [10]. Hence, given the limited payload capacity of light UAVs, it is essential for the flight controller to have low complexity. This requirement is usually fulfilled by using the time-scale separation

criteria in order to divide the flight control problem into an inner and an outer loop; the former is designed to ensure the stability of the vehicle whereas the latter guides the vehicle along the trajectory. This methodology is referred to as the second typical approach to the path following problem.

Following this approach, many solutions have been developed taking advantage of the autopilots that are normally installed on board UAVs in order to ensure the internal stability of the vehicle and proposing guidance strategies based on Line-of-Sight (LOS) design [11, 12, 13], Lyapunov theory [14], vector fields [1, 15], etc. In [12] a LOS inspired nonlinear guidance logic is presented for tight tracking of curved trajectories. The approach approximates PD control for straight-line paths and an additional anticipatory control element that improves the tracking capability is implemented for curved paths. The guidance logic accounts for wind by focusing on the ground track of the UAV, the same strategy being considered also in [14, 1, 16]. However, in practice this information is given from GPS feedback signals which are usually delayed, have low rate and questionable accuracy. Moreover, the reflective choice of the visibility distance in LOS strategy demands high computational power and local adjustments for changes in either the speed or the direction of the wind.

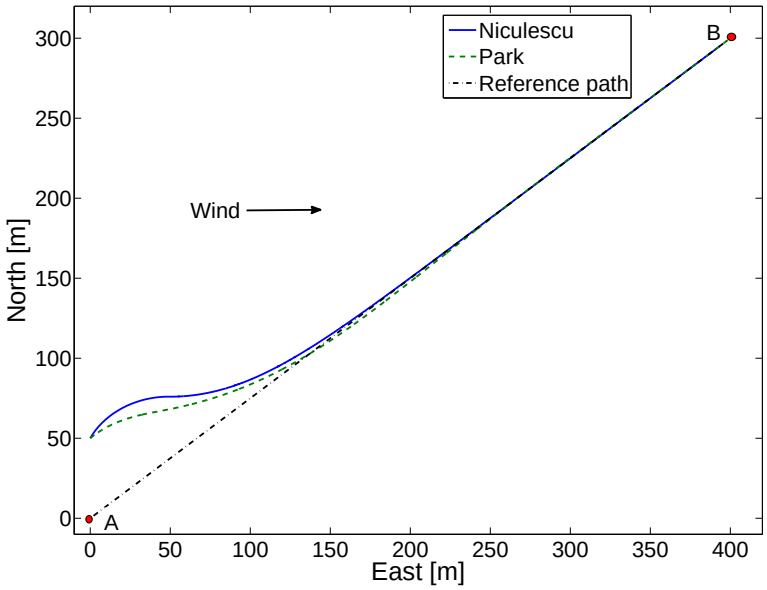

Figure 3-2: LOS inspired path following controllers

3.2 Modeling for control

Building on the time-scale separation approach, our analysis proposes an inner-outer control structure taking advantage of the fact that the outer kinematic loop is designed separately from the internal vehicle dynamics. Stated intuitively, the guidance loop first generates a commanded attitude of the aircraft based on the position error derived at a kinematic level and then the inner dynamic loop uses deflections of the flight control surfaces in order to achieve the commanded attitude.

For the sake of clarity, only the guidance control loop will be discussed in this chapter. In addition, it is assumed that the vehicle flies in two dimensions (in the horizontal plane) and thus, only the lateral equations of motion are of primary interest. It follows that the longitudinal variables of the airplane (airspeed, pitch and flight path angle) are stabilized around nominal values by means of the inner autopilot and their time derivatives can be neglected in further analysis [17].

On the basis of the above considerations, in this section we first introduce the simplified airplane model that will be used in the design of the guidance controller and then we present an application of light fixed-wing UAVs that consists in following straight-line paths between geo-referenced waypoints.

3.2.1 Translational and rotational kinematics

Corresponding to the above assumptions, the airplane motion relative to the inertial frame, as presented in Chapter 2, simplifies to

$$\dot{p}_n = V\cos\psi + W\cos\psi_\omega \tag{3.1a}$$

$$\dot{p}_e = V\sin\psi + W\sin\psi_\omega \tag{3.1b}$$

$$\dot{\psi} = \frac{g}{V}\tan\phi^c \tag{3.1c}$$

where p_n and p_e represent the inertial position of the airplane, $W\cos\psi_\omega = W_N$, $W\sin\psi_\omega = W_E$, W is the wind velocity and ψ_ω describes the wind direction and ϕ^c stands for the commanded bank angle.

The motion of the airplane governed by equations (3.1) corresponds to a truly banked turn maneuver in which both rudder and ailerons are used to change the aircraft heading. First, the ailerons are used to bank the airplane to one side, which produces a side component of the lift force. The rudder is used to provide corrections for unwanted motions such as adverse yaw, and to coordinate the turn. If turning at large bank angles, the elevator must also be used to provide more lift needed to balance the gravity. Consequently, the airplane flies in a circular arc. Further, the inner autopilot of the airplane implements a bank-hold loop whose dynamics is described by the differential equation

$$\dot{\phi} = k_{\phi} \left(\phi^{c} - \phi \right) \tag{3.2}$$

where k_{ϕ} is a positive constant and its value depends on the structure of the inner control loop.

Stated in the form of equations (3.1), the airplane kinematic model can be used to formulate the following control problem of a certain paths, i.e. straight-line trajectories aligned with one of the inertial frame axes. In this particular case, equations $(3.1a)$ or $(3.1b)$ supply the cross track error velocity equation and the guidance problem to be solved simplifies to commanding the bank angle, ϕ^{c}, required for the airplane to change its direction in order to minimize p_n or p_e.

3.2.2 Motion relative to a straight-line path

In the previous subsection, the simplified aircraft equations of motion in the direction of the inertial frame axes were used to formulate the path following problem in terms of a state vector and a control input. Nevertheless, the airplane may be required to follow paths which are not aligned with any of these axes. Consequently, the main purpose of this subsection is to express the motion of the airplane relative to a straight-line path of given orientation.

To this end, let us consider the segment line defined by the points (A, B) and the orientation ψ_s in Figure $3-3$. In order to obtain the motion of the airplane relative

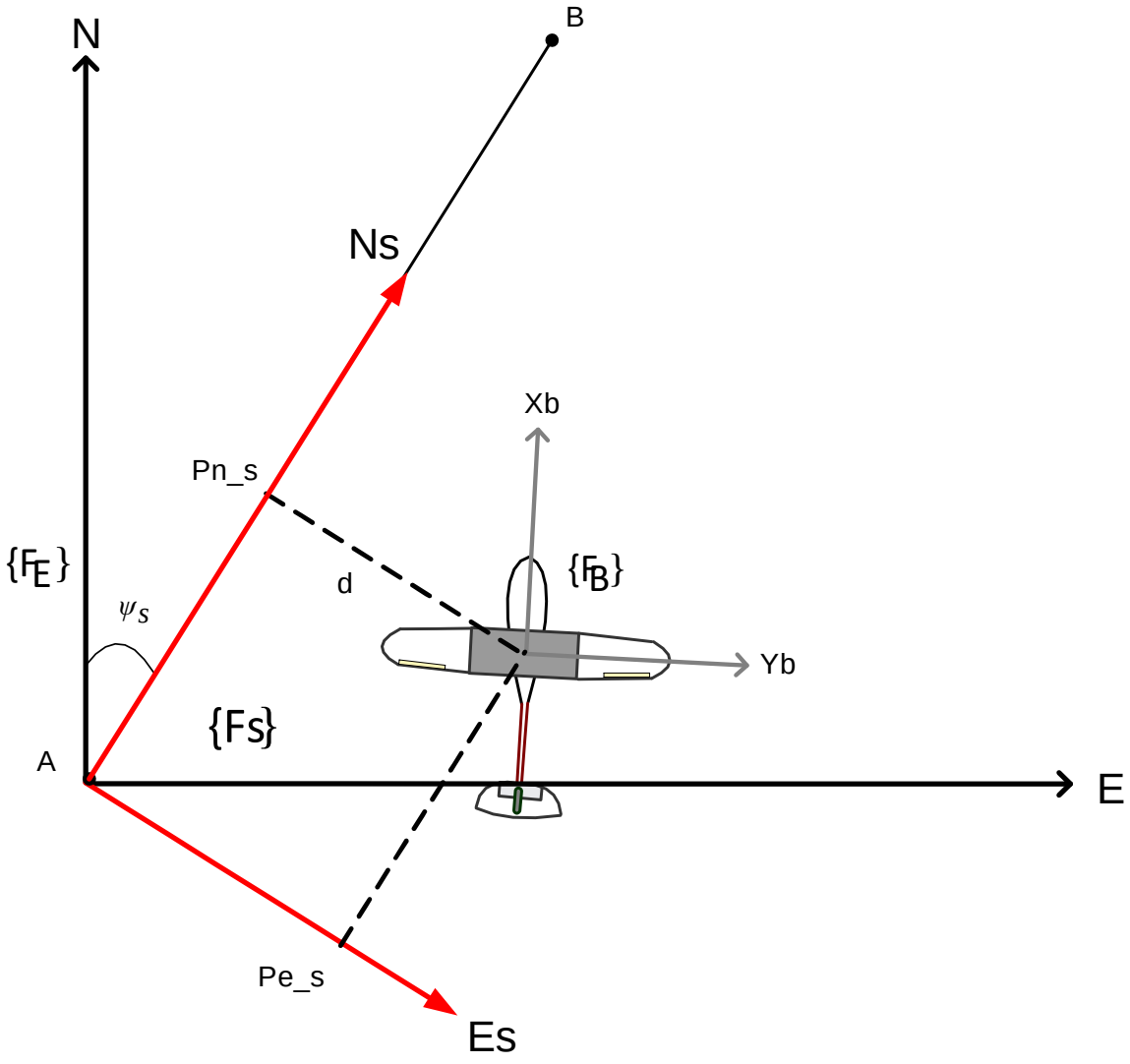

Figure 3-3: Airplane motion relative to a straight-line path

to such a path, it is appropriate to introduce a reference frame which has one of its axis aligned with the line-segment itself while the other is chosen to define a clockwise rotation of the inertial frame, represented by F_E, through angle ψ_s. The new reference frame is highlighted by the red color in the figure above and it is denoted by F_S.

The coordinates of the velocity vector, expressed in the rotated frame, are given by the rotation matrix $R(\psi_s)$ as it follows

$$\begin{bmatrix} \dot{p}_{ns} \\ \dot{p}_{es} \end{bmatrix} = R_E^S(\psi_s) \begin{bmatrix} \dot{p}_n \\ \dot{p}_e \end{bmatrix} \tag{3.3}$$

where

$$R_E^S(\psi_s) = \begin{pmatrix} \cos\psi_s & \sin\psi_s \\ -\sin\psi_s & \cos\psi_s \end{pmatrix}$$

represents the rotation from F_E to F_S and p_{ns} and p_{es} are the components of the airplane position in the segment frame.

The motion of the airplane with respect to a stationary desired straight-line path of angle ψ_s can then be expressed from equations (3.1) and (3.3) as

$$\dot{p}_{ns} = V\cos(\psi - \psi_s) + W\cos(\psi_\omega - \psi_s) \tag{3.4a}$$

$$\dot{p}_{es} = V\sin(\psi - \psi_s) + W\sin(\psi_\omega - \psi_s) \tag{3.4b}$$

Equations (3.4) can be used to formulate the following problem of straight-line segments of any given orientation as the one plotted in Figure $3-3$. In this case, the control objective is the regulation of p_{ns} or p_{es} by commanding the ϕ^c bank angle, which corresponds to non-zero inertial coordinates of the airplane position.

3.2.3 Following multiple segments

In this subsection we aim to extend the above results to the case of multiple segments following. Comparing to the others scenarios, this case has the particularity to contain segments that are translated from the origin of the inertial frame, as it will be highlighted in the following lines.

First, let us introduce the inertial path (C) denoted by dotted line in Figure $3-4$. In order to minimize the airplane position error relative to the reference trajectory, one can use the assumption that every smooth path can be divided into a series of successive straight-line segments. Therefore, the path (C) can been discretized by a series of three successive segments, as shown in the figure, in order to facilitate the formulation of the following control problem.

Therefore, F_S is preferred, rather than F_E, to define the aircraft kinematics, since it allows to formulate the path following problem as a regulation problem. As depicted in the geometrical representation from Figure $3-4$, following the segment line AB

by the airplane is equivalent to driving to zero the conveniently defined cross track error Pe_s while Pn_s moves along the segment, where Pe_s and Pn_s are defined in F_S.

Since the airplane position is usually measured in the inertial frame, a transformation of the position vector to the segment frame is necessary. Therefore, for a complete transformation from F_E to F_S, a translation is performed first and then a rotation.

$$\begin{bmatrix} p_{ns} \\ p_{es} \end{bmatrix} = R_E^S(\psi_s) \begin{bmatrix} p_n - WP_{1n} \\ p_e - WP_{1e} \end{bmatrix}$$

where WP_{1n} and WP_{1e} represent the position of the start point of the segment. On the other hand, first a rotation and then a translation is needed when passing a position vector from F_S to F_E

$$\begin{bmatrix} p_n \\ p_e \end{bmatrix} = R_S^E(\psi_s) \begin{bmatrix} p_{ns} \\ p_{es} \end{bmatrix} + \begin{bmatrix} WP_{1n} \\ WP_{1e} \end{bmatrix}$$

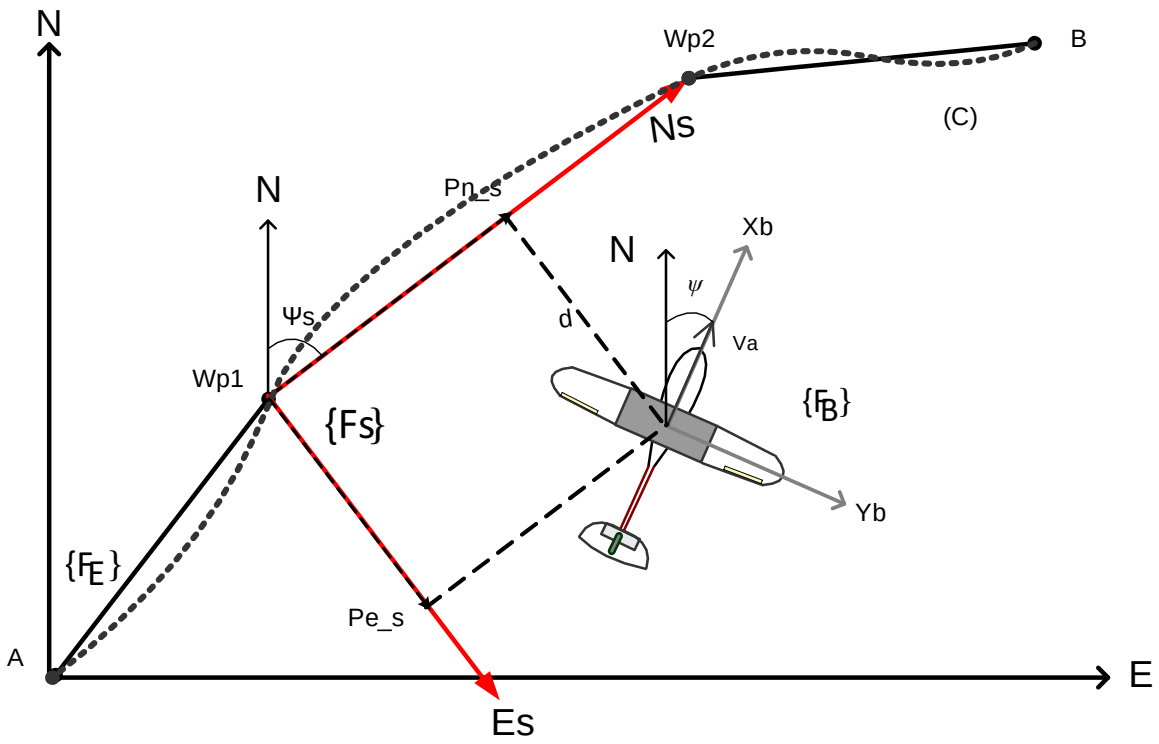

Figure 3-4: Frames of reference

Notice from Eq. (3.4) that the deviation from the desired trajectory, parameterized by its orientation ψ_s, depends on the airplane velocity and on the wind parameters. Thus, without loss of generality, the airplane equations for multiple straight-line path following purpose can be defined as

$$\dot{d} \equiv \dot{p}_{es} = V \sin(\psi - \psi_s) + W \sin(\psi_\omega - \psi_s) \tag{3.5a}$$

$$\dot{\psi} = \frac{g}{V} \tan\phi \tag{3.5b}$$

$$\dot{\phi} = k_\phi (\phi^c - \phi) \tag{3.5c}$$

3.3 Lyapunov stability theory

Lyapunov theory offers some of the most useful tools for stability analysis, which is a fundamental property of any dynamical system. The difficulty in using Lyapunov based design lies in finding a different Lyapunov function for any given system, which would prove the stability of the system. However, the *backstepping* procedure allows the Lyapunov function to be constructed successively, along with the control law. For these reasons, this section first introduces fundamentals of Lyapunov theory and then it explains the main concepts of the backstepping control design with the aim of obtaining airplane path following capabilities.

3.3.1 Basic definitions and main stability theorems

The most important property of any dynamical system is related to its stability. For this purpose, Lyapunov theory contains a collection of results that are widely used for studying the stability properties of nonlinear systems. In order to define the guidance problem in the sense of Lyapunov, let us review the most basic concepts of this theory in terms of autonomous[1] systems, as they are stated in [3, 4, 10].

As for the case of aircraft guidance control, many stability problems are related to the stability around the equilibrium points. In Lyapunov theory, usually the stability

[1]Nonlinear systems are traditionally classified as either *autonomous* or *non-autonomous*, depending whether the system depends or not on time [10].

of such points is characterized. First, consider the autonomous system

$$\dot{x} = f(x) \tag{3.6}$$

where x is the state vector and f is a nonlinear vector function. Let $x = x_e$ be an equilibrium of the system, that is $f(x_e) = 0$.

Definition 3.1. The equilibrium point $x = x_e$ of (3.6) is

1. stable if for each $\epsilon > 0$ there is $\delta = \delta(\epsilon) > 0$ such that

$$\|x(0)\| < \delta \Rightarrow \|x(t)\| < \epsilon, \forall t \geq 0$$

2. unstable if it is not stable

3. asymptotically stable if it is stable and δ can be chosen such that

$$\|x(0) - x_e\| < \delta \Rightarrow \lim_{t\to\infty} x(t) = x_e$$

4. globally asymptotically stable (GAS) if it is asymptotically stable for all initial states, that is, if

$$\lim_{t\to\infty} x(t) = x_e, \forall x(0)$$

The stability of an equilibrium point being defined, the next challenge is to find ways to determine the stability for a particular system. As a solution to this problem, the mathematician Lyapunov showed that the stability of a system can be examined by studying a single appropriate scalar function $V(x)$ and its time derivative along the trajectories of (3.6). This idea is nothing else then a fundamental physical observation, namely that if the total energy of a mechanical (or electrical) system is continuously dissipated, then the system, whether linear or nonlinear, must eventually settle down to an equilibrium point [10]. Let us introduce first a useful theoretical background for Lyapunov's stability theorem to be stated.

Definition 3.2. A scalar function $V(x)$ is

1. positive definite if $V(0) = 0$ and $V(x) > 0, x \neq 0$
2. positive semidefinite if $V(0) = 0$ and $V(x) \geq 0, x \neq 0$
3. negative (semi-)definite if $-V(x)$ is positive (semi-)definite
4. radially unbounded if $V(x) \to \infty$ as $\|x\| \to \infty$

Definition 3.3. A continuously differentiable positive definite function $V(x)$ for which $\dot{V}(x)$ is negative semidefinite is called a Lyapunov function.

Based on the terminology introduced by the above definitions, the stability of an equilibrium point in the sense of Lyapunov can be determined by the use of the following theorem (Theorem 4.1 from [4])

Theorem 3.1. *(Lyapunov's stability theorem). Let $x = 0$ be an equilibrium point for (3.6) and $D \subset R^n$ be a domain containing $x = 0$. Let $V : D \to R$ be a Lyapunov function. Then, $x = 0$ is stable. Moreover, if $\dot{V}(x)$ is negative definite then the origin is asymptotically stable.*

The above theorem is concerned with establishing the stability or asymptotic stability of an equilibrium point but it can not be used to prove that the equilibrium is unstable. Moreover, if the origin is asymptotically stable, no conclusion can be drawn using this theorem if the point is whether or not GAS, that is for any initial state x the trajectory approaches the origin as $t \to \infty$, no matter how large $\|x\|$ is. In order to ensure the global asymptotic stability, any point x from the whole space R^n should be included in the interior of bounded set Ω_c. For this constraint to be satisfied, we need the conditions of the Theorem [3.1, p. 50] to hold globally, that is $D = R^n$, and the Lyapunov function to be radially unbounded, that is

$$V(x) \to \infty \quad as \quad \|x\| \to \infty \tag{3.7}$$

Theorem 3.2. *(Barbashin-Krasovskii theorem, Theorem 4.2 from [4]). Let $x = 0$ be an equilibrium point for (3.6). Let $V : R^n \to R^n$ be a positive definite, radially unbounded, continuously differentiable function such that*

$$\dot{V}(x) < 0, \forall x \neq 0$$

then $x = 0$ is globally asymptotically stable.

A system possessing a global asymptotically stable origin $x = 0$ has a unique equilibrium point which is x. In some cases, the (global) asymptotic stability of the equilibrium point can be determined when $\dot{V}(x)$ is only negative semidefinite with the help of the powerful invariant set theorems attributed to LaSalle[2] (Corollary 4.1 and 4.2 from [4]).

Theorem 3.3. *(Local invariant set theorem). Let $x = 0$ be an equilibrium point for (3.6). Let $V : D \to R$ be a continuously differentiable positive definite function on a domain D containing the origin $x = 0$, such that $\dot{V}(x) \leq 0$ in D. Let $S = \{x \in D | \dot{V}(x) = 0\}$ and suppose that no solution can stay identically in S, other than the trivial solution $x(t) \equiv 0$. Then, the origin is asymptotically stable.*

Theorem 3.4. *(Global invariant set theorem). Let $x = 0$ be an equilibrium point for (3.6). Let $V : R^n \to R^n$ be a continuously differentiable, radially unbounded, positive definite function such that $\dot{V}(x) \leq 0$ for all $x \in R^n$. Let $S = \{x \in R^n | \dot{V}(x) = 0\}$ and suppose that no solution can stay identically in S, other than the trivial solution $x(t) \equiv 0$. Then, the origin is globally asymptotically stable.*

The above definitions and theorems can be used in order to analyze the stability properties of a given system. However, if we are interested in creating closed loop systems with asymptotically stable equilibrium points, then control design using Lyapunov theory should be employed. In order to illustrate this idea, let us consider the

[2]Theorems 3.3 and 3.4 are known as the theorems of Barbashin and Krasovskii, who proved them before the introduction of LaSalle's invariance principle.

autonomous system

$$\dot{x} = f(x, u), \qquad x \in R^n, \qquad u \in R, \qquad f(0, 0) = 0 \tag{3.8}$$

with the control objective being the design of a control law $u = \alpha(x)$ such that the equilibrium $x = 0$ is a globally asymptotically stable point of the closed-loop system. Lyapunov based control design refers to constructing a control law $\alpha(x)$ and a Lyapunov function $V(x)$ satisfying the conditions of the above theorems. Accordingly, let us state the following definition, which is an extension of the Lyapunov function concept ([3], Definition 2.4)

Definition 3.4. A smooth, positive definite, radially unbounded function $V : R^n \rightarrow R_+$ is called a control Lyapunov function (clf) for (3.8) if

$$\inf_{u \in R} \{ \frac{\partial V}{\partial x}(x) f(x, u) \} < 0, \qquad \forall x \neq 0$$

Further, Artstein [18] showed that the existence of a clf for a system is sufficient to prove the existence of a stabilizing control law for that system, which is equivalent to global asymptotic stability.

3.3.2 Related Lyapunov design

Backstepping

The main deficiency in applying Lyapunov theory is that there is no systematic method for finding a Lyapunov function. In addition, the control problem becomes more complicated when the real input of the system does not directly influence the state which formulates the control objective. This is illustrated by the example of the system of equations (3.5) in which the cross track error, d, is one integrator away from the control input, ϕ^c. In this case, the construction of the Lyapunov function becomes a difficult task. Moreover, finding the appropriate control law to stabilize the system represents also a complex problem which may require considerable caution.

The backstepping method solves these two tasks for a class of nonlinear systems by approaching the problem in a backward manner, constructing the control law along with a Lyapunov function. The procedure is based on the idea that a stabilizing control law and a Lyapunov function are easier to find for a scalar system. Consequently, the task of stabilizing a higher-order system is accomplished by using a recursive scalar design in which the states act as virtual controls. The deviation of the states from their real value is considered in the progressive construction of a candidate Lyapunov function. The procedure repeats until the real control input, u, could be chosen such that the candidate function becomes a control Lyapunov function, which shows that the equilibrium is GAS in view of Definition 3.4.

3.4 Lyapunov-based guidance control

The main objective of this section is to cast the airplane guidance problem in the framework of the Lyapunov theory in order to use the above tools for control design to create a closed-loop system with global asymptotically stability properties. In this context, the airplane yaw angle is of great interest since manipulating ψ leads to changes in the velocity vector direction, thus in the airplane heading direction. This motivates the development of a backstepping controller where the yaw angle can be used as a virtual control. However, before applying the backstepping procedure, let us first resume the wind correction angle technique which is a correction applied to the heading in order to counteract wind drift and maintain a desired course.

3.4.1 Wind correction angle

The wind is an important factor for the airplane performance when required to fly a constant inertial course. Indeed, any inert object with no contact with the Earth (clouds, birds, balloons, etc.) is blown along by the moving air mass. Assuming no correction is made for wind effect, the airplane will be similarly affected so that its inertial track will fall laterally of the desired course. However, airplane control systems act typically to offset this effect by determining the amount of the drift and

by heading the airplane away from the intended course accordingly. Then, the track of the airplane follows the desired course.

The correction applied to the airplane heading in order to counteract the effect of wind is called the wind correction angle (WCA) and it is expressed in terms of degrees right or left of the true course (see Figure $3-5$).

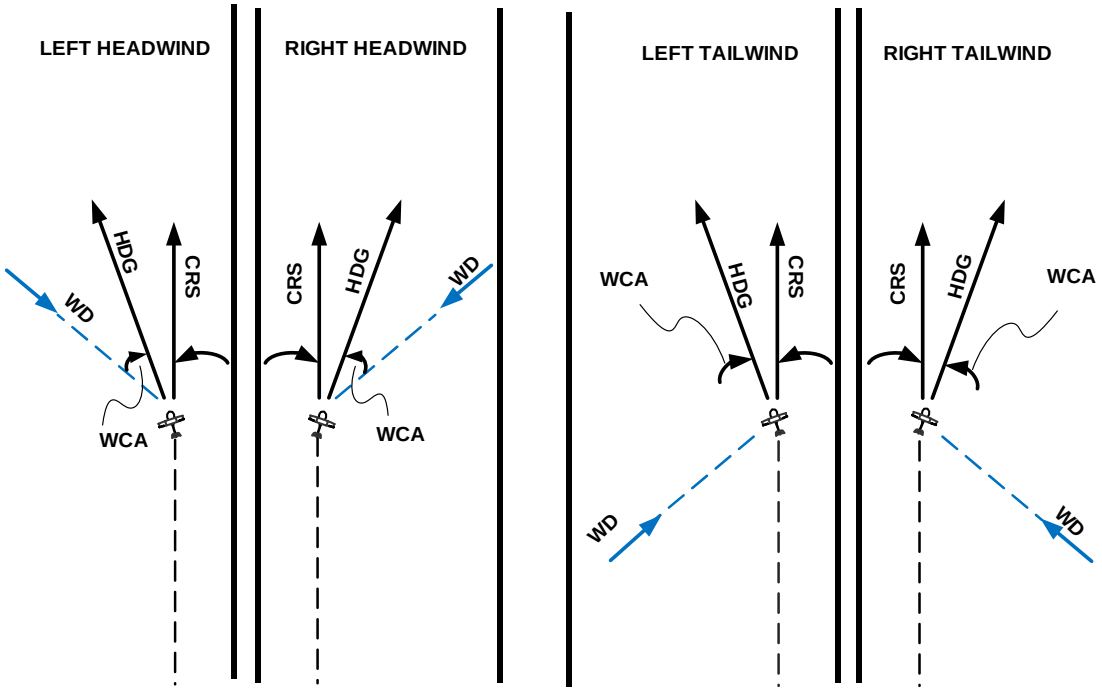

Figure 3-5: Wind correction angle definition

Based on these considerations, the control objective of the path following problem introduced in section 3.2.3 by equations (3.5), is twofold:

1. $d \to 0$, regulation of the cross track error

2. $\psi \to \psi_s \pm WCA$, convergence of the airplane heading to the intended course adding or subtracting the WCA, depending on whether the wind is on the left or on the right of the intended course

In order to meet these goals, it is worth mentioning that both the position and the orientation errors can be controlled by variations of ψ which manipulates the direction of the velocity vector. For this purpose, let us consider that the yaw angle has two

components: one will be used to minimize the position error and it is denoted by ψ_e, and the other to counteract the wind and it is represented by ψ_c, i.e.,

$$\psi = \psi_e + \psi_c \tag{3.9}$$

Consider, in a first time, the airplane aligned with the desired trajectory with the position error very small, thus, $\psi_e \approx 0$ and $d, \dot{d} \approx 0$, then it yields

$$V \sin(\psi_c - \psi_s) + W \sin(\psi_\omega - \psi_s) = 0$$

and from the above

$$\psi_c = -\arcsin\left(\frac{W \sin(\psi_\omega - \psi_s)}{V}\right) + \psi_s \tag{3.10}$$

It follows from the above that the control system must provide a heading angle equal to ψ_c given by (3.10) in order to offset the effect of the wind and to maintain alignment with a desired course ψ_s. When there is a position error relative to the reference trajectory, ψ_e, in addition to ψ_c, needs to be provided such that d from

$$\dot{d} = V \sin(\psi_e - \psi_s) \tag{3.11a}$$

$$\dot{\psi} = \frac{g}{V} \tan\phi^c \tag{3.11b}$$

to be minimized. A straightforward method to stabilize the system (3.11) is to impose a linear behavior of the airplane position by choosing the control input so that the closed loop system to act as a stable polynomial. In order to illustrate this principle, let us considerate the second derivative of d from (3.11a) with respect to time

$$\ddot{d} = g \tan\phi^c \cos(\psi_e - \psi_s)$$

Proposing

$$\phi^c = \arctan\left(\frac{-2\dot{d} - d}{g \cos(\psi_e - \psi_s)}\right) \tag{3.12}$$

where $\psi_e = \psi - \psi_c$, then, the closed-loop system becomes

$$\ddot{d} = -2\dot{d} - d$$

or $s^2 + 2s + 1 = 0$, which represents a stable polynomial.

Stability analysis

A natural choice of a Lyapunov function candidate is

$$V = \frac{1}{2}z_1^2 + \frac{1}{2}z_2^2 \tag{3.13}$$

with $z_1 = d$ and $z_2 = \dot{d}$.

Taking the derivative of V along the trajectories of the system it yields

$$\dot{V} = -2z_2^2$$

Let us study the stability of the equilibrium point at the origin. Let $D \subset R^2$ be a domain containing $z = 0$. V is a continuously differentiable, radially unbounded, positive definite function in D since $V(0) = 0$ and $V(z) > 0, z \neq 0$. In addition, the derivative of V along the trajectories of the system is negative semidefinite; it is not negative definite because $\dot{V}(z) = 0$ along the z_1 axis, that is $\dot{V}(z) = 0$ for $z_2 = 0$ irrespective of the value of z_1. Then, according to Definition [3.3, p. 50], V is a Lyapunov function and we can conclude that the origin is stable in view of Theorem [3.1, p. 50].

Let us now find $S = \{z \in D | \dot{V}(z) = 0\}$. For this purpose, note that

$$\dot{V}(z) = 0 \Rightarrow z_2 = 0$$

Thus, $S = \{z \in D | z_2 = 0\}$. Let $z(t)$ be a solution that belongs identically to S.

$$z_2(t) = 0 \Rightarrow \dot{z}_2(t) = 0 \Rightarrow \dot{d}(t), \ddot{d}(t) = 0 \Rightarrow d(t) = 0 \Rightarrow z_1(t) = 0 \tag{3.14}$$

This implies that the only solution that can stay identically in S is the trivial solution $z(t) = 0$. Thus, the origin is asymptotically stable in view of Theorem [3.3, p. 51].

Numerical simulations

This section addresses the results obtained from the simulation of three scenarios, aimed to validate the performance of the proposed controller. In all three scenarios, the value of the airplane velocity relative to the air was considered constant and set to 10 m/s, the bank angle was limited to a maximum value of $\pm 45°$ while a low-altitude/low-turbulence dryden gust model was added to simulate the environmental wind, whose components are shown in Figure $3-6$.

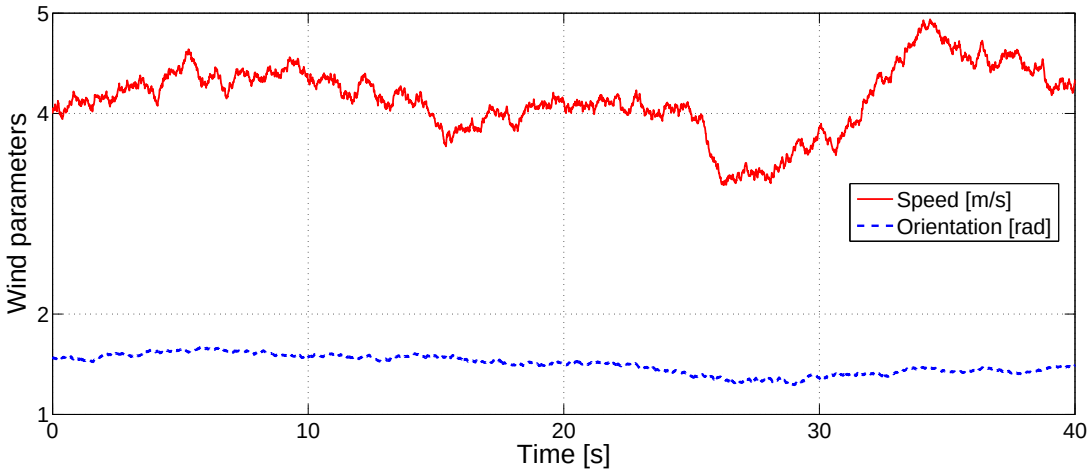

Figure 3-6: Low altitude, low turbulence Dryden Gust Model. Windspeed vs. Wind direction

A. Wind influence on inertial track

The first scenario includes a simple analysis of the open-loop nonlinear system in order to illustrate the effect of the wind on the airplane performance. Figure $3-7$ shows the behavior of the airplane when no correction is made for wind effect. Notice from this figure that the airplane advancing direction is North-East although it is headed continuously North. Hence, if the control system does not account for wind disturbances, the trajectory tracking ability of the aircraft are compromised.

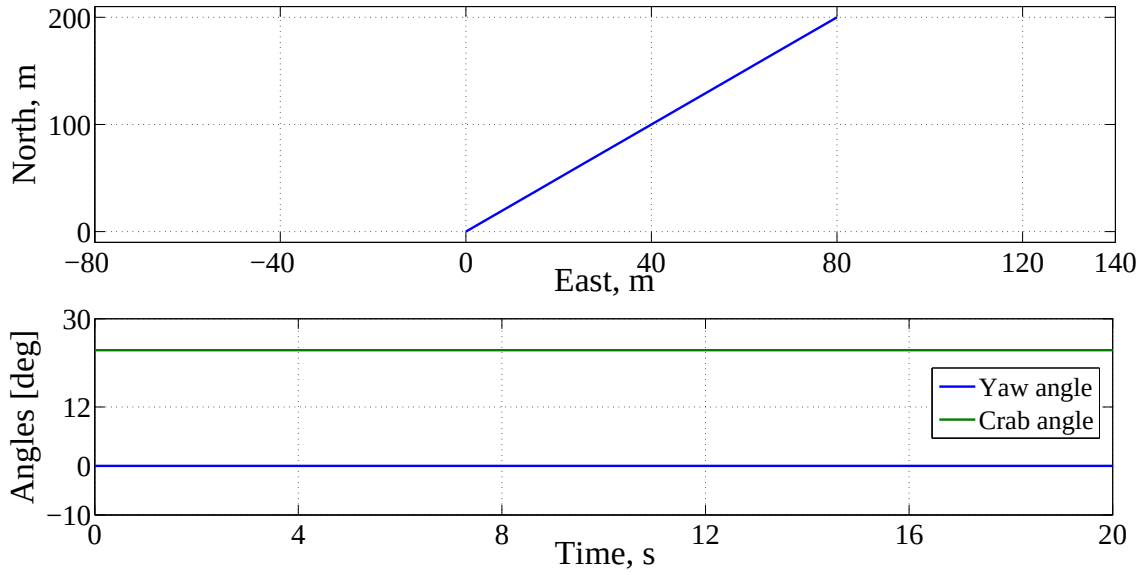

Figure 3-7: Airplane states in presence of wind

B. Wind angle computation

Further, the proposed control strategy was validated in closed-loop simulations. The airplane was commanded to follow the north direction based on the controller (3.12) without any initial path deviation. For comparative studies, a controller based on the same strategy was developed but without computing the WCA. The controller has the same form as (3.12) except the fact that it manipulates the yaw angle, ψ, so that the position and the orientation errors are controlled simultaneously.

The airplane response is shown in Figure $3-8$ based on the two similar controllers. Notice from this figure that the error corresponding to the controller developed in (3.12), plotted in blue line, is ~ 7.5 m. On the other hand, not using the knowledge of the WCA results in a larger error of ~ 13 m from the path.

C. Waypoint Guidance

Last simulations were performed to test the capabilities of the controller (3.12) to navigate between a series of predefined waypoints. For this purpose, Table 3.1 summarizes both the inertial coordinates of the points and the course to be flown, based on two neighboring waypoints. Figure $3-9$ illustrates the ground track of the airplane when commanded to fly this scenario.

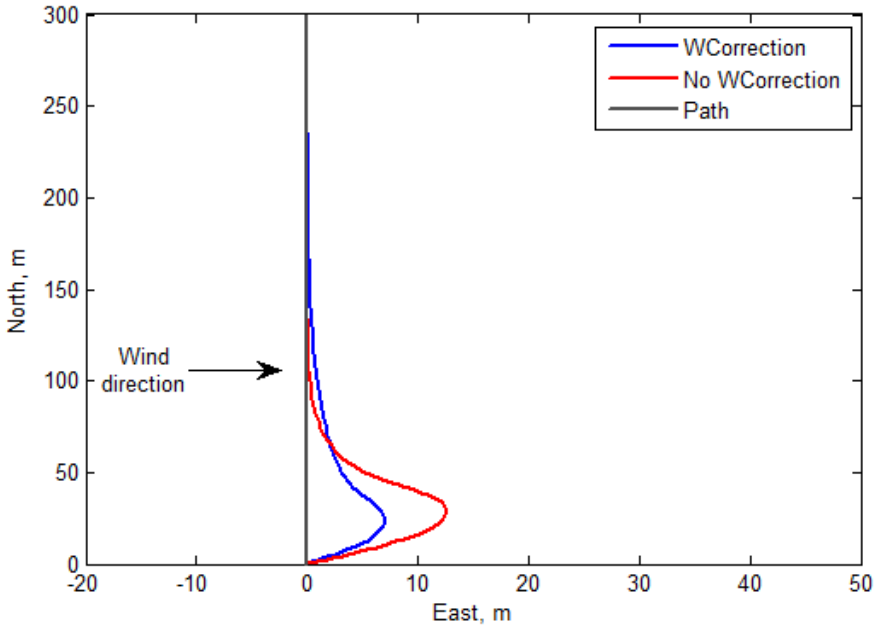

Figure 3-8: Airplane response in presence of wind

$A = (0, 0)$; $B = (0, 0)$; $C = (150, 100)$; $D = (100, 0)$; $E = (200, 0)$; $F = (200, 150)$; $G = (0, 150)$; $H = (-50, 0)$;
$\psi_{AB} = 0°$; $\psi_{BC} = 90°$; $\psi_{CD} \simeq -153°$; $\psi_{DE} = 90°$; $\psi_{EF} = 0°$; $\psi_{FG} = -90°$; $\psi_{GH} \simeq -161°$

Table 3.1: Waypoints list and course

The aircraft starts West of the current waypoint at a distance of 10 m, with a 0° heading and wings level. It recovers relatively fast from the cross track error and it manages to follow the straight-line segments between the given waypoints. The cross track error, plotted in Figure $3-10$, remains bounded and it converges to zero as the airplane approaches the desired trajectory. The WCA is shown in Figure $3-11$ and it changes depending on the direction of the wind relative to each segment line. Notice from this figure that the WCA is positive for right cross wind, negative for left cross wind and zero when the wind has the same direction as the intended course.

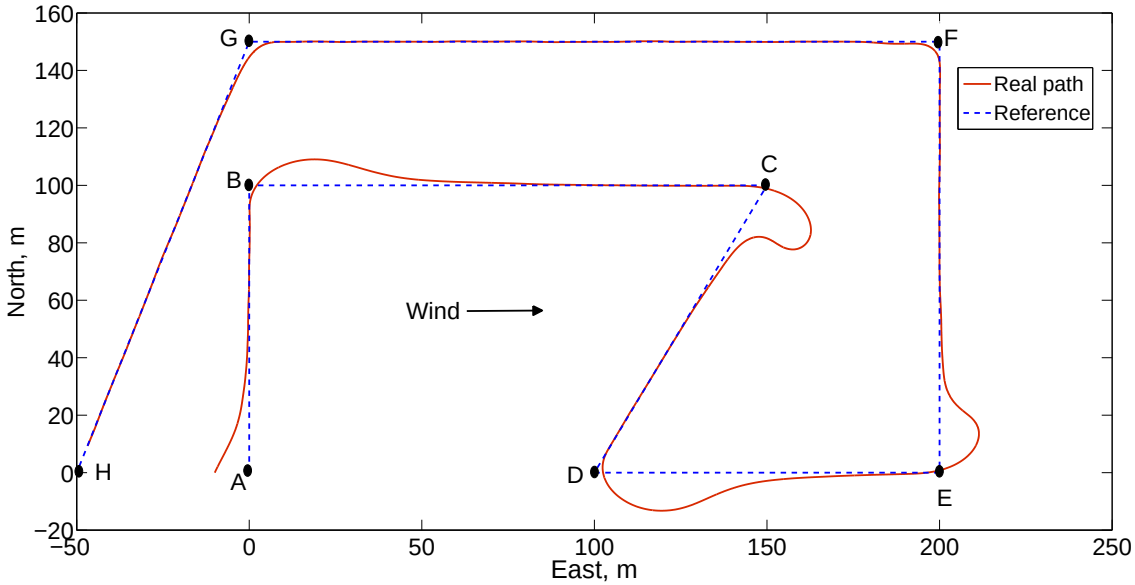

Figure 3-9: Following multiple straight-line segments

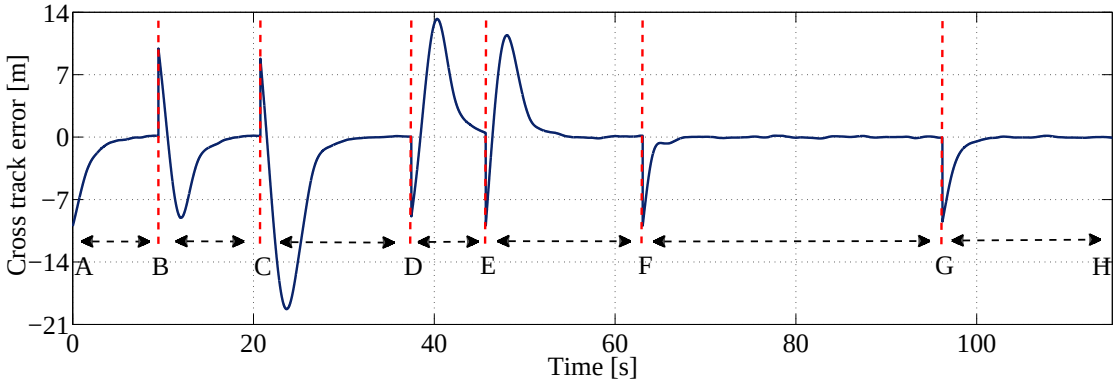

Figure 3-10: Cross track error relative to different segment lines

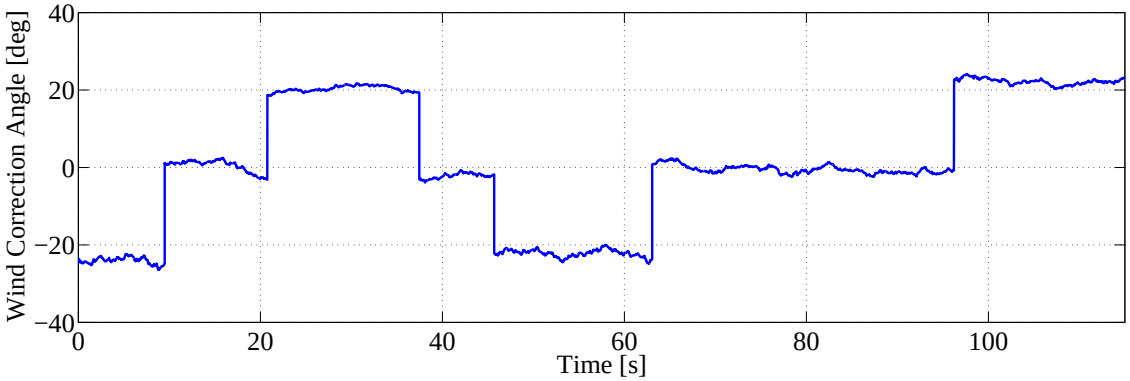

Figure 3-11: The Wind Correction Angle computed for each segment

The airplane orientation is plotted in Figure 3−12 along with the intended and the real courses. Notice from this figure that the airplane follows the inertial straight-line path by heading the nose into the wind. As a matter of fact, the difference between the airplane heading and the ground track is the value of the WCA depicted in Figure 3−11. Likewise, the commanded and the real bank angles are plotted in Figure 3−13. Positive values of the bank angle correspond to right turns while negative values to left turns.

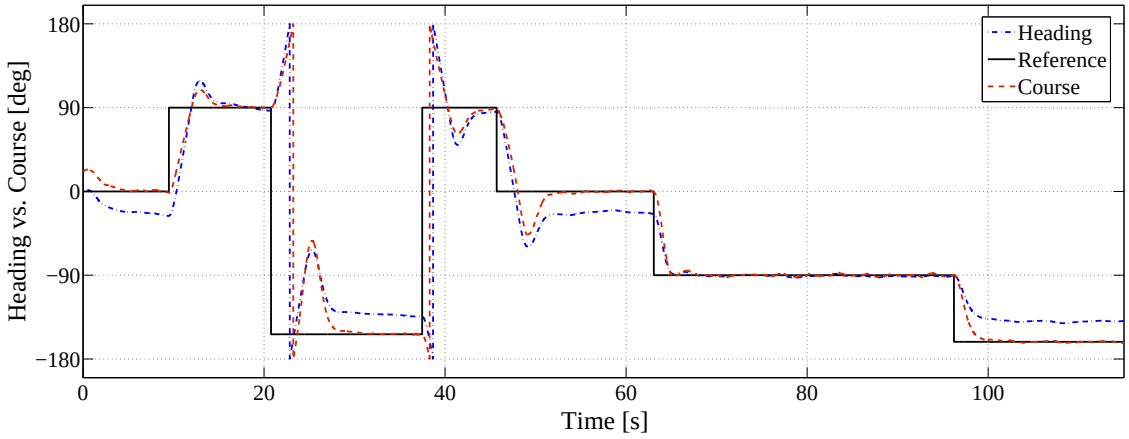

Figure 3-12: Airplane heading and real course relative to the intended course

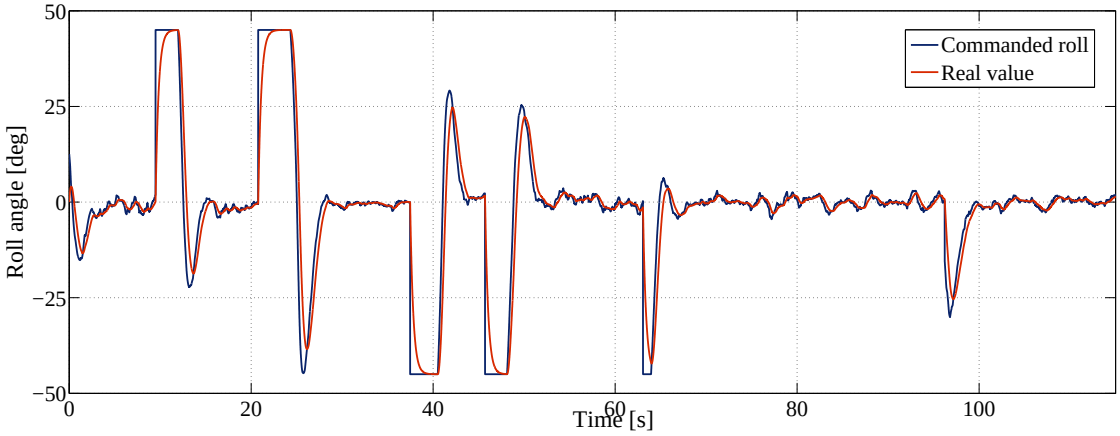

Figure 3-13: The commanded roll and the value provided by the inner control system

3.4.2 Standard backstepping design

In the previous section, the Lyapunov stability theorem failed to show the asymptotic stability of the closed-loop system due to a poor choice of the Lyapunov function. Nevertheless, an important feature of the Lyapunov's stability theorem is that its conditions are only sufficient, which means that for an inappropriate Lyapunov function no conclusions can be drawn on the stability of the system. This powerful property allowed us to determine the asymptotic stability of the system by using the LaSalle invariance principle.

However, many Lyapunov functions may exist for a given system and a specific choice of such a function may provide more precise results than others. Therefore, in this section we propose a backstepping design for the aircraft path following problem in windy conditions, which allows us to construct a proper Lyapunov function progressively, along with a stabilizing controller.

The following commonly steps in the development of a backstepping based controller will be illustrated for the path following problem of an aerial vehicle:

1. define a control objective

2. choose a virtual control among the states that could meet the control objective and find a stabilizing function for the scalar system

3. propose an error variable based on the deviation of the state from its commanded value and reformulate the control objective as the regulation of the error variable

4. derive the error variable dynamics and repeat the procedure until the real control input can be proposed

For this purpose, let us rewrite the nonlinear system described by (3.5)

$$\begin{aligned} \dot{d} &= V \sin(\psi - \psi_s) + W \sin(\psi_\omega - \psi_s) \\ \dot{\psi} &= \frac{g}{V} \tan\phi \\ \dot{\phi} &= k_\phi (\phi^c - \phi) \end{aligned}$$

We intend to achieve regulation of d designing backstepping control, thus we define the following error variable

$$e_1 = d - d_{min}$$

where d_{min} is the minimum allowed constant distance from the desired trajectory. The dynamics of e_1 yields

$$\dot{e}_1 = V \sin(\psi - \psi_s) + W \sin(\psi_w - \psi_s) \tag{3.15}$$

Let us consider the following positive function

$$V_{L_1} = \frac{1}{2} e_1^2$$

thus

$$\dot{V}_{L_1} = e_1 \left[V \sin(\psi - \psi_s) + W \sin(\psi_w - \psi_s) \right]$$

The e_1 term can be stabilized if we introduce ψ^v as virtual control in the form

$$V \sin(\psi^v - \psi_s) = -c_1 e_1 - W \sin(\psi_w - \psi_s)$$

Evaluating $\dot{V}_{L_1}$ when $\psi \to \psi^v$ it follows that

$$\dot{V}_{L_1}|_{\psi=\psi^v} = -c_1 e_1^2$$

Note from the above that, if $\psi \to \psi^v$ then the proposed control objective will be achieved. However, since ψ is a state variable and not an input control, let us define the deviation from its desired value

$$e_2 = V \sin(\psi - \psi_s) - V \sin(\psi^v - \psi_s) = V \sin(\psi - \psi_s) + c_1 e_1 + W \sin(\psi_w - \psi_s) \tag{3.16}$$

and rewrite (3.15) in terms of e_1 and e_2

$$\dot{e}_1 = e_2 - c_1 e_1$$

This implies that

$$\dot{e}_2 = g \tan\phi \cos(\psi - \psi_s) + c_1 e_2 - c_1^2 e_1 \tag{3.17}$$

Notice that $\cos(\psi - \psi_s) = \sqrt{1 - \sin^2(\psi - \psi_s)}$. From equation (3.16)

$$\sin(\psi - \psi_s) = \frac{e_2 - c_1 e_1 - W \sin(\psi_w - \psi_s)}{V} \tag{3.18}$$

and assuming that $-\frac{\pi}{2} < \psi - \psi_s < \frac{\pi}{2}$ it follows that equation (3.17) becomes

$$\dot{e}_2 = \frac{g}{V} R \tan\phi + c_1 e_2 - c_1^2 e_1$$

with $R = \sqrt{V^2 - [e_2 - c_1 e_1 - W \sin(\psi_w - \psi_s)]^2}$.
Introducing $V_L = \frac{1}{2}e_1^2 + \frac{1}{2}e_2^2$ as the Lyapunov function, then

$$\dot{V}_L = -c_1 e_1^2 + e_2 \left[\frac{g}{V} R \tan\phi + c_1 e_2 + e_1(1 - c_1^2) \right] \tag{3.19}$$

Let us propose the control input as

$$\phi^c = \arctan\left(\frac{V\left[-e_1(1 - c_1^2) - e_2(c_1 + c_2)\right]}{gR} \right) \tag{3.20}$$

Thus, (3.19) becomes

$$\dot{V}_L = -c_1 e_1^2 - c_2 e_2^2$$

Stability analysis

The Lyapunov function V_L is positive definite for all $e \in R^2$ and radially unbounded since it tends to infinity as $|e| \to \infty$. In addition, its derivative is negative definite since $\dot{V}_L(e) < 0 \ \forall \ e \neq 0$. Thus, using Theorem [3.2, p. 50], the origin $(0, 0)$ is a GAS equilibrium of the system represented in the (e_1, e_2) coordinates. It follows that $d \to d_{min}$. Moreover, from (3.16) it yelds

$$\psi \to -\arcsin\left(\frac{W \sin(\psi_\omega - \psi_s)}{V} \right) + \psi_s$$

Remark: The model presented above assumes that the airplane is equipped with an autopilot which stabilizes the vehicle and provides roll-angle tracking capabilities. If the autopilot disposes of angular momentum tracking capabilities instead of roll angle, the simplified model, introduced in Chapter 2, will have the form

$$\dot{d} = V \sin(\psi - \psi_s) + W \sin(\psi_w - \psi_s) \tag{3.21a}$$

$$\dot{\psi} = r \tag{3.21b}$$

$$\dot{r} = cN \tag{3.21c}$$

where r stands for yaw rate, N represents the yawing moment and c is a constant related to the aircraft moment of inertia. Employing the standard nonlinear backstepping algorithm, the commanded yaw moment is given by[3]

$$cN^c = -3r + \tan(\psi - \psi_s)(r^2 - 5) - \frac{3d + 5W \sin(\psi_w - \psi_s)}{V \cos(\psi - \psi_s)} \tag{3.22}$$

Numerical simulations

In this subsection we present several simulations which were carried out in order to validate the control structure proposed in (3.20) whose performance is mainly affected by wind. However, the stability analysis presented in the previous subsection has shown that the closed-loop system is also constrained by the choice of the constant parameters in the design of the Lyapunov function. For this reason, two sets of simulations will be further conducted, the goal of the first being to analyze the sensitivity of the controller to different choices of the constant parameters while the second concerns the controller robustness relative to slowly varying wind when following straight-line paths between geo-referenced waypoints.

[3]For a detailed description of the controller 3.22 see Appendix A.

A. The choice of the tuning parameters

First set of simulations addresses the constant parameters choice problem. For this purpose, the aircraft was commanded to follow a straight-line path defined by the geo-referenced waypoints $A(0,0)$ and $B(0,400)$, as shown in Figure 3-14. Thus, the minimum distance to the path, d_{min}, was required to be zero and different values of the constant parameters, listed in Table 3.2, were employed in order to analyze the risk that the aircraft exits the nominal flight envelope compromising the trajectory following abilities of the controller.

Figure 3-14 shows the time evolution of the airplane position related to the Earth when employing the controller (3.20) with three different sets of tuning parameters listed in the table above. The initial position of the aircraft was given by the point of coordinates S(-30; 10), with an orientation of 0° relative to North and wings level.

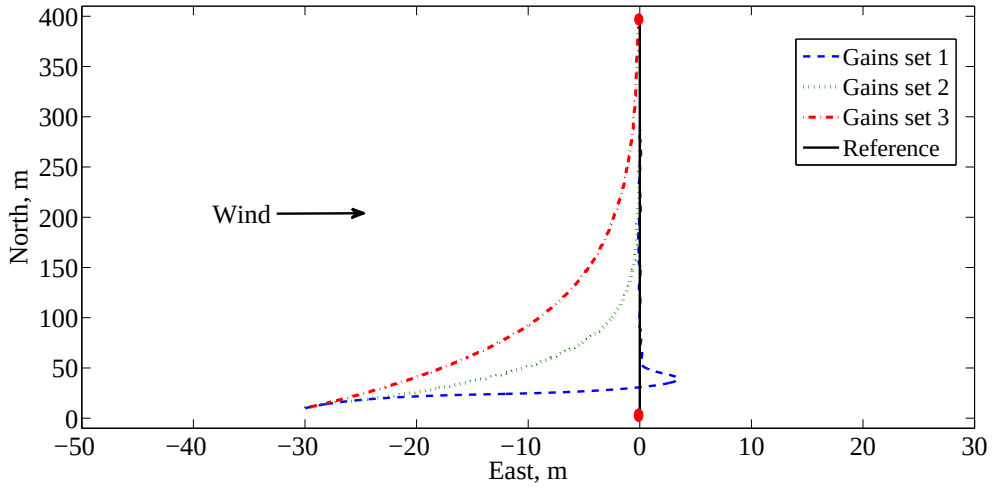

Figure 3-14: Airplane paths for different values of the constant parameters.

1st Scenario	$c_1 = 0.5$; $c_2 = 2$;
2nd Scenario	$c_1 = 0.1$; $c_2 = 6$;
3rd Scenario 3	$c_1 = 0.03$; $c_2 = 10$;

Table 3.2: Tuning parameters choice

The aircraft performance is shown to be affected by the choice of the constant parameters in the controller design. For example, the first scenario corresponds to the case when the airplane convergence to the reference path is oscillatory although the reaction time is short. The large values of the parameters, especially for c_1 which controls the convergence rate of $d \to 0$, make the airplane to move fast toward the desired trajectory in presence of large cross track errors but they cause oscillations when the airplane is close to the path. By reducing the values of this parameter in the second scenario and increasing the value of c_2, we have obtained a smoother response in airplane motion but a shorter convergence time. The smoothest convergence but also the slowest, was obtained for the set of constant gains.

The controller points the nose of the airplane into the wind in order to balance sideways displacements with engine thrust. This technique is displayed in Figure $3-15$ which shows the heading angle stabilized around $-25°$. However, as shown in Figure 3-14, the airplane keeps moving towards the North since it follows a straight-line path which makes a course of $0°$. In terms of stability, Figure $3-15$ proves that a sharp convergence towards the reference trajectory increases the risk that the aircraft will exit the nominal flight envelope since $|\psi - \psi_d| \approx \frac{\pi}{2}$ for the first set of parameters. In the case of the second scenario the system presents a better stability since the heading does not exceed $20°$ while a slow convergence, as obtained in the third scenario, presents the lowest risk of instability for the system.

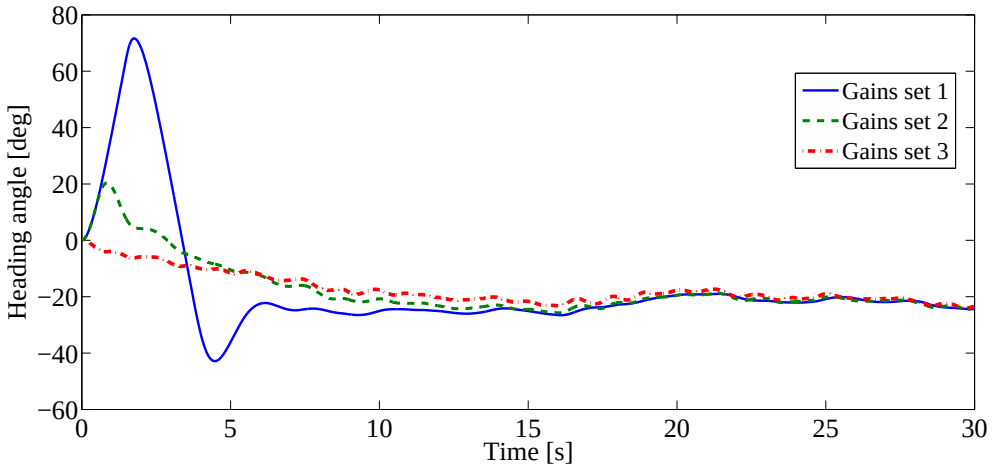

Figure 3-15: Airplane headings for different values of the constant parameters.

B. Waypoint guidance

The second set of simulations addresses a "Waypoint Guidance" scenario in which the airplane navigates between a series of predefined waypoints. As it was previously shown, the most important parameter in designing the guidance controller is c_1 since it affects the convergence rate of the airplane to the reference position. On the other hand, c_2 is also important but it affects the performance of a virtual input in the system, ie ψ^v. Thus, given the the second scenario envisaged, the parameters employed in simulation are : $c_1 = 0.05; c_2 = 10$. The airplane performance, as well as the state variables, are plotted in the following figures.

Figure $3-16$ illustrates the ground track of the airplane which recovers from the initial cross track error and it manages to maintain the course of the first segment by heading the airplane nose into the wind which blows perpendicular to the desired segment line. When the aircraft reaches the second waypoint, it starts the course correction according to the next segment to be followed. This time, the wind has the same direction with the intended course, affecting just the groundspeed/airspeed relation and no correction needs to be made in order to offset lateral movements due to the wind. When flying the third segment, the wind comes from the side direction of the forward motion which creates mainly a difference between aircraft course and

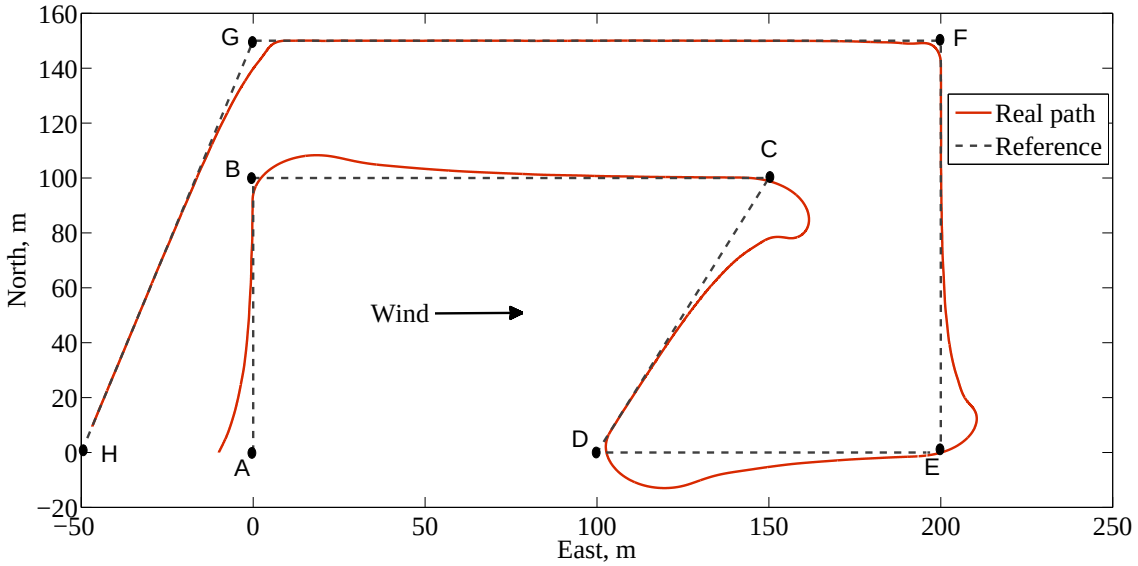

Figure 3-16: Airplane response when employing standard backstepping design

heading. Following the forth and the fifth segments requires similar effort from the airplane as for the second and the first segments. Contrary to the forth segment, the airplane encounters a headwind when flying the FG segment, which is favorable in takeoffs and landings since it generates greater lift but it makes the forward movement difficult.

In Figure $3-17$ we show the time evolution of the airplane deviation from the desired trajectory when commanded to follow this scenario. Notice from this figure that the developed controller provides cross track error regulation. Crosswind flight requires the controller to use an intentional crab maneuver in order to adjust the ground track of the airplane. As a result, the airplane moves in the direction of the line segment orientation while the airplane nose is yawed into the wind, see Figure $3-18$. The required and the provided control effort is illustrated in Figure $3-19$.

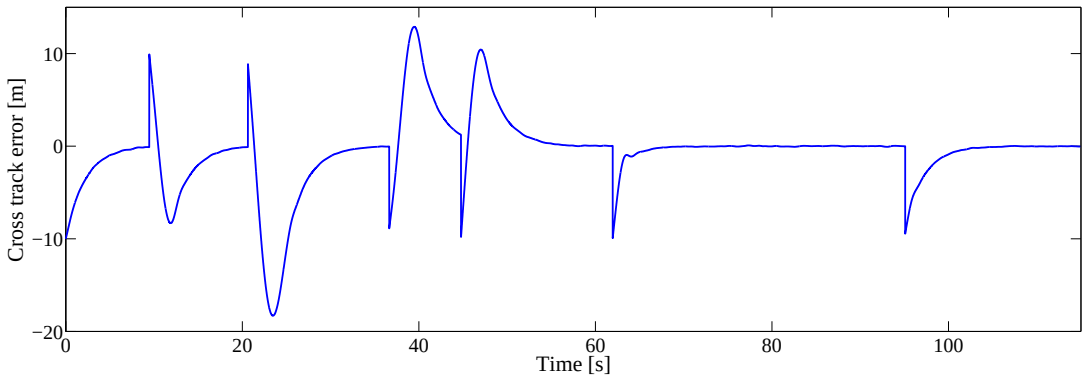

Figure 3-17: Airplane cross track error

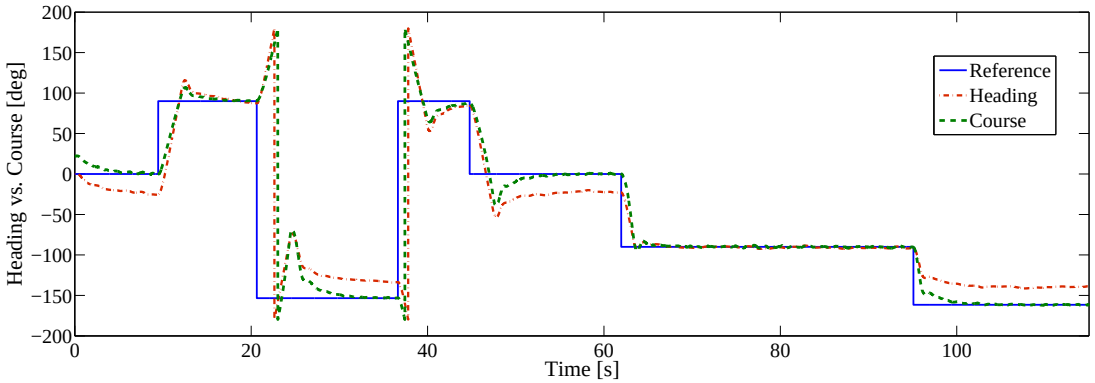

Figure 3-18: Airplane heading vs. inertial course

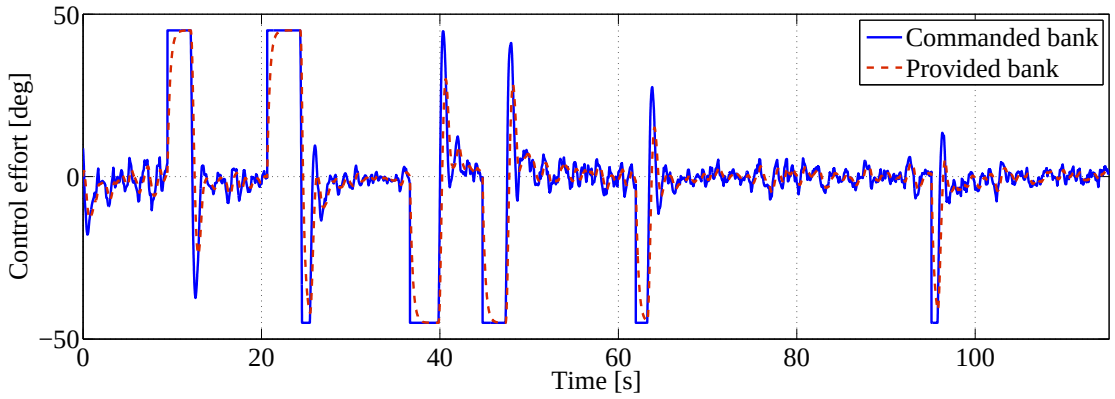

Figure 3-19: Control effort

3.5 Summary of results

This chapter has addressed the directional control problem of autonomous air vehicles in order to obtain path following capabilities when flying in a moving atmosphere with respect to the Earth. The motion of the atmosphere, i.e. the wind, was considered constat and known (measurable online with onboard sensors or from a ground location and sent to the aircraft via radio links) for control design. However, the performance of the controller was evaluated in presence of a low-altitude/low-turbulence dryden gust model to simulate real-flight conditions.

In what concerns the airplane guidance problem, first a general description has been given from a control design point of view and then an application consisting in following straight-line paths between geo-referenced waypoints was formulated. In order to obtain the dynamic of the cross track error with respect to such trajectory, a segment-fixed reference frame was introduced and the transformation of the latter relative to the inertial frame has been derived combining rotation and translation operations.

The control strategy is designed in the framework of Lyapunov theory and it uses a flight maneuver commonly employed in the landing approach of the airplanes which is known as "*the crab technique*" and which was described in the previous chapter. To this end, first some fundamentals of the Lyapunov theory were introduced and the main stability theorems were stated. The importance of applying a correction to the

airplane heading in order to counteract the effect of wind was emphasized by means of an example which compares the performance of a simple Lyapunov-based trajectory following controller and a similar design but incorporating the wind correction angle in its parameters. By illustrating the response of the aircraft to control signals from the two similar controllers, it can be noticed that using the knowledge of the wind correction angle results in small deviations from the path.

The general applicability of a Lyapunov-based control design is limited by the difficulty of finding a Lyapunov function. However, employing the backstepping approach we have constructed a stabilizing function along with a Lyapunov function for the simplified system describing the motion of the aircraft relative to a stationary straight-line path. Using this methodology, the closed-loop system was shown to be asymptotically stable. Several numerical simulations were carried out in order to validate the proposed control structure and they were divided into two main categories: the first one addressed the constant parameters choice problem while the second one addressed a waypoint guidance scenario.

Chapter 4

Wind identification with application to autonomous flight

The flight controllers developed in the previous chapter consider that local wind field data is available. In reality, measuring the wind from a moving aircraft platform is a challenging problem which requires accurate measurements of the airflow around the aircraft together with inertial velocity and orientation. Consequently, this chapter investigates conventional wind computation methods and addresses the estimation precision problem by taking into account the expected uncertainty in sensor measurements. Furthermore, an approach to improve the wind estimation accuracy and to maintain consistent aircraft performance for the path following application introduced in the previous chapter is proposed by employing adaptive control techniques.

4.1 Prior work on aircraft control in unknown wind

Generally, flight controllers proposed in literature do not account for wind or the wind conditions are assumed to be known and several control techniques are developed for different applications. Nevertheless, it is reasonable to consider that the airplane does not have full knowledge of the experienced wind given its sudden variations in velocity or orientation. For this reason, this section explores prior research on relevant methods to offset undesirable wind effect on airplane performance.

The problem of the aircraft flight in unknown wind is usually approached from two points of view, depending on whether or not it relies on knowledge of the local wind. On the one hand, a flight controller can account for wind perturbations by using ground-referenced measurements (i.e., course and groundspeed) instead of airspeed and flow angles. An important amount of research has been conducted following this direction with works developed in [1, 16, 29] being typical examples. However, this method is not likely to give good results in practice since accurate airdata has become a general requirement for the autopilot of an aircraft flying in presence of wind shear [23, 30]. In addition, the ground position and velocity are usually provided by sensors with questionable accuracy as it will be discussed later in this chapter.

On the other hand, the problem can be addressed by taking the wind into account during the construction of the flight controller. Although it requires knowledge of the wind vector, the approach has been employed in a wide range of literature and several strategies have been adopted to deal with the wind identification problem. First, measurements of the wind can be made from ground based devices and transmitted via radio signals to the aircraft. The ground station should also be capable of tracking the position of the aircraft, namely its altitude, since the wind parameters at the aircraft level are computed as a function of altitude based on a standard atmosphere model. However, the wind data processed in this way may have significant errors due to sudden variations in the wind profile.

Therefore, onboard sensors capable of measuring or algorithms for estimating the wind parameters are necessary in order to obtain better flight capabilities. Accurate measurements of wind have been obtained by using arrays of multihole pitot probes [19]. Nevertheless, our study addresses the flight of small light UAVs for which the payload capacity is limited. Thus, rather than adding additional sensors which increase weight and costs, we intend to use only sensors that are typically included in standard autopilots, such as inertial measurement unit (IMU), global positioning system (GPS) or air data sensors.

There is an increasing amount of literature highlighting methods to compute the wind from a moving aircraft platform. For example, in [25] the authors compute the

wind by comparing Earth relative measurements of the aircraft motion and predictions of the same quantities obtained from the aircraft dynamic model in which the influence induced by the wind field can be separated by the influence induced by the control input. A second approach proposed in this paper uses the vehicle kinematics and sensor measurements of the inertial velocity to directly compute the wind. This method follows from the graphical representation of the relationship between aircraft motion and wind and it is known as the *wind triangle*. Indeed, in [26] the authors use this approach to estimate the wind comparing the aircraft airspeed with estimates of the inertial speed. Artificial noise was injected in simulations in order to obtain real flight measurements while the critical parameters to be computed were chosen to be the wind bearing and the variation of wind speed with altitude. Even though the proposed algorithm introduces a delay in computation of the wind acceleration, it has low complexity which makes it usable on small UAVs with limited computational power. The same strategy to compute the wind is considered in [20, 21].

In the same way, the authors explore in [27] the joint estimation problem of vehicle heading, wind speed and wind direction using air data and inertial measurements. A nonlinear recursive filter associated with a reduced kinematic model is implemented and high fidelity simulations are conducted.

4.2 Common techniques for wind computation

As the above discussion attests, wind identification involves various measured quantities which can be separated in two main categories: air data and inertial navigation sensing. Estimates of these quantities are computed by standard autopilots and they represent a potential uncertainty source that will propagate through the wind identification algorithm. Thus, the error in the wind estimates depends on how the data provided by sensors are combined. Thereby, this section starts by establishing the common quantities which are required to evaluate the wind and the sensors needed to measure them. Further, relevant methods to compute the wind are explored in detail and an associated error analysis is conducted based on sensors uncertainty.

4.2.1 Required quantities for wind sensing capabilities

This subsection introduces the minimum sensing suite needed by an autopilot to provide wind estimates. The sensors that are commonly used to measure the required quantities are discussed along with the corresponding uncertainties provided by manufacturers and quantified by one standard deviation referred as σ.

Air data

Knowing the airstream surrounding the aircraft is vital for the flight control system to ensure flight safety. Generally, airdata include static and dynamic pressures, which are converted into airspeed, vertical speed, altitude and airflow angles represented by angle of attack and sideslip. The static and dynamic pressures are measured using air data probes called Pitot tubes while the flow angles are typically measured using mass flow vanes connected to potentiometers or fixed differential pressure probes. The measurements are subject to errors due to sensor uncertainty. In addition, the movement of the airplane creates distortion of the surrounding air generating errors that are sometimes larger than those inherent in the measuring instruments. Furthermore, the location of the sensors greatly affects their measurements [22]. Nevertheless, standard air data sensors offer smooth airspeed measurements with an accuracy of $\sigma_{V_a} = \pm 0.2\ m/s$ and flow angles with a high $\sigma_{\alpha,\beta} = \pm 0.2^\circ$ accuracy.

Inertial navigation data

A complete Earth relative data set can be determined from several sensors such as INS, GPS, ground based radar, etc. Since an INS determines velocity from integrated acceleration, the computed data set is not accurate being subject to drift errors. On the other hand, Earth relative data without drift errors can be computed by a GPS unit which has, however, the deficiency of a large uncertainty in position measurements of the order of $\sigma_{P_I} = \pm 2.5\ m$. GPS sensors provide smooth velocity measurements which are not affected by this problem, having an accuracy of $\sigma_{V_I} = \pm 0.1\ m/s$. Using carrier phase differential GPS significantly increases the position

accuracy but the signal is still noisy to be used for accurate wind identification. The orientation of the airplane can be measured using an Inertial Measurement Unit (IMU) with $\sigma_{\psi,\theta,\phi} = \pm 0.5^{\circ}$ accuracy.

4.2.2 Computing the wind from the velocity vectors diagram

The Earth-relative motion of an airplane is the resultant of the aircraft motion through the airmass and the motion of the airmass over the ground. The equation connecting these quantities is captured by the graphical diagram in Figure $4-1$ and it is given by

$$\overrightarrow{V}_g = \overrightarrow{V}_a + \overrightarrow{V}_w \tag{4.1}$$

Equation (4.1) is known as the wind triangle equation and it represents the relationships among the velocities involved in the navigation of an aircraft. Its terms are vector quantities, each being described by both magnitude and orientation as it follows: the ground vector, $\overrightarrow{V}_g$, is represented by ground speed V_g and course χ, the air vector, $\overrightarrow{V}_a$, is defined by airspeed V_a and heading ψ while the wind vector, $\overrightarrow{V}_w$, is described by wind speed W and wind direction ψ_w.

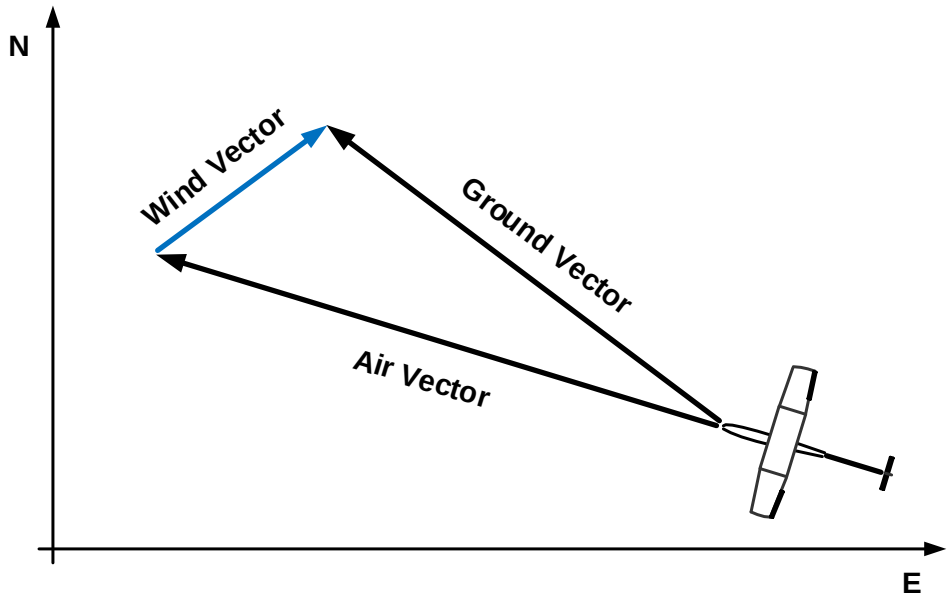

Figure 4-1: The graphical representation of the relationship between aircraft motion and wind.

Wind sensing capabilities can be obtained from the vector difference of $\overrightarrow{V}_g$ and $\overrightarrow{V}_a$ in equation (4.1) when these quantities are known. Apparently, this approach is straightforward and it relies on navigation and air-relative velocity measurements. However, solving the wind triangle equation for the inertial components of the wind vector requires the use of several coordinate systems and, implicitly, the angles to transform between them.

This inconvenient is due to the fact that there is no direct measurement of the required quantities in the same frame of reference, i.e. ground vector is directly measured by the navigation sensor in the inertial coordinate system while the air vector is essentially measured by the air data sensor in the directions of the axes of a reference frame aligned with the airflow referred as the aerodynamic reference frame. Therefore, several calculations have to be applied in order to allow for the vector difference in the Earth-fixed reference frame.

To begin with, air data sensors provide measurements of the airspeed, V_a, and airflow angles, α and β. The air vector is then obtained by employing the aerodynamic coordinate system, in which it has the components $\overrightarrow{V}_a = (V_a, 0, 0)$. Further, the air vector is brought into the body-fixed coordinate system by successive rotations through angles β and α using the transformation introduced in [28] and given by

$$\{\overrightarrow{V}_a\}_B = R_{BA}\overrightarrow{V}_a = \frac{V_a}{D}\begin{bmatrix} 1 \\ \tan\beta \\ \tan\alpha \end{bmatrix}$$

with the normalization factor $D = \sqrt{1 + \tan^2\alpha + \tan^2\beta}$, the subscript B describing a vector in the body frame and the matrix R_{BA} representing the transformation from aerodynamic to body frame.

The vector describing the motion of the aircraft through the airmass has been obtained and transformed in the orientation of the body frame but it can still not be exploited in equation (4.1). For this purpose, the complete transformation from the body coordinate system into the inertial frame, achieved by successive rotations

through angles (ψ, θ, ϕ) and introduced in Chapter 2 by R_{IB}, is required

$$\{\overrightarrow{V}_a\}_I = R_{IB}\{\overrightarrow{V}_a\}_B \tag{4.2}$$

Thus, from (4.1) and (4.2) the wind vector can be obtained as

$$\overrightarrow{V}_w = \overrightarrow{V}_g - R_{IB}R_{BA}\overrightarrow{V}_a$$

where $\overrightarrow{V}_w = (w_e, w_n, w_h)$ and $\overrightarrow{V}_g = (v_e, v_n, v_h)$ are two vectors expressed in the Earth-relative reference frame and $\overrightarrow{V}_a = (V_a, 0, 0)$ is described in the aerodynamic coordinate system. Writing for the inertial components of the wind vector it yields

$$\begin{aligned}
w_e &= v_e - V_a D^{-1}\left[\cos\theta\sin\psi + \tan\beta\left(\sin\phi\sin\theta\sin\psi + \cos\phi\cos\psi\right)\right] \\
&\quad + V_a D^{-1}\tan\alpha\left(\cos\phi\sin\theta\sin\psi - \sin\phi\cos\psi\right) \qquad (4.3a) \\
w_n &= v_n - V_a D^{-1}\left[\cos\theta\cos\psi + \tan\beta\left(\sin\phi\sin\theta\cos\psi - \cos\phi\sin\psi\right)\right] \\
&\quad + V_a D^{-1}\tan\alpha\left(\cos\phi\sin\theta\cos\psi + \sin\phi\sin\psi\right) \qquad (4.3b) \\
w_h &= v_h - V_a D^{-1}\left(-\sin\theta + \tan\beta\sin\phi\cos\theta\right) \\
&\quad + \tan\alpha\cos\phi\cos\theta \qquad (4.3c)
\end{aligned}$$

4.2.3 Wind computation using the vehicle response approach

Another approach to compute wind from a fixed wing UAV platform is to compare measurements of the aircraft inertial motion, provided by a navigation sensor, with predictions of the same quantities resulted from the dynamic model of the vehicle [25]. Indeed, the Earth-relative aircraft motion can be stimulated by two inputs: aerodynamic or propulsive commands sent by the autopilot and external perturbing forces typically represented by wind. In addition, the contribution of each of these inputs in the induced motion of the aircraft can be emphasized in the equations of motion. Therefore, any potential difference between predictions of the aircraft motion induced by autopilot commands and actual measurements provided by embedded sensors can be assigned to wind which can thus be estimated.

Writing the equation for the rate of change of translational position, it yields

$$\dot{p}_I = R_{IB} V_b + V_w \tag{4.4}$$

where $p_I = [p_e \; p_n \; p_h]^T$ is the inertial position of the airplane and $V_b = [u \; v \; w]^T$ represents the air-mass relative velocity in the body axes direction.

Equation (4.4) relates the aircraft inertial motion to the Earth-relative wind, V_w, velocity with respect to the air-mass, V_b, and angular position through the transformation matrix from body to inertial frame, R_{IB}. Further, let the aircraft motion induced by autopilot inputs be denoted by p^{AP}. Therefore, one can write

$$\dot{p}^{AP} = R_{IB} V_b$$

In the above equation, the aircraft air-relative velocity and angular position are controlled by aerodynamic and propulsive inputs and predictions of their values are provided by the autopilot system based on the dynamic model of the aircraft. Consequently, the airplane motion induced by control inputs can be estimated. Further, if the vehicle is equipped with a sensor capable of measuring the Earth-relative velocity of the aircraft, then the wind field yields from

$$V_w = \dot{p}_I^{SEN} - \dot{p}^{AP} \tag{4.5}$$

The wind estimates provided by equation (4.5) rely on inertial velocity measurements and aircraft state predictions. Another approach, similar in principle with the one previously presented, uses numerical differentiation of position measurements instead of inertial velocity. To this end, the discrete form of the aircraft mathematical model needs to be derived in order to obtain the wind speed as

$$V_{w_{k-1}} = \frac{1}{\Delta t} \left(p_{I_k} - p_{I_{k-1}} \right) - f_u \left(x_{k-1}, u_{k-1} \right) \tag{4.6}$$

where p_{I_k} and $p_{I_{k-1}}$ are two successive measurements of the aircraft Earth-relative

position, x_{k-1} represents an estimations of the aircraft state commanded by the control input u_{k-1}, $f_u\left(x_{k-1}, u_{k-1}\right)$ is the prediction of the change in aircraft state over the time interval from $k-1$ to k ignoring the effects of wind and ΔT is the sampling time determined by the navigation sensor. The methods based on the vehicle response differ by the fact that one relies on velocity while the other on position measurements. Thus, depending on the employed sensor and its corresponding uncertainty, one can give more precise results than the other.

4.2.4 Expected uncertainty in the computed wind

The calculation of the wind vector based on the methods presented above involves several measured and/or predicted quantities, each representing a potential source of uncertainty in the wind values. As discussed in section 4.2.1, the uncertainty in sensor measurements can be quantified by one standard deviation provided by manufacturers. Regarding predicted quantities, their uncertainty depends on the accuracy of the airplane dynamic model to describe the real behavior of the vehicle. Thus, this subsection focuses on determining the wind computation precision based on expected errors in sensor measurements and aircraft state predictions.

Wind triangle approach

Equations (4.3) shows that the velocity vectors diagram method involves nine measured quantities and several trigonometric functions to compute the wind field. The nonlinear form of the equations implies that the measurement precision can not be straightforward addressed. In order to transparently quantify the overall system accuracy, one can use a linearized uncertainty propagation model in the wind vector equations. For this purpose, let us write the compact form of the computed nonlinear equation (4.3)

$$V_w = f(v_e, v_n, v_h; V_a, \alpha, \beta; \psi, \theta, \phi)$$

which becomes after linearization

$$\Delta V_w \approx f(x_n) + H\,(x - x_n)$$

where x is the vector containing the measured quantities and it is given by $x = [v_e\ v_n\ v_h\ V_a\ \alpha\ \beta\ \psi\ \theta\ \phi]^T$, $f(x_n)$ represents the computed wind evaluated at nominal value x_n of the state vector and $H_w = \frac{\partial V_w}{\partial x}$ is the Jacobian of the wind equations.

Therefore, the overall uncertainty of the wind computation method is determined through Gaussian uncertainty propagation by evaluating the *trace* of the wind error covariance matrix Σ_W

$$\sigma_W^2 = Tr\Sigma_w = \sum_{j=1}^{9} \Sigma_w(j,j)$$

with Σ_w resulting from the covariance of the expected noise denoted by Σ_x

$$\begin{aligned} \Sigma_x &= diag(\sigma_{v_e}^2\ \sigma_{v_n}^2\ \sigma_{v_h}^2\ \sigma_{V_a}^2\ \sigma_\alpha^2\ \sigma_\beta^2\ \sigma_\psi^2\ \sigma_\theta^2\ \sigma_\phi^2\ ) \\ \Sigma_w &= H_w \Sigma_x H_w^T \end{aligned}$$

Approaches based on vehicle response

Equations (4.5) and (4.6) involves two measured quantities of known uncertainty and predictions of the aircraft state which require an accurate mathematical model of the aircraft. However, this can be a challenging problem for small UAVs whose dynamic properties change frequently due to changes in the embedded system setup. Therefore, another uncertainty source needs to be considered but a potential deviation from the real values of the aircraft state can not be generally quantified and the overall quality of the vehicle based wind measurement methods can not be completely evaluated.

Nevertheless, denoting the uncertainties of the inertial velocity predicted vector by $\sigma_{V_g}^{AP}$ and employing σ_{V_g} and σ_{p_I} to represent the navigation sensor uncertainties for the velocity and position vectors parameters measurement, then the Gaussian uncertainty propagation model can be used to estimate the errors in the computed wind. However, $\sigma_{V_g}^{AP}$ is difficult to predict and it can be subject to large ranges.

4.3 Adaptive control theory

The wind computation methods presented in the previous section have the deficiency to directly rely on sensors measurements which are subject to noise and large errors. Hence, all the false readings are translated into inaccurate wind measurements which might result in excessive and insecure control efforts. In order to deal with this drawback, one can consider the wind components as unknown parameters in the aircraft equations of motion and employ adaptive control techniques to achieve global stabilization with online parameter estimation.

To this end, this section introduces basic concepts of adaptive control theory together with an illustrative example of adaptive control design for a simple scalar system. Further, relevant literature on adaptive flight control is discussed.

4.3.1 Basic concepts

Adaptive control is an approach to control systems with uncertain parameters such as robots, airplanes, ships, etc. Lately, an increasingly number of practical problems are addressed using adaptive control techniques and several examples can be illustrated. For instance, commercial airplanes fly long courses and account for considerable mass changes, large speed or altitude variations. In addition, the adaptive control system of a ship is able to adjust depending on ship loading or wave conditions. On the other hand, robots can manipulate loads of different sizes or unknown weights. As a matter of fact, the theory describing this methodology was originally developed for high-performance aircraft control purposes. Indeed, airplanes have a large flight envelope depending on changes in speed, altitude, configuration, payload, etc. Thus, in order to achieve and maintain consistent performance under varying operating conditions, flight controllers need to adjust their parameters such that a satisfactory plant response is reached.

Nevertheless, despite their usefulness in many practical contexts, a significant issue to be considered in the adaptation designs is the stability and the convergence of the closed-loop adaptive system. It can be then concluded that the design of an

adaptive controller, compared to conventional control design, involves three steps that are further listed [10]

1. the choice of a control law containing the uncertain parameters
2. the choice of an adaptation law in order to adjust these parameters
3. the analysis of the stability properties of the resulting control system

Adaptive controllers are usually flexible and they allow the coupling of various control techniques, employed to meet the objective of the first step, with estimation techniques, used to adjust the uncertain parameters. Nevertheless, the stability of the resulting system is difficult to guarantee. Various tools from nonlinear control theory, such as Lyapunov theory, can be used to this end. In reality, an appropriate choice of the Lyapunov function can coordinate, in some cases, the three steps usually involved in the design of an adaptive controller. In this particular case, guessing the Lyapunov function at the beginning of the design process, allows the choice of the control and adaptation laws so that the proposed function decreases, fulfilling all the requirements of an efficient adaptive system. This property will guide our choice of estimation technique for Lyapunov stability theory as it will be illustrated in the following example.

4.3.2 Example: aerodynamic velocity control

Let us illustrate the Lyapunov-based adaptive control for a simple application which requires the stabilization of the aircraft aerodynamic velocity, V_a, at predefined values. The equation governing the velocity dynamics is given by

$$\dot{V}_a = \frac{F_{wx}}{m} - g \sin \gamma$$

where $F_{wx} = T_{wx} - D$ is the total force along the x-axis of the aerodynamic reference frame and it is determined by the thrust component in the direction of the same axis, T_{wx}, and the drag force, D, while γ describes the flight path angle. Using the

transformation matrix from body to aerodynamic frame, R_{AB}, in order to write the equation in appropriate form, ie depending on the body-axis thrust, it yields

$$\dot{V}_a = \frac{1}{m}\left(F_T \cos\alpha \cos\beta - D - mg\sin\gamma\right)$$

Since the purpose of this example is to illustrate the typical steps to follow in adaptive control design, let us consider for simplicity that the aircraft flies at zero angle of attack, sideslip and flight path angle. Therefore, the velocity equation reads

$$\dot{V}_a = \frac{1}{m}\left(F_T - D\right) \tag{4.7}$$

where the drag force is the uncertain parameter and the body-axis thrust force represents the control input. Thus, the problem to be solved involves the estimation of the uncertain parameter based on the measured velocity and the use of the estimated parameter in the flight controller in order to make the system to follow a given reference in velocity.

For this purpose consider the velocity error

$$e_V = V_a - V_{ref}$$

whose evolution is given by

$$\dot{e}_V = \frac{1}{m}\left(F_T - D\right)$$

In order to stabilize e_V, one can employ Lyapunov theory design proposing the candidate function

$$V_1 = \frac{1}{2}e_V^2$$

whose derivative reads

$$\dot{V}_1 = \frac{e_V}{m}\left(F_T - D\right)$$

At this point we should choose F_T such that V_1 decreases. An intuitive selection of the required engine thrust would be $F_T = D - c_1 e_V$ with c_1 a positive definite constant gain. However, the term D is not known and it can not be employed in the

controller. For this reason, D is replaced by its estimate $\hat{D}$ and the new error variable is considered in the candidate Lyapunov function

$$V_L = \frac{1}{2}e_V^2 + \frac{1}{2k_\gamma}\tilde{D}$$

with $\tilde{D} = D - \hat{D}$ being the difference between the unknown parameter and its estimate and k_γ a constant positive adaptation gain. The derivative of this function, for slowly-varying D, is given by

$$\dot{V}_L = \frac{e_V}{m}\left(F_T - D\right) - \frac{1}{k_\gamma}\tilde{D}\dot{\hat{D}}$$

Choosing

$$F_T = \hat{D} - mc_1 e_V$$

the derivative of V_L reads

$$\dot{V}_L = -c_1 e_V^2 - \frac{\tilde{D}}{k_\gamma}\left(\frac{k_\gamma e_V}{m} + \dot{\hat{D}}\right)$$

Then, the adaptation law for the unknown drag force is

$$\dot{\hat{D}} = -\frac{k_\gamma e_V}{m}$$

which makes the derivative of the Lyapunov function

$$\dot{V}_L = -c_1 e_V^2$$

proving the stability of the closed-loop adaptive system in the sense of Lyapunov.

Simulations have been carried out with the purpose of testing the capabilities of the developed adaptive controller. The variation of the Drag force with airspeed for a typical airplane in steady, level flight was considered in order to reproduce conditions similar to real flight and it is shown in Figure $4-2$. Note from equation (4.7) that thrust must equal drag in steady flight; thus, the curve for the total drag also represents the required thrust. Based on these considerations, the scenario envisaged

in simulations was to stabilize the aircraft airspeed at several nominal values, each corresponding to a different value of the Drag force. The performance of this simple adaptive system is provided in Figure $4-3$.

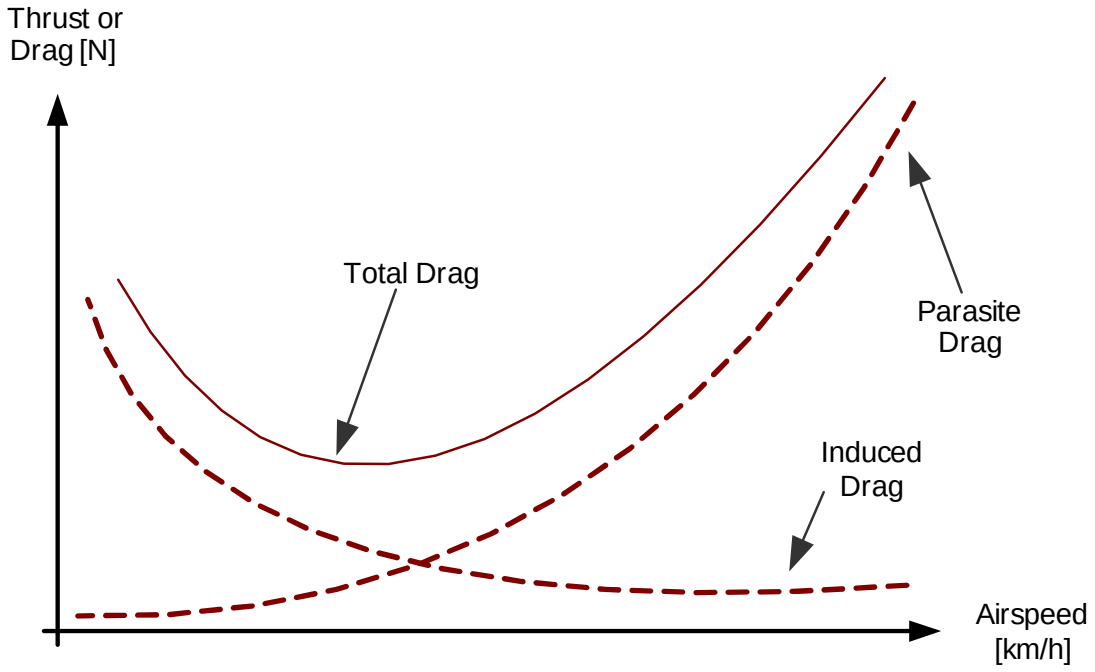

Figure 4-2: The variation of the Drag force with airspeed.

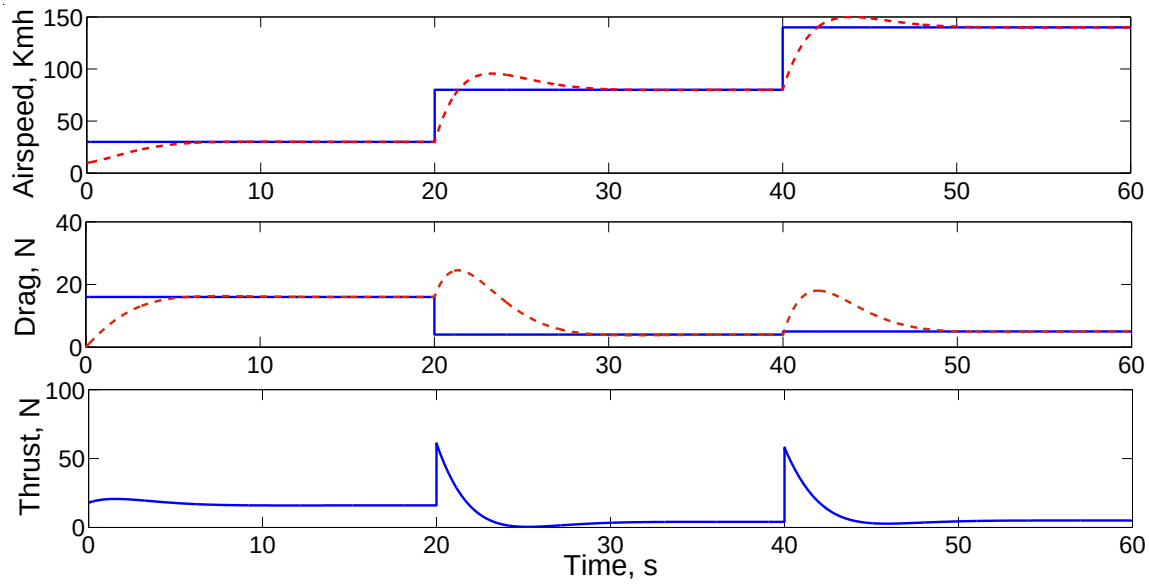

Figure 4-3: The parameters of the adaptive system.

4.4 Path following with online wind estimation

The adaptive design in the above example is straightforward because the matched uncertainty condition is satisfied, i.e. the uncertainty is in the span of the control input. Systems with uncertainties separated from the control input can be addressed using an extended framework of the backstepping approach introduced in the previous chapter, which contains a dynamic feedback part as the uncertain parameter update law. This approach, referred to as adaptive backstepping, allows the design of an adaptive controller in a structured and recursive way. In addition, boundedness of the closed-loop states and convergence of the tracking error to zero are properties that adaptive backstepping handles well due to its Lyapunov foundation.

Based on these considerations, this section addresses the guidance problem of a small fixed-wing UAV when flying in unknown wind field. Rather than accounting for uncertain dynamics of the aircraft, adaptive control design is employed in order to estimate and to eliminate the wind influence on the vehicle performance. For this purpose, the application consisting in following straight-line paths, introduced in Chapter 3, is formulated in the framework of the adaptive backstepping theory.

Let us rewrite the nonlinear system (3.5) describing the motion of an aircraft relative to a stationary straight-line path

$$\begin{aligned} \dot{d} &= V \sin(\psi - \psi_s) + k_\omega \\ \dot{\psi} &= \frac{g}{V} \tan\phi \\ \dot{\phi} &= k_\phi (\phi^c - \phi) \end{aligned}$$

where $k_\omega = W \sin(\psi_\omega - \psi_s)$ is unknown and it is due to the wind perturbation.

In practice, the uncertain parameters describing the dynamic systems are often time-varying. This is also the case for the unknown wind field which is generally slowly-varying but it can also be associated with significant variations in speed or direction. Although wind gust is likely to occur in real flight conditions, a complete analysis of the airplane behavior in such conditions involves mathematical difficul-

ties in the adaptive control design and requires high computation capabilities of the embedded autopilot. For this reason, we will assume further that the wind vector varies slowly so that it can be considered constant in the development of the adaptive control structure. However, at the end of the section we will provide an analysis based on simulation results relative to the behavior of the adaptive control system in presence of time-varying wind.

In what follows, we will propose a path following controller correlated with adaptation laws for on-line wind estimation. The controller will be developed based on the adaptive backstepping approach and it will use the estimated values of the wind. For this purpose, define the following error variable

$$e_1 = d - d_{min} \tag{4.8}$$

where d_{min} represents the minimum allowed distance from the desired. Thus,

$$\dot{e}_1 = V \sin(\psi - \psi_s) + k_\omega \tag{4.9}$$

4.4.1 Regulation of the cross track error

Propose the following positive function

$$V_{L_1} = \frac{1}{2} e_1^2$$

thus

$$\dot{V}_{L_1} = e_1 \left[V \sin(\psi - \psi_s) + k_\omega \right]$$

To stabilize e_1 we introduce ψ^v as a virtual control in the following form

$$V \sin(\psi^v - \psi_s) = -c_1 e_1 - \hat{k}_{\omega_1}$$

where $\hat{k}_{\omega_1}$ is the estimate of k_ω and $c_1 > 0$ is a constant. Evaluating $\dot{V}_{L_1}$ when $\psi \to \psi^v$

it follows that

$$\dot{V}_{L_1}|_{\psi=\psi^v} = -c_1 e_1^2 + e_1 \tilde{k}_{\omega_1}$$

where $\tilde{k}_{\omega_1} = k_\omega - \hat{k}_{\omega_1}$.

Notice from the above equation that if $\hat{k}_{\omega_1} \to k_\omega$ then $\dot{V}_{L_1} \leq 0$. Thus, rewriting V_{L_1}, it yields

$$V_{L_1} = \frac{1}{2}\left(e_1^2 + \frac{1}{\gamma_1}\tilde{k}_{\omega_1}^2\right)$$

where $\gamma_1 > 0$ denotes a constant adaptation gain. Then

$$\dot{V}_{L_1}|_{\psi=\psi^v} = -c_1 e_1^2 + \left(e_1 - \frac{\dot{\hat{k}}_{\omega_1}}{\gamma_1}\right)\tilde{k}_{\omega_1}$$

Choosing the update law as

$$\dot{\hat{k}}_{\omega_1} = \gamma_1 e_1$$

It follows that

$$\dot{V}_{L_1}|_{\psi=\psi^v} = -c_1 e_1^2$$

4.4.2 Convergence of ψ to ψ^v

Define the error

$$e_2 = V\sin(\psi - \psi_s) - V\sin(\psi^v - \psi_s) = V\sin(\psi - \psi_s) + c_1 e_1 + \hat{k}_{\omega_1} \tag{4.10}$$

and rewrite (4.9) in terms of e_1 and e_2

$$\dot{e}_1 = e_2 - c_1 e_1 + \tilde{k}_{\omega_1}$$

This implies that

$$\dot{e}_2 = g\tan\phi^c\cos(\psi - \psi_s) + \left(\gamma_1 - c_1^2\right)e_1 + c_1 e_2 + c_1\tilde{k}_{\omega_1}$$

Finally, introduce the following Lyapunov function

$$V_L = \frac{1}{2}\left(e_1^2 + \frac{1}{\gamma_1}\tilde{k}_{\omega_1}^2 + e_2^2\right)$$

then

$$\dot{V}_L = -c_1 e_1^2 + e_2\left[g\tan\phi^c\cos\left(\psi-\psi_s\right) + c_1 e_2 + (1+\gamma_1-c_1^2)e_1 + c_1\tilde{k}_{\omega_1}\right] \tag{4.11}$$

Propose the control input as

$$\phi^c = \arctan\left[-\frac{e_1(1+\gamma_1-c_1^2) + e_2(c_1+c_2) + c_1(\hat{k}_{\omega_2}-\hat{k}_{\omega_1})}{g\cos\left(\psi-\psi_s\right)}\right] \tag{4.12}$$

where $\tilde{k}_{\omega_2} = k_\omega - \hat{k}_{\omega_2}$, $\hat{k}_{\omega_2}$ represents a new estimate for k_ω and c_2 denotes a positive constant gain. Notice that if we had employed the existing estimate $\hat{k}_{\omega_1}$, we would have had no design freedom left to cancel the unknown parameter from $\dot{V}_L$. Additionally, $\hat{k}_{\omega_2}$ could be seen as a factor correction for $\hat{k}_{\omega_1}$.

Introducing the above into (4.11), we have

$$\dot{V}_L|_{\phi=\phi^c} = -c_1 e_1^2 - c_2 e_2^2 + c_1 e_2\tilde{k}_{\omega_2}$$

Observe that $\dot{V}_L \leq 0$ if $\hat{k}_{\omega_2} \to k_\omega$. Therefore augmenting V_L, it yields

$$V_L = \frac{1}{2}\left(e_1^2 + \frac{1}{\gamma_1}\tilde{k}_{\omega_1}^2 + e_2^2 + \frac{1}{\gamma_2}\tilde{k}_{\omega_2}^2\right) \tag{4.13}$$

and

$$\dot{V}_L|_{\phi=\phi^c} = -c_1 e_1^2 - c_2 e_2^2 + \tilde{k}_{\omega_2}\left(c_1 e_2 - \frac{\dot{\hat{k}}_{\omega_2}}{\gamma_2}\right)$$

Choosing

$$\dot{\hat{k}}_{\omega_2} = \gamma_2 c_1 e_2$$

$\dot{V}_L$ becomes

$$\dot{V}_L = -c_1 e_1^2 - c_2 e_2^2 \tag{4.14}$$

The error representation of the closed-loop adaptive system is summarized below

$$\begin{bmatrix} \dot{e}_1 \\ \dot{e}_2 \end{bmatrix} = \begin{bmatrix} -c_1 & 1 \\ -1 & -c_2 \end{bmatrix} \begin{bmatrix} e_1 \\ e_2 \end{bmatrix} + \begin{bmatrix} \tilde{k}_{\omega_1} \\ c_1 \tilde{k}_{\omega_2} \end{bmatrix}$$

$$\begin{bmatrix} \dot{\hat{k}}_{\omega_1} \\ \dot{\hat{k}}_{\omega_2} \end{bmatrix} = \begin{bmatrix} \gamma_1 & 0 \\ 0 & c_1\gamma_2 \end{bmatrix} \begin{bmatrix} e_1 \\ e_2 \end{bmatrix} \tag{4.15}$$

4.4.3 Stability analysis

The stability of the equilibrium $(e_i, \tilde{k}_{\omega_i}) = 0$; $i = 1,\ 2$; follows from (4.13) and (4.14). From the LaSalle-Yoshizawa theorem [3] we have that e_i and $\hat{k}_{\omega_i}$ are bounded and $e_i, \tilde{k}_{\omega_i} \to 0$ as $t \to \infty$. From (4.8), it follows that $d \to d_{min}$. The boundedness of ψ follows from the boundedness of e_1, $\hat{k}_{\omega_1}$ and e_2 defined in (4.10). Observe that the convergence to zero of e_i does not imply the convergence to zero of ψ. From (4.10) it can be noted that ψ is bounded, i.e.

$$\lim_{t\to\infty} \psi = \arcsin\left(-\frac{\hat{k}_{\omega_1}}{V}\right) + \psi_s$$

Observe that from (4.15) it follows that $\dot{\hat{k}}_{\omega_i} \to 0$; $i = 1,\ 2$. Finally, from (4.12) we conclude that the control ϕ^c is also bounded.

LaSalle's invariance principle [4] assures that the state $(e_i, \tilde{k}_{\omega_i})$ converges to the largest invariant set M contained in $\{(e_1, e_2, \tilde{k}_{\omega_1}, \tilde{k}_{\omega_2}) \in \mathbb{R}^4 | \dot{V}_L = 0\}$. On this invariant set, we have $e_i \equiv 0$ and $\dot{e}_i \equiv 0$. From (4.15) it yields $\dot{\tilde{k}}_{\omega_i} = 0$ and $\tilde{k}_{\omega_i} = 0$. Thus, the largest invariant set M is

$$\begin{aligned} M =& \{(e_i, \tilde{k}_{\omega_i}) \in \mathbb{R}^4 | e_i = 0, \tilde{k}_{\omega_i} = 0\} \\ =& \{(d, \psi, \hat{k}_{\omega_1}, \hat{k}_{\omega_2}) \in \mathbb{R}^4 | (d, \psi, \hat{k}_{\omega_1}, \hat{k}_{\omega_2}) = (0, \arcsin(-\frac{\hat{k}_{\omega_1}}{V}) + \psi_s, k_\omega, k_\omega)\} \end{aligned}$$

The manifold M is the single point $d = 0$, $\psi = \arcsin(-\frac{\hat{k}_{\omega_1}}{V}) + \psi_s$, $\hat{k}_{\omega_i} = k_\omega$ for $i = 1$ and 2, which is asymptotically stable.

Remark: The model presented above assumes that the airplane is equipped with an autopilot which stabilizes the vehicle and provides roll-angle tracking capabilities. If the autopilot disposes of angular momentum tracking capabilities instead of roll angle, then the simplified model introduced by equations (3.21) needs to be used. Thus, employing the adaptive backstepping algorithm, the commanded yaw moment reads[1]

$$cN^c = -\bar{L}_1 r + \tan(\psi - \psi_s)(r^2 - \bar{L}_2) - \frac{\bar{L}_3 d + \bar{L}_4 \hat{k}_{\omega 1} + \bar{L}_5 \hat{k}_{\omega 2} + \bar{L}_6 \hat{k}_{\omega 3}}{V_a \cos(\psi - \psi_s)} \tag{4.16}$$

$$\begin{aligned}
\dot{\hat{k}}_{\omega 1} &= \bar{\gamma}_1 d && (4.17a)\\
\dot{\hat{k}}_{\omega 2} &= \bar{\gamma}_2 \bar{c}_1 \left(V \sin(\psi - \psi_s) + \bar{c}_1 d + \hat{k}_{\omega 1} \right) && (4.17b)\\
\dot{\hat{k}}_{\omega 3} &= \bar{\gamma}_3 \bar{L}_6 V \left[r \cos(\psi - \psi_s) + (\bar{c}_1 + \bar{c}_2) \sin(\psi - \psi_s) \right] \\
&\quad + \bar{\gamma}_3 \bar{L}_6 \left[d\bar{L}_6 + \bar{c}_1 \hat{k}_{\omega 2} + \bar{c}_2 \hat{k}_{\omega 1} \right] && (4.17c)
\end{aligned}$$

where $\bar{L}_1 = \bar{c}_1 + \bar{c}_2 + \bar{c}_3$, $\bar{L}_2 = \bar{c}_1\bar{c}_2 + \bar{c}_1\bar{c}_3 + \bar{c}_2\bar{c}_3 + 2 + \bar{\gamma}_1 + \bar{c}_1^2\bar{\gamma}_2$, $\bar{L}_3 = \bar{c}_1 + \bar{c}_3 + \bar{c}_1\bar{c}_2\bar{c}_3 + \bar{\gamma}_1(\bar{c}_2 + \bar{c}_3)$, $\bar{L}_4 = \bar{c}_2\bar{c}_3 + \bar{c}_1^2\bar{\gamma}_2 + 1$, $\bar{L}_5 = \bar{c}_1\bar{c}_3$, $\bar{L}_6 = \bar{c}_1\bar{c}_2 + \bar{\gamma}_1 + 1$ with $\bar{c}_1, \bar{c}_2, \bar{c}_3, \bar{\gamma}_1, \bar{\gamma}_2, \bar{\gamma}_3 > 0$.

The choice of the adaptation laws given by equations (4.17) has been made so that the derivative of the Lyapunov function

$$\bar{V}_L = \frac{1}{2}\left[\bar{\epsilon}^T I \bar{\epsilon} + \tilde{\omega}^T I_\gamma \tilde{\omega} \right]$$

with

$$\bar{\epsilon} = \begin{bmatrix} \bar{e}_1 \\ \bar{e}_2 \\ \bar{e}_3 \end{bmatrix} = \begin{bmatrix} d \\ V \sin(\psi - \psi_s) + \bar{c}_1 \bar{e}_1 + \hat{k}_{\omega 1} \\ rV \cos(\psi - \psi_s) + (\bar{c}_1 + \bar{c}_2)\bar{e}_2 + (1 - \bar{c}_1^2 + \bar{\gamma}_1)\bar{e}_1 \\ + \bar{c}_1 \left(\hat{k}_{\omega 2} - \hat{k}_{\omega 1} \right) \end{bmatrix}$$

[1]For a detailed description of the controller 4.16 see Appendix B.

$$\tilde{\omega}_E = k_\omega \quad - \quad \hat{k}_\omega = \begin{bmatrix} k_\omega - \hat{k}_{\omega_1} \\ k_\omega - \hat{k}_{\omega_2} \\ k_\omega - \hat{k}_{\omega_3} \end{bmatrix}$$

$$I_\gamma \quad = \quad \begin{bmatrix} \frac{1}{\gamma_1} & 0 & 0 \\ 0 & \frac{1}{\gamma_2} & 0 \\ 0 & 0 & \frac{1}{\gamma_3} \end{bmatrix}$$

to be always negative, which proves the stability of the closed-loop adaptive system, hence the boundedness and the convergence of $d \to 0$ and of $\hat{k}_{\omega_i} \to k_\omega$, $i = 1, 2, 3$.

4.5 Wind estimation with minimum-order design

The main deficiency of the resulting adaptive system consisting of equations (3.5) with control law (4.12) and update laws (4.15) is the increased dynamic order of the closed-loop system despite the cross track error regulation even in presence of unknown wind. The overparametrization, i.e. more than one update law for each parameter, can be avoided by using the tuning functions method [3]. Instead of using two adaptation laws for the unknown wind (as it was the case in the previous design), this approach reduces the dynamic order of the adaptive controller to its minimum.

Consider the system (3.5) with the design objective being the convergence of the cross track error d to a minimum allowed distance from the path, d_{min}. Therefore, the following error variable is defined

$$e_1 = d - d_{min} \tag{4.18}$$

Thus,

$$\dot{e}_1 = V \sin(\psi - \psi_s) + k_\omega \tag{4.19}$$

4.5.1 Regulation of e_1

Propose the following positive function

$$V_{L_1} = \frac{1}{2}e_1^2$$

thus

$$\dot{V}_{L_1} = e_1 \left[V \sin\left(\psi - \psi_s\right) + k_\omega \right] \tag{4.20}$$

define the second error as

$$e_2 \;\; = \;\; V \sin\left(\psi - \psi_s\right) - V \sin\left(\psi^v - \psi_s\right) \tag{4.21}$$

where ψ^v defines the virtual control with the form

$$V \sin\left(\psi^v - \psi_s\right) = -c_1 e_1 - \hat{k}_\omega$$

with $\hat{k}_\omega$ an estimate of k_ω and $c_1 > 0$ a constant. Then, (4.21) becomes

$$e_2 \;\; = \;\; V \sin\left(\psi - \psi_s\right) + c_1 e_1 + \hat{k}_\omega \tag{4.22}$$

Rewriting (4.19)

$$\dot{e}_1 = e_2 - c_1 e_1 + \tilde{k}_\omega$$

where $\tilde{k}_\omega = k_\omega - \hat{k}_\omega$. Hence, (4.20) yields

$$\dot{V}_{L_1} = -c_1 e_1^2 + e_1 e_2 + e_1 \tilde{k}_\omega$$

Notice from the above equation that if $\hat{k}_\omega \to k_\omega$ and $e_2 \to 0$ then $\dot{V}_{L_1} \leq 0$ and this implies that $e_1 \to 0$.

In order to converge $\tilde{k}_\omega \to 0$, propose the following positive function

$$V_{L_2} = \frac{1}{2\gamma}\tilde{k}_\omega^2$$

where $\gamma > 0$ is a constant adaptation gain. Then

$$\dot{V}_{L_2} = -\frac{\dot{\hat{k}}_\omega}{\gamma}\tilde{k}_\omega$$

Define the following tuning function

$$\tau_1 = \gamma e_1 \tag{4.23}$$

Thus

$$\dot{V}_{L_1} + \dot{V}_{L_2} = -c_1 e_1^2 + e_1 e_2 + \left(\tau_1 - \dot{\hat{k}}_\omega\right)\frac{\tilde{k}_\omega}{\gamma}$$

4.5.2 Regulation of e_2

From (4.22), it follows that

$$\dot{e}_2 = g\cos(\psi - \psi_s)\tan\phi^c + c_1 e_2 - c_1^2 e_1 + c_1\tilde{k}_\omega + \dot{\hat{k}}_\omega$$

Consider the following positive function

$$V_{L_3} = \frac{1}{2}e_2^2$$

Taking the time derivative leads to

$$\dot{V}_{L_3} = e_2\left[g\cos(\psi - \psi_s)\tan\phi^c + c_1 e_2 - c_1^2 e_1 + c_1\tilde{k}_\omega + \dot{\hat{k}}_\omega\right]$$

Observe in the above equation the term $\tilde{k}_\omega$. To reduce the adaptive error, we introduce the second tuning function of the form

$$\tau_2 = \tau_1 + \gamma c_1 e_2 \tag{4.24}$$

Finally, define the Lyapunov function

$$V_L = V_{L_1} + V_{L_2} + V_{L_3} = \frac{1}{2}\left(e_1^2 + \frac{1}{\gamma}\tilde{k}_\omega^2 + e_2^2\right) \tag{4.25}$$

thus

$$\begin{aligned}\dot{V}_L = &- c_1 e_1^2 + \frac{\tilde{k}_\omega}{\gamma}(\tau_2 - \dot{\hat{k}}_\omega) + e_2\left(\dot{\hat{k}}_\omega - \tau_2\right) \\ &+ e_2\left[g\cos(\psi - \psi_s)\tan\phi^c + \tau_2 + c_1 e_2 + (1 - c_1)e_1\right]\end{aligned}$$

Proposing the commanded bank angle as

$$\phi^c = \tan^{-1}\left[\frac{L_1 e_1 + L_2 e_2}{g\cos(\psi - \psi_s)}\right] \tag{4.26}$$

and the update law

$$\dot{\hat{k}}_\omega = \tau_2 \tag{4.27}$$

consequently, it follows that

$$\dot{V}_L = -c_1 e_1^2 - c_2 e_2^2 \tag{4.28}$$

where $L_1 = c_1^2 - 1 - \gamma$ and $L_2 = -c_1 - c_2 - c_1\gamma$.

The error system representation of the resulting closed-loop adaptive system is summarized below

$$\begin{aligned}\dot{e}_1 &= -c_1 e_1 + e_2 + \tilde{k}_\omega \\ \dot{e}_2 &= -e_1 - c_2 e_2 + c_1\tilde{k}_\omega \\ \dot{\tilde{k}}_\omega &= -\gamma e_1 - \gamma c_1 e_2\end{aligned}$$

Rewriting (4.26) and (4.27) in terms of d and ψ we have

$$\phi^c = \tan^{-1}\left[\frac{L_3(d - d_{min}) + L_2 V\sin(\psi - \psi_s) + L_2\hat{k}_\omega}{g\cos(\psi - \psi_s)}\right]$$

and

$$\dot{\hat{k}}_\omega = L_4(d - d_{min}) + \gamma c_1 V \sin(\psi - \psi_s) + \gamma c_1 \hat{k}_\omega$$

with $L_3 = L_1 + c_1 L_2$ and $L_4 = \gamma + \gamma c_1$.

4.5.3 Stability analysis

Notice that, the stability of the equilibrium $(e_i, \tilde{k}_\omega) = 0$ follows from (4.25) and (4.28). (4.28) implies that $V_L \leq 0$ and from the LaSalle-Yoshizawa theorem [4] we have that e_i and $\hat{k}_\omega$ are bounded and $e_i,\ \tilde{k}_\omega \to 0$ as $t \to \infty$; $i = 1, 2$. From (4.18), it follows that $d \to d_{min}$. The boundedness of ψ follows from the boundedness of e_1, $\hat{k}_\omega$ and e_2 defined in (4.22). Observe that the convergence to zero of e_i does not imply the convergence to zero of ψ. From (4.22) it can be noted that ψ is bounded, i.e.

$$\lim_{t\to\infty} \psi = \arcsin\left(-\frac{\hat{k}_\omega}{V}\right) + \psi_s$$

Observe that from (4.23), (4.24) and (4.27) it follows that $\dot{\hat{k}}_\omega, \tau_i \to 0$; $i = 1, 2$. Finally from (4.26), we conclude that the control ϕ^c is also bounded.

LaSalle's invariance principle [4] assures that the state $(e_i, \tilde{k}_\omega)$ converges to the largest invariant set M contained in $\{(e_1, e_2, \tilde{k}_\omega) \in \mathbb{R}^3 | \dot{V}_L = 0\}$. On this invariant set, we have $e \equiv 0$ and $\dot{e} \equiv 0$. From (4.27) it yields $\dot{\tilde{k}}_\omega = 0$ and $\tilde{k}_\omega = 0$. Thus, the largest invariant set M is

$$\begin{aligned} M &= \{(e, \tilde{k}_\omega) \in \mathbb{R}^3 | e = 0, \tilde{k}_\omega = 0\} \\ &= \{(d, \psi, \hat{k}_\omega) \in \mathbb{R}^3 | \\ &\quad (d, \psi, \hat{k}_\omega) = (0, \arcsin(-\frac{k_\omega}{V}) + \psi_s, k_\omega)\} \end{aligned}$$

The manifold M is the single point $d = 0, \psi = \arcsin(-\frac{k_\omega}{V}) + \psi_s, \hat{k}_\omega = k_\omega$ which is asymptotically stable.

For a perturbed system it is very important to estimate if not delimitate the region of attraction of its equilibrium points. Equation (4.22) can be rewritten as

$$e_2 = V \sin\psi + e_1 + \left(\hat{k}_\omega - k_\omega\right) + k_\omega$$

Thus

$$|V \sin\psi| \leq |e_2| + |e_1| + |\tilde{k}_\omega| + |k_\omega| \tag{4.29}$$

From the proposed Lyapunov function we can write the inequalities

$$\begin{aligned}
\frac{1}{2}e_1^2 &\leq V_L \leq V(0) \Rightarrow |e_1| \leq \sqrt{2V(0)} \\
\frac{1}{2}e_2^2 &\leq V_L \leq V(0) \Rightarrow |e_2| \leq \sqrt{2V(0)} \\
\frac{1}{2}\tilde{k}_\omega^2 &\leq V_L \leq V(0) \Rightarrow |\tilde{k}_\omega| \leq \sqrt{2V(0)}
\end{aligned}$$

Using the above and (4.29) we can write

$$|\sin\psi| \leq \frac{3\sqrt{2V(0)}}{V} + \frac{|k_\omega|}{V}$$

To remove the singularities we impose $|\sin\psi| < 1$. Therefore, the region of attraction is $\frac{|k_\omega|}{V} \leq 1 - \varepsilon$, where $\varepsilon = 3\sqrt{2V(0)}$.

Remark: The model presented above assumes that the airplane is equipped with an autopilot which stabilizes the vehicle and provides roll-angle tracking capabilities. If the autopilot disposes of angular momentum tracking capabilities instead of roll angle, then the simplified model introduced by equation (3.21) needs to be used.

Introducing the error variables

$$\begin{aligned}
\underline{e}_1 &= d - d_{min} \\
\underline{e}_2 &= V \sin\psi - V \sin\psi^v \\
\underline{e}_3 &= Vr \cos\psi - Vr^v \cos\psi
\end{aligned}$$

where ψ^v and r^v are stabilizing functions given by

$$\begin{aligned} V \sin \psi^v &= -\underline{c}_1 \underline{e}_1 - \hat{w}_E \\ V r^v \cos \psi &= -\left(\underline{c}_1 + \underline{c}_2 + \gamma \underline{c}_1\right) \underline{e}_2 - \left(1 - \underline{c}_1^2 + \gamma\right) \underline{e}_1 \end{aligned}$$

one can verify that the adaptive controller consisting of the feedback control and of the parameter update law given by[2]

$$c\tau_\psi = -\underline{L}_1 r + \tan\psi(r^2 - \underline{L}_2) - \frac{\underline{L}_3 d + \underline{L}_2 \hat{w}_E}{V_a \cos\psi} \tag{4.30a}$$

$$\dot{\hat{w}}_E = \tau_3 \tag{4.30b}$$

with the tuning function obtained from

$$\begin{aligned} \tau_1 &= \gamma \underline{e}_1 \\ \tau_2 &= \tau_1 + \gamma \underline{c}_1 \underline{e}_2 \\ \tau_3 &= \tau_2 + \gamma \left[\underline{c}_1 \left(\gamma \underline{c}_1 + \underline{c}_2\right) + 1 + \gamma\right] \underline{e}_3 \end{aligned}$$

and the coefficients

$$\begin{aligned} \underline{L}_1 &= \underline{c}_3 + \left(\underline{c}_1 + \underline{c}_2 + \gamma \underline{c}_1\right)\left(1 + \gamma + \gamma^2 + \gamma^2 \underline{c}_1^2 + \gamma \underline{c}_1 \underline{c}_2\right) \\ \underline{L}_2 &= 2\left(1 + \gamma\right) + \gamma^2\left(1 + \underline{c}_1^2\right) - \left(\underline{c}_1^2 + \underline{c}_1 \underline{c}_2 + \underline{c}_2^2 + \gamma\right) + \underline{L}_1\left(\underline{c}_1 + \underline{c}_2 + \gamma \underline{c}_1\right) \\ \underline{L}_3 &= c_1 \gamma^2\left(1 + \underline{c}_1^2\right) - \underline{c}_2\left(1 + \underline{c}_1 + \underline{c}_2\right) + \underline{L}_1\left(1 + \gamma + \underline{c}_1 \underline{c}_2 + \gamma \underline{c}_1^2\right) \end{aligned}$$

guarantees the asymptotic stability of the equilibrium $(e_i, \tilde{k}_\omega) = (0, 0)$ through the Lyapunov function

$$\underline{V}_L = \frac{1}{2}\left(\underline{e}_1^2 + \frac{1}{\gamma}\tilde{w}_E^2 + \underline{e}_2^2 + \underline{e}_3^2\right)$$

and its derivative

$$\dot{\underline{V}}_L = -\underline{c}_1 \underline{e}_1^2 - \underline{c}_2 \underline{e}_2^2 - \underline{c}_3 \underline{e}_3^2 \ .$$

[2]For a detailed description of the controller 4.30 see Appendix C.

4.6 Simulation results and performance analysis

The performance of the wind computation methods has been evaluated in simulations along with the developed path following controllers and relevant results are further presented. The airplane velocity relative to the air was considered constant and equal to 10 m/s, the bank angle was limited to a maximum value of 45° while the low-altitude/low-turbulence dryden gust model, shown in Figure $3-6$, was added to simulate the environmental wind.

4.6.1 Path following based on computed wind

First simulations were carried out in order to test the capabilities of the wind computation methods introduced in Sections 4.2.2 and 4.2.3. For this reason, the path following application formulated in the previous chapter, for which a stabilizing controller was designed in equation (3.20), has been considered. The airplane was commanded to follow the north direction based on the developed controller and employing successively the values of the wind computed in equations (4.3), (4.5) and (4.6). The error analysis developed in Section 4.2.4 will be used in order to quantify the overall uncertainty of the computed wind for the studied case.

Based on the wind triangle

Let us first discuss the precision of the wind estimation algorithm for the path following application introduced in the previous chapter. Remember that several assumptions have been considered in order to derive the simplified equations (3.5) which describe the flight in horizontal plane, stabilized longitudinal variables and truly banked turn. Introducing these assumptions in the velocity vectors diagram based computed wind given in equations (4.3), the wind components in the direction of the (E, N) axes of the inertial frame simplify to

$$w_e = v_e - V_a \sin\psi \tag{4.31a}$$

$$w_n = v_n - V_a \cos\psi \tag{4.31b}$$

where v_e, v_n, V_a and ψ are measured quantities whose uncertainties σ, provided by manufacturers, are summarized in Table 4.1.

The Jacobian of the simplified wind equations (4.31) reads

$$H_w = \begin{bmatrix} 1 & 0 & -\sin\psi & -V_a\cos\psi \\ 0 & 1 & -\cos\psi & V_a\sin\psi \end{bmatrix}$$

and the covariance of the expected noise and of the expected error in the wind velocity estimate are given by

$$\begin{aligned} \Sigma_x &= diag\left(\sigma_{v_e}^2\ \sigma_{v_n}^2\ \sigma_{V_a}^2\ \sigma_\psi^2\right) \\ \Sigma_w &= H_w \Sigma_x H_w^T \end{aligned}$$

After computations, Σ_w reads

$$\Sigma_w = \begin{bmatrix} \sigma_{v_e}^2 + \sigma_{V_a}^2\sin^2\psi + V_a^2\sigma_\psi^2\cos^2\psi & \sigma_{V_a}^2\sin\psi\cos\psi - V_a^2\sigma_\psi^2\sin\psi\cos\psi \\ \sigma_{V_a}^2\sin\psi\cos\psi - V_a^2\sigma_\psi^2\sin\psi\cos\psi & \sigma_{v_n}^2 + \sigma_{V_a}^2\cos^2\psi + V_a^2\sigma_\psi^2\sin^2\psi \end{bmatrix}$$

The error in the wind estimates can be evaluated computing the *trace* of the covariance matrix

$$e_w^2 \ = \ Tr\Sigma_w \ = \ \sigma_{v_e}^2 + \sigma_{v_n}^2 + \sigma_{V_a}^2 + V_a^2\sigma_\psi^2 \tag{4.32}$$

Equation (4.32) shows that the airspeed is a critical parameter in reducing the estimates error of the wind speed, together with the noise in sensor measurements. Minimizing the error in the computed wind requires flying at low airspeed as shown in Figures $(4-4)$ - $(4-9)$. .

Sensor	Measured quantity	Provided uncertainty
Pitot tube	Airspeed	$\sigma_{V_a} = 0.2$
GPS	Inertial velocity	$\sigma_{v_e} = \sigma_{v_n} = 0.1$
GPS	Inertial position	$\sigma_{p_e} = \sigma_{p_n} = 2.5$
IMU	Heading	$\sigma_\psi = 0.5$

Table 4.1: Sensors uncertainty.

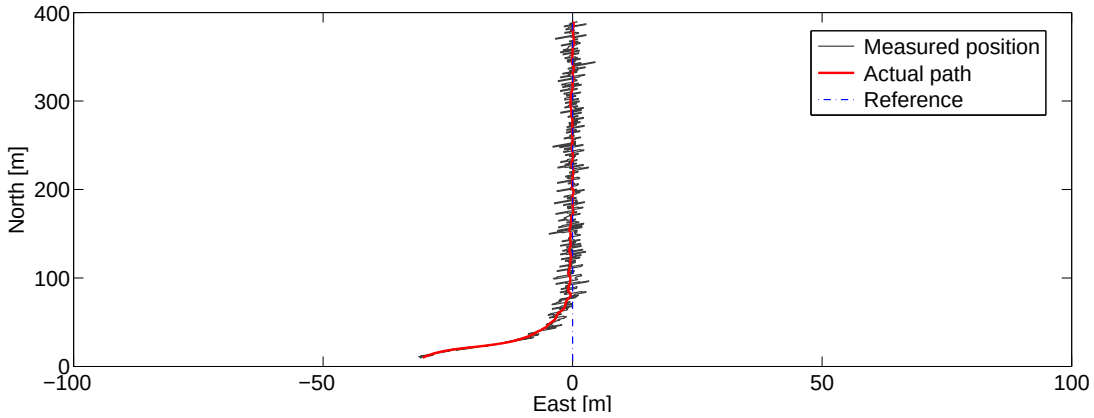

Figure 4-4: Airplane inertial position when computing wind from the wind triangle and $V_a = 10$ m/s.

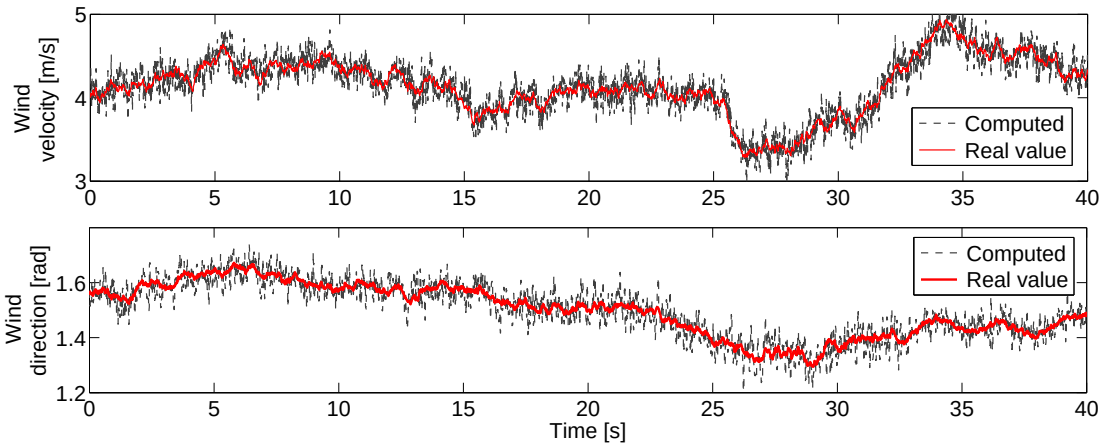

Figure 4-5: Computed wind from the velocity vectors diagram for $V_a = 10$ m/s.

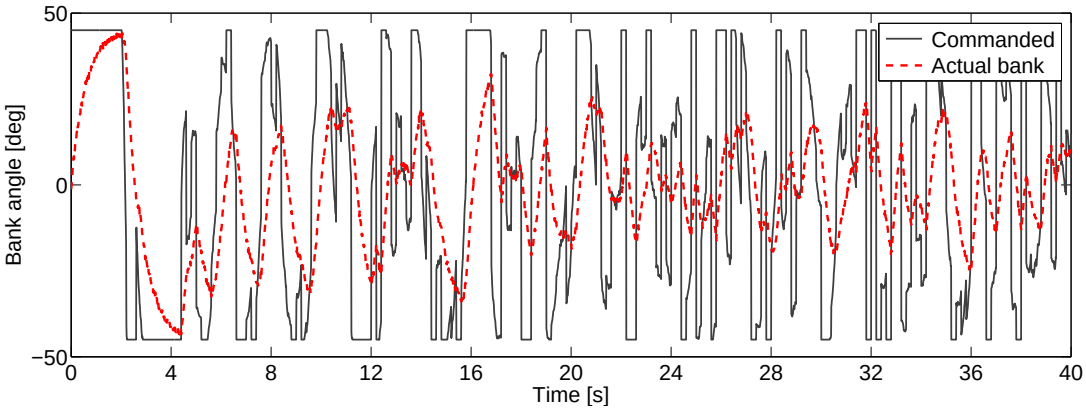

Figure 4-6: Control effort for the path following application based on computed wind for $V_a = 10$ m/s.

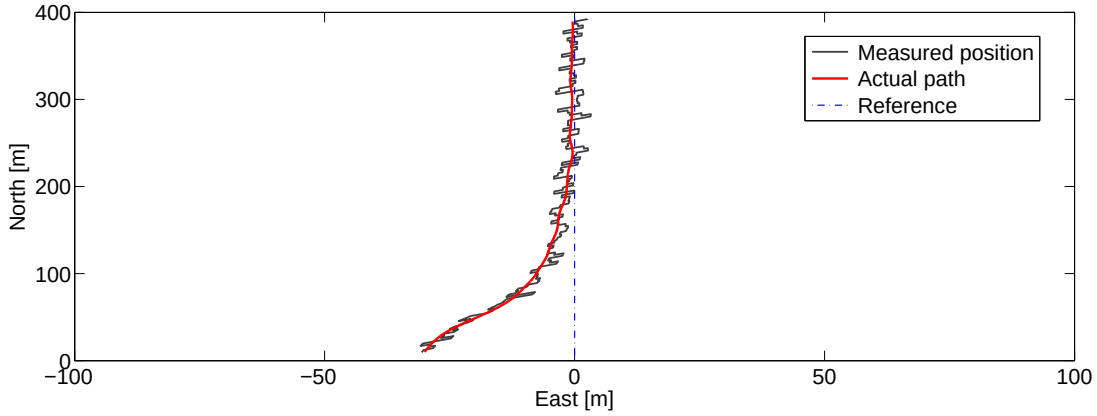

Figure 4-7: Airplane inertial position when computing wind from the wind triangle and $V_a = 30$ m/s.

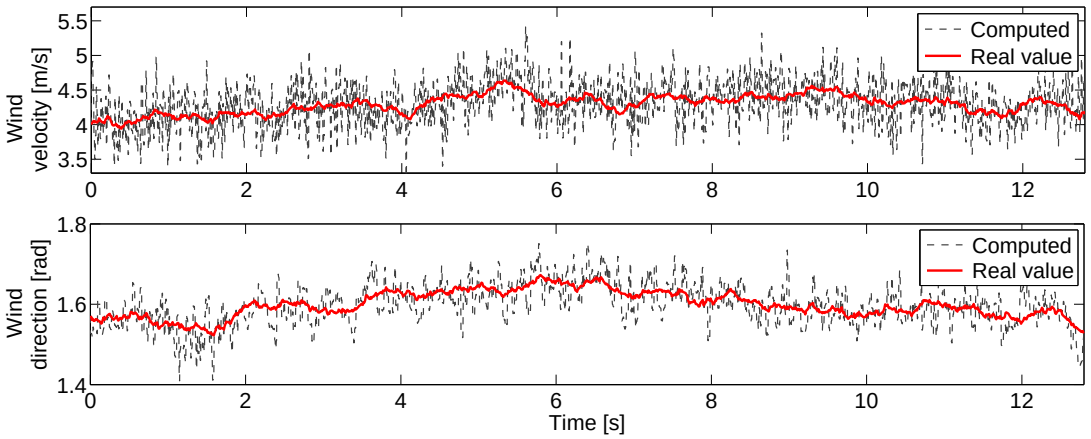

Figure 4-8: Computed wind from the velocity vectors diagram for $V_a = 30$ m/s.

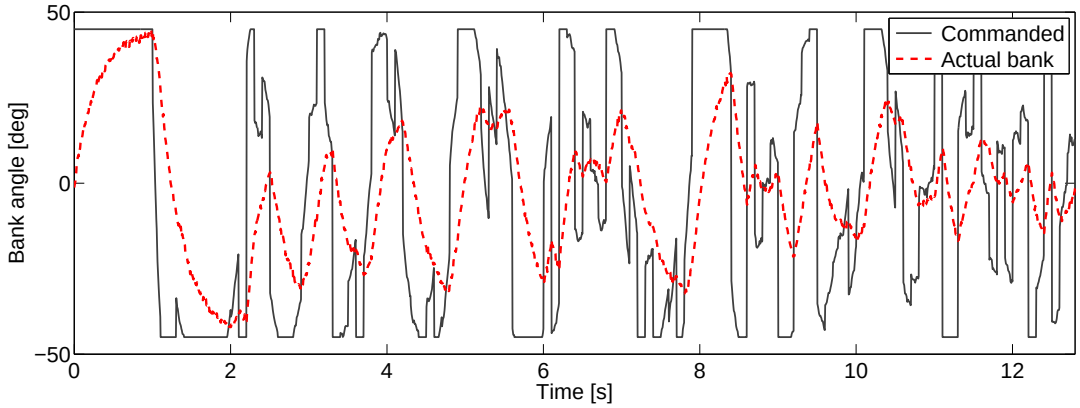

Figure 4-9: Control effort for the path following application based on computed wind for $V_a = 30$ m/s.

Based on vehicle response and velocity measurements

Developing equation (4.5) for the considered assumptions, we get the relationships for the wind components in the inertial coordinate system

$$w_e = v_e^{SEN} - V_a^{AP} \sin \psi^{AP} \tag{4.33a}$$

$$w_n = v_n^{SEN} - V_a^{AP} \cos \psi^{AP} \tag{4.33b}$$

where v_e^{SEN} and v_n^{SEN} are measured quantities provided by a GPS sensor and V_a^{AP} and ψ^{AP} are predictions provided by the autopilot system based on the aircraft dynamic model.

The way the terms of equations (4.31) and (4.33) are obtained represents the only difference between the two wind computation methods for the simplified case studied here. The precision of the vehicle response based approach depends on the accuracy of the equations to describe the dynamic behavior of the vehicle, which is difficult to quantify. Therefore, the analysis concerning the error in the wind estimates can not be further continued. Simulations based on this method are presented in Figures $(4-10)$ - $(4-12)$.

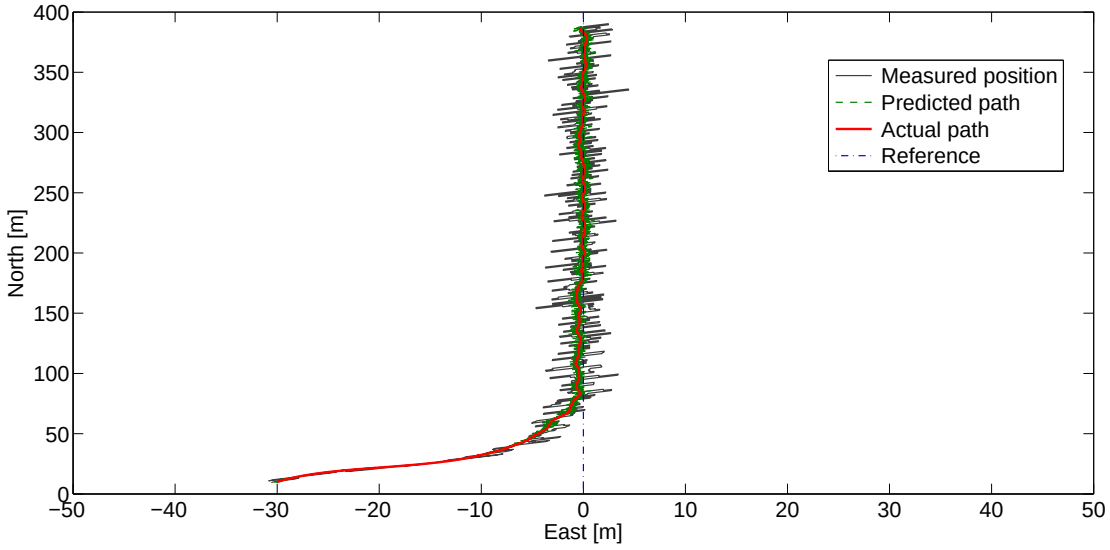

Figure 4-10: Airplane inertial position when computing wind from the vehicle response and velocity measurements.

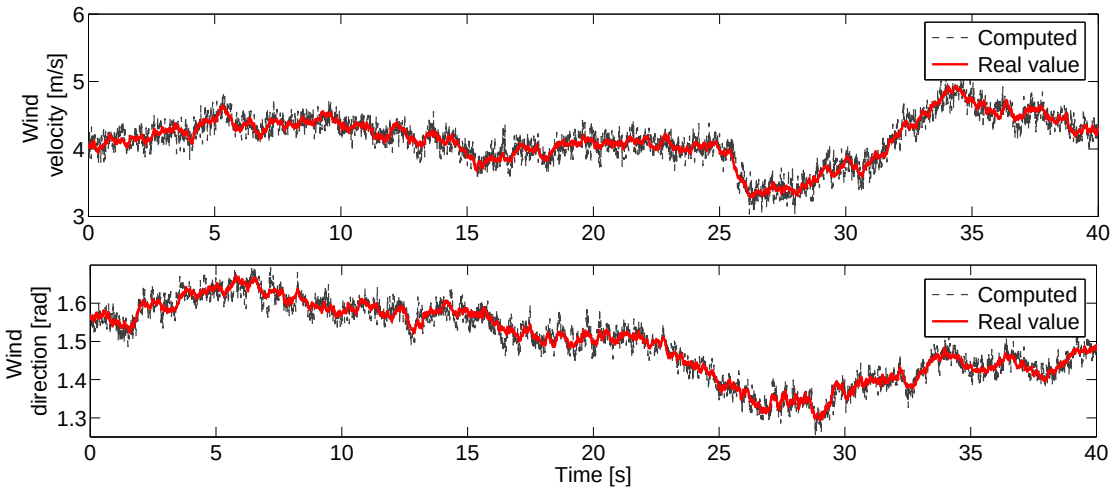

Figure 4-11: Computed wind from the vehicle response and velocity measurements.

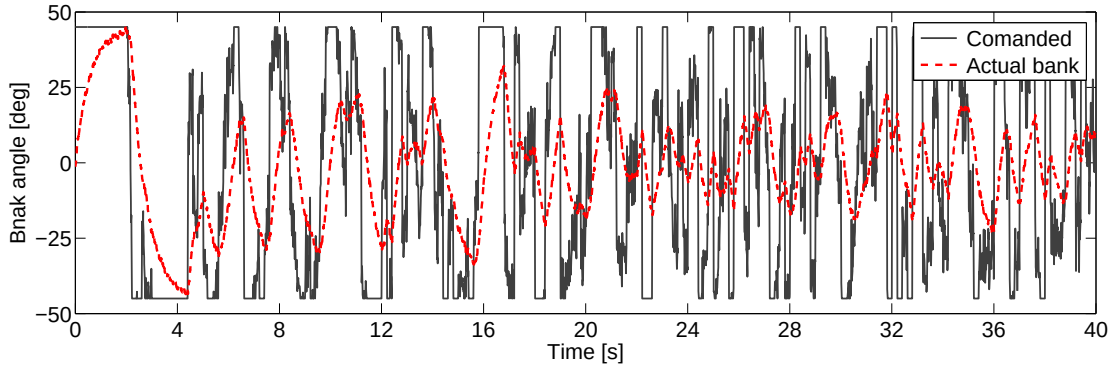

Figure 4-12: Control effort for the path following application based on computed wind from the vehicle response and velocity measurements.

Based on vehicle response and position measurements

In order to emphasize the wind computation method based on inertial position measurements, let us write the equations (3.5) in discrete form using a forward Euler integration.

Thus, it yields

$$\begin{aligned} x_{e_k} &= x_{e_{k-1}} + \Delta T \left(V_a \sin \psi_{k-1} + w_{e_{k-1}} \right) \\ y_{n_k} &= y_{n_{k-1}} + \Delta T \left(V_a \cos \psi_{k-1} + w_{n_{k-1}} \right) \\ \psi_k &= \psi_{k-1} + \Delta T \frac{g}{V_a} \tan \phi_{k-1} \\ \phi_k &= \phi_{k-1} + \Delta T k_\phi (\phi^c_{k-1} - \phi_{k-1}) \end{aligned}$$

According to equation (4.6), the wind speed components along the x_e and y_n axes are given by

$$\begin{aligned} w_{e_{k-1}} &= \frac{1}{\Delta T}\left(x_{e_k} - x_{e_{k-1}}\right) - V_a \sin\psi_{k-1} \\ w_{n_{k-1}} &= \frac{1}{\Delta T}\left(y_{n_k} - y_{n_{k-1}}\right) - V_a \cos\psi_{k-1} \end{aligned}$$

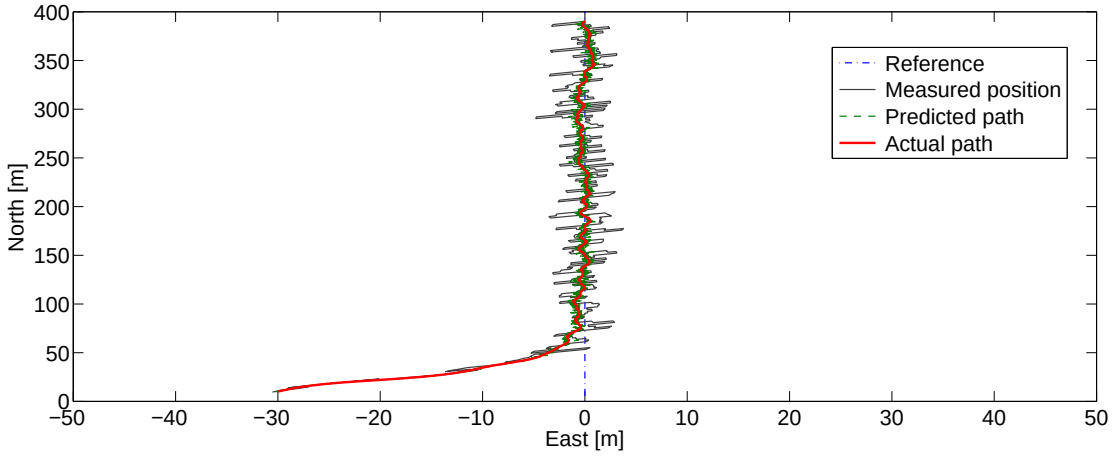

Figure 4-13: Airplane inertial position when computing wind from the vehicle response and position measurements.

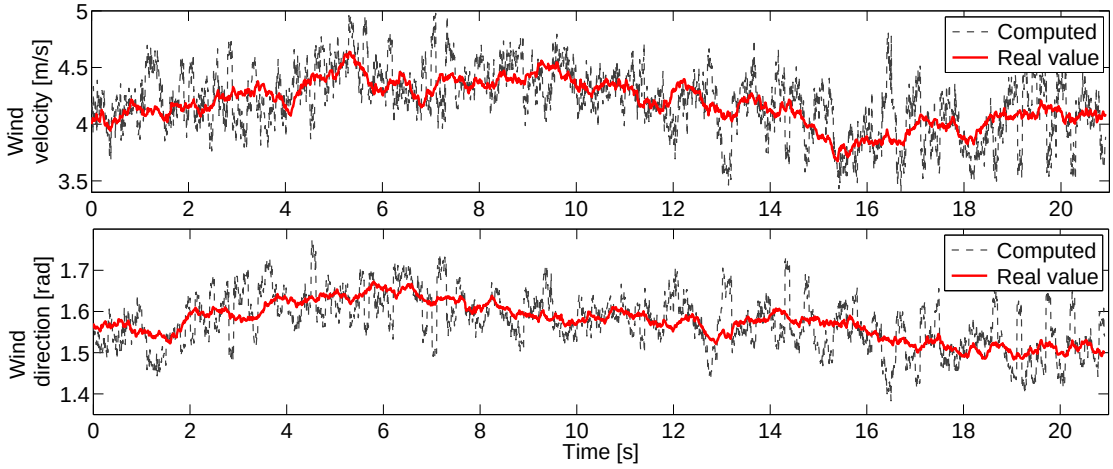

Figure 4-14: Computed wind from the vehicle response and position measurements.

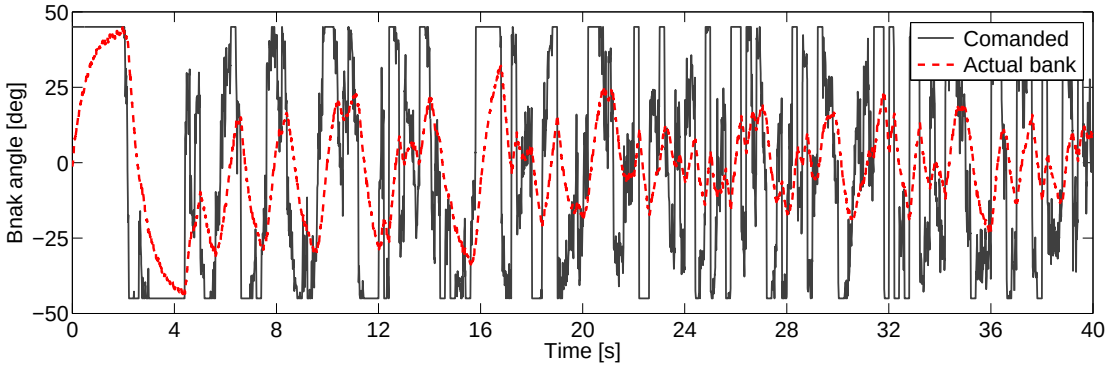

Figure 4-15: Control effort for the path following application based on computed wind from the vehicle response and position measurements.

4.6.2 Adaptive backstepping with overparametrization

Waypoint guidance

In order to test the performance of the closed loop adaptive system consisting of the flight controller (4.12) and adaptation laws (4.15), the same "waypoint guidance" scenario introduced in Chapter 3 was considered. The airplane response when commanded to fly between geo-referenced points is shown in figures 4-16.

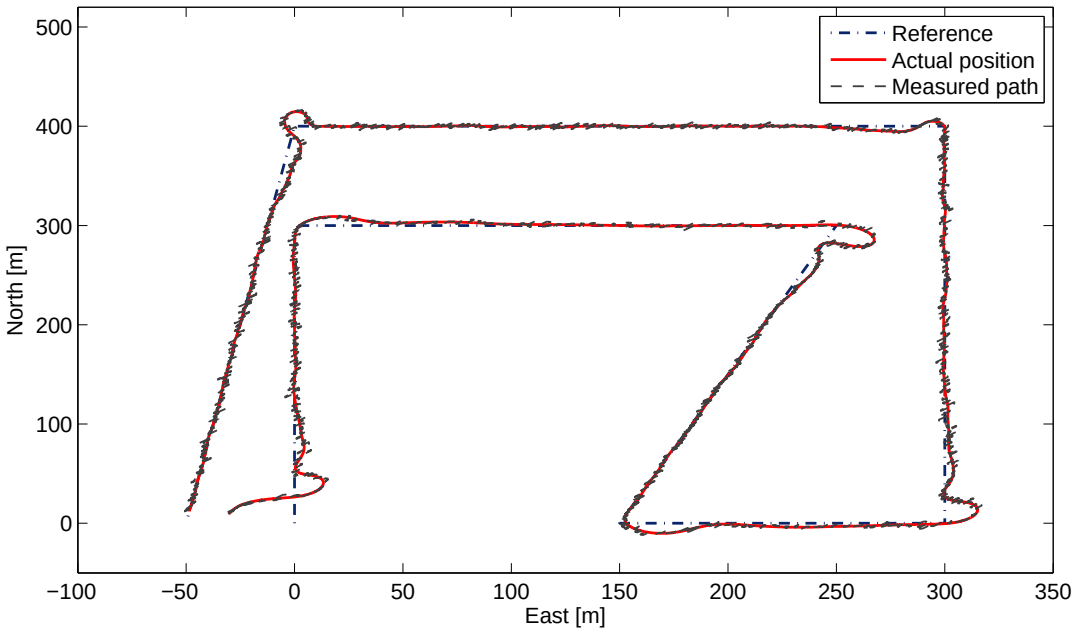

Figure 4-16: Earth relative path when flying in unknown wind.

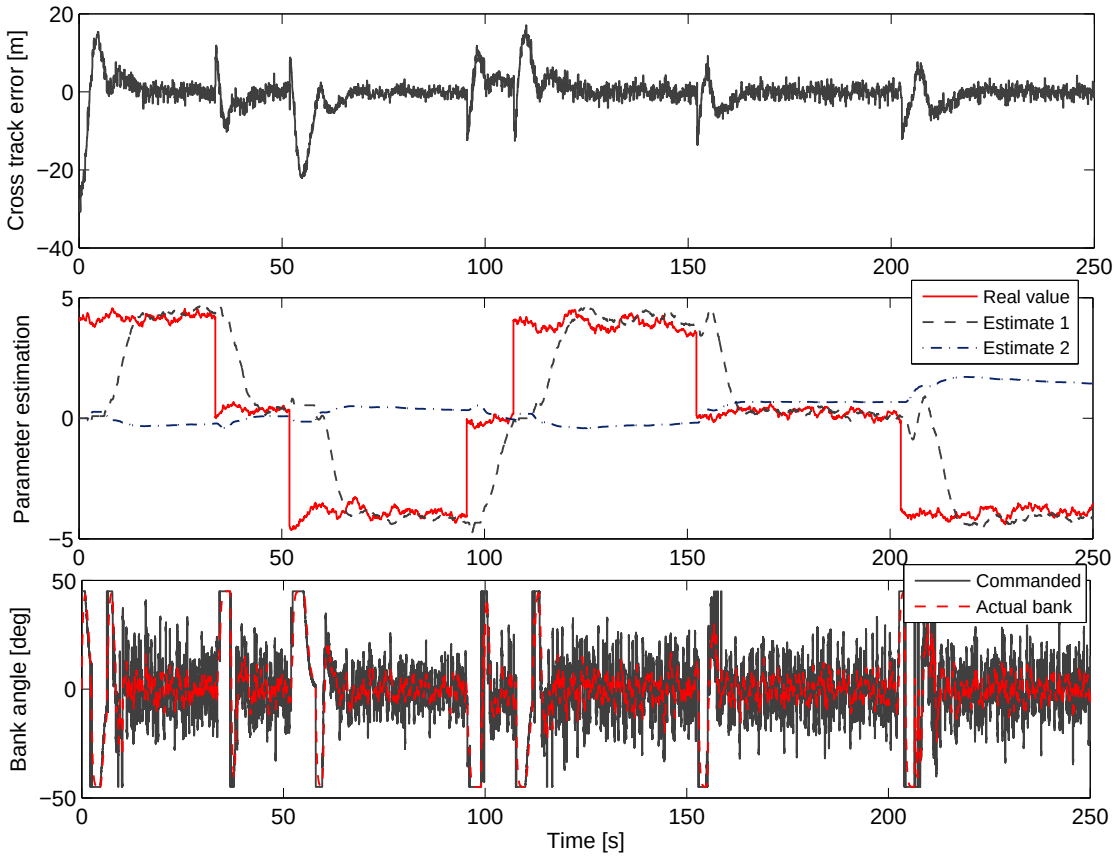

Figure 4-17: Flight parameters when flying between predefined waypoints in unknown wind.

4.6.3 Tuning functions adaptive backstepping

Waypoint guidance

First simulations were performed to test the capabilities of the controller to navigate in unknown wind between a series of predefined waypoints. Figure 4-18 illustrates the ground track of the airplane when commanded to fly the first scenario. The flight controller recovers the airplane from the initial cross track error of 30 m, see Figure 4-19, and it manages to maintain the course of the first segment flying with lateral wind. When the aircraft flies the second segment it encounters a tail wind while, for the third segment, the wind has a cross side component almost equally with the tailwind component.

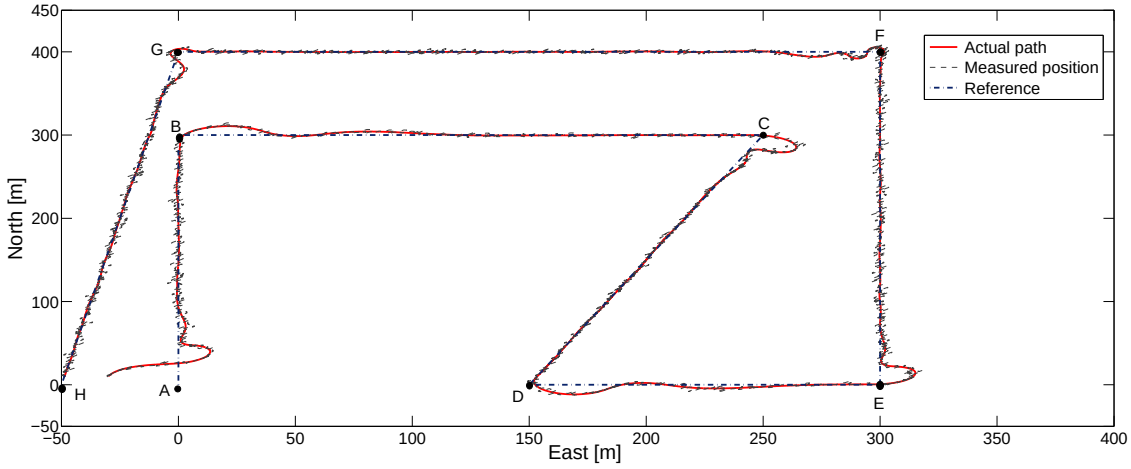

Figure 4-18: Airplane inertial position when flying between predefined waypoints in unknown wind.

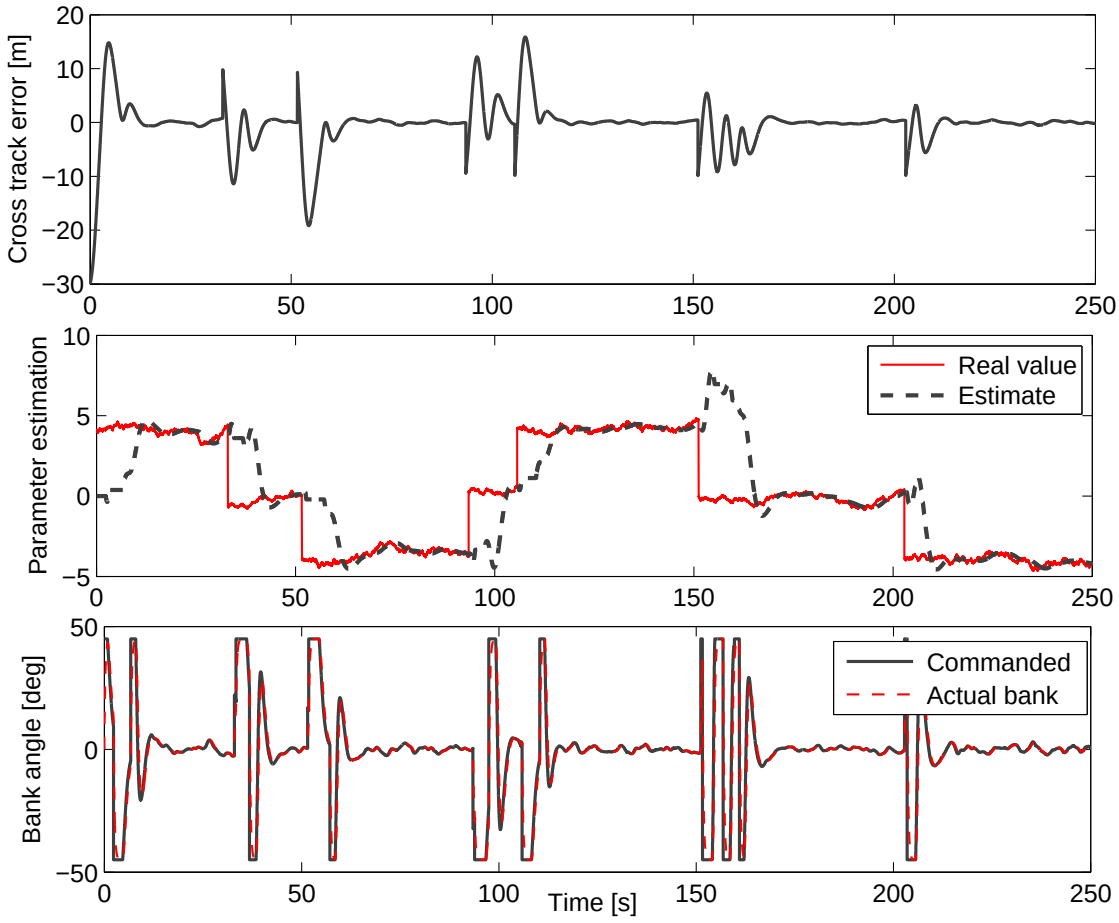

Figure 4-19: Flight parameters when flying between predefined waypoints in unknown wind.

Notice from Figure 4-19a that the controller developed in equation (4.26) is able to provide cross track error regulation due to the adaptation law presented in (4.27). For this case the closed-loop adaptive system shows good response even in presence of unknown disturbance. The proposed adaptation law employs one estimate for the unknown parameter whose convergence to its real value is guaranteed in a relatively short time, see Figure 4-19b. The adaptation law is used to estimate the value of $k_\omega = W\sin(\psi_w - \psi_s)$, which varies depending on ψ_s and on changes in wind parameters. The control effort is illustrated in Figure Figure 4-19c.

Wind influence on inertial track

The second scenario envisaged was to command different courses for the airplane, each course flown the same period of time. If there were no wind and excluding the transient errors from the turns, the ground course would be the same as the heading and the airplane would fly several line segments of the same length. On the other hand, flying in wind requires the autopilot to provide a drift correction, which is usually obtained heading the airplane into the wind while following a desired ground track. In this way, the length of the flown segments is different depending on the relation between the course of the segment and the wind direction and speed.

The performance of the airplane when commanded to fly this scenario is illustrated in Figure 4-20. Notice from the figure that the wind plays an important role for the path that the airplane traces over the ground. It navigates a maximum inertial distance of $\approx$ 275m when flying with a wind blowing in the direction of motion (the distances from A to B and from E to F). Next, it covers an average of $\approx$ 220m from B to C and from D to E, when still flying with a tail wind but also with crosswind. Finally, when the wind blows against the direction of travel, the airplane tracks the smallest distance over the ground ($\approx$ 125m from C to D and from F to G).

$t_0 = 0\text{s} \mapsto \chi = 0^\circ$; $t_1 = 20\text{s} \mapsto \chi = 90^\circ$; $t_2 = 40\text{s} \mapsto \chi = 180^\circ$;
$t_3 = 60\text{s} \mapsto \chi = 90^\circ$; $t_4 = 80\text{s} \mapsto \chi = 0^\circ$; $t_5 = 100\text{s} \mapsto \chi = -90^\circ$

Table 4.2: The course to follow

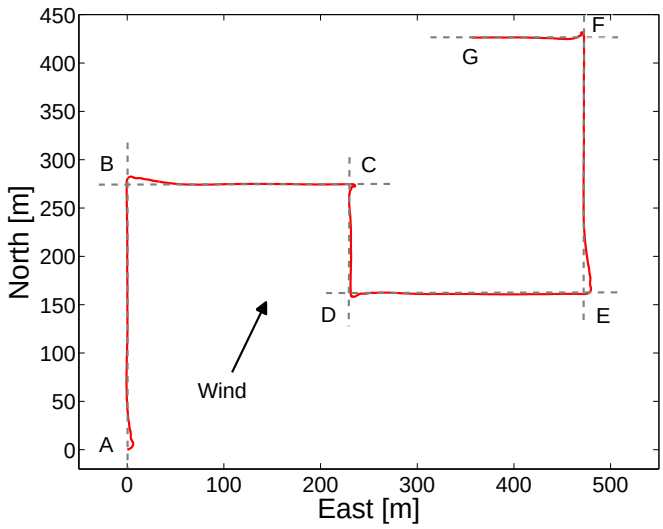

Figure 4-20: Airplane ground track. The course to follow changes each 20 seconds according to table 4.2. The distance covered on ground varies for each course being affected by wind.

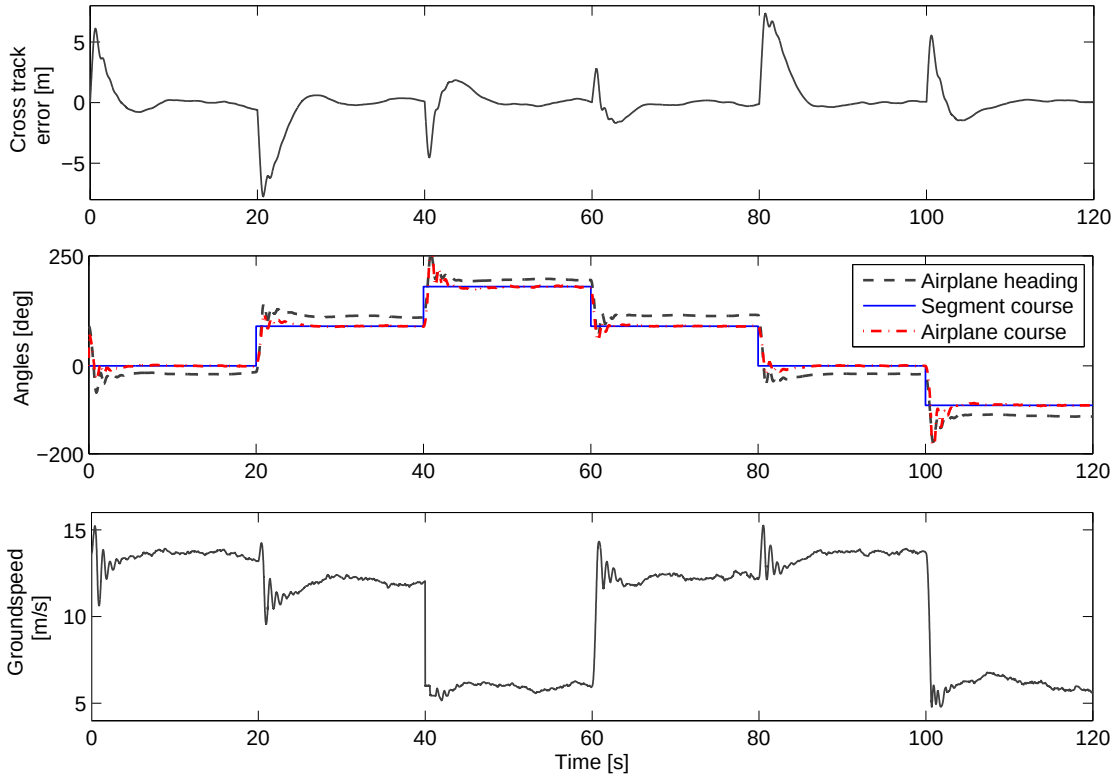

Figure 4-21: Flight parameters. (a) Tracking errors are small since the airplane follows the desired course closely. (b) Airplane heading and course. (c) The groundspeed varies according to the wind direction relative to the desired course.

The first plot in Figure 4-21 shows that the proposed control algorithm keeps the tracking errors small when the system is subjected to large course change demands. As mentioned above, the inertial course and the groundspeed, shown in the second and the third plots of this figure, are strongly affected by wind. The desired course is maintained by heading the airplane into the wind and the length of the distances traveled by the airplane decreases with the groundspeed. The estimated parameter, which is in agreement with the real values, and the control effort required to follow the commanded courses are illustrated in Figure 4-22.

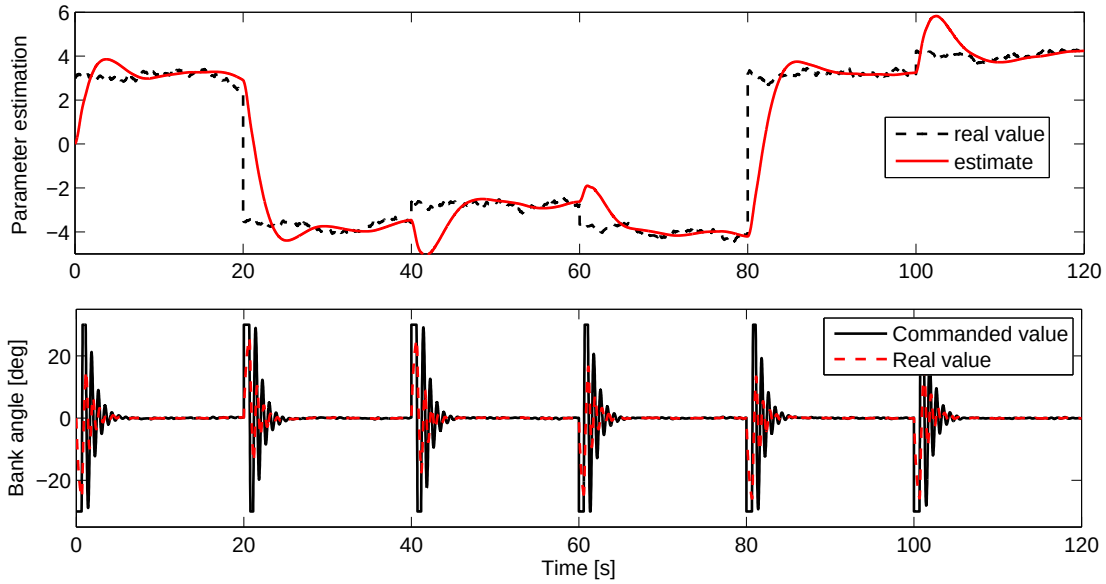

Figure 4-22: Flight parameters. (a) Parameter estimation. (b) The control effort required to follow the desired course.

4.7 Summary of results

The main contribution of this chapter is twofold. On the one hand, it extends the results obtained in Chapter 3 by dealing with unknown wind which is considered as an unknown parameter in the aircraft equations of motion and estimated using adaptive control design. On the other hand, the solution proposed in this chapter overcomes the initial condition constraint.

The first adaptive backstepping method employed overparametrization, i.e. more

than one update law was used for each parameter, which is not very efficient in a numerical implementation of the controller. With the introduction of the tuning functions adaptive backstepping method the overparametrization was removed so that only one dynamic update law for each unknown parameter is needed.

Chapter 5

Experimental setup

The real-time implementation of the proposed flight controllers and wind estimation algorithms requires the setup of an embedded autopilot architecture containing an airframe platform equipped with appropriate avionics. Optionally, a ground station can be developed for monitoring purposes or to interact with the flight platform in real time in order to change its mission or to adjust the controller parameters.

Therefore, the main purpose of this chapter is to introduce an overview of the experimental setup used to carry out flight tests. First, typical avionics equipment for actuation, data processing, navigation and communication is briefly presented followed by different airframes that have been developed within the HEUDIASYC Laboratory. Further, a ground station designed to be used for monitoring and control purposes is described. Finally, data from manual flight tests are presented.

5.1 Embedded autopilot

Developing an aircraft platform and equipping it with required sensors and actuators yields many difficulties. On the one hand, the propulsion system must produce enough thrust to offset the drag. On the other hand, the power source needs to have large capacity to allow for long duration flight. At the same time, sensors to measure the state of the aircraft or to enable radio communications with a ground human pilot, must be selected from a wide choice of devices. Further, once all the components have

been integrated, a central processing unit is necessary in order to read the information from sensors, compute the control law and send the corrections to the actuators. This section gives an overview of the developed embedded autopilot describing general features of its component parts.

5.1.1 Central processing unit (CPU)

The CPU used in our experiments is the $RCM4300$ series of RabbitCore modules which takes advantage of the features of a Rabbit 4000 microprocessor such as clock speeds of up to 60 MHz, I/O lines shared with six serial ports, variable-phase PWM, input capture, A/D converter and removable memory card [46]. The module is fast, efficient, and it has the essentials required to design a microprocessor-based system. Therefore, $RCM4300$ offers an ideal solution for a wide range of embedded applications such as the one addressed in our work.

The microprocessor shown in Figure $5-1$ is programmed using a C language compiler called Dynamic C. The sensors measure the state of the vehicle and they transmit the data to the CPU through different communication interfaces (serial port, I^2C, SPI, A/D convertor). The information is processed in order to compute the control law, which is sent to the actuators in terms of control signals (deflections of the control surfaces or adjustments of the engine thrust). In addition, the microprocessor is able to exchange information with a ground station in order to transmit data relative to the aircraft state or to receive signals with respect to the ongoing mission.

Figure 5-1: RabbitCore RCM4300.

5.1.2 GPS-Aided Inertial Navigation System (GPS/INS)

A miniature Microstrain 3DM-GX3-45 GPS-Aided Inertial Navigation System, illustrated in Figure $5-2$, was used to generate a range of navigation-related output quantities, including estimated position, velocity and attitude [47]. The sensor combines MEMS inertial sensors, a highly-sensitive embedded GPS receiver, and a complex Extended Kalman Filter. In addition, fully-calibrated inertial measurements provided by the GPS/INS sensors include acceleration, angular rate, magnetic field, Euler angles (pitch, roll, and heading), rotation matrix and quaternion. Unprocessed GPS data quantities include LLH position, NED velocity, ECEF position and velocity, UTC and GPS time.

The 3DM-GX3-45 possesses three communications modes, namely the NAV mode, AHRS Direct and GPS Direct. Each packet can contain any combination of data quantities from the same data descriptor set (any combination of GPS, AHRS or NAV data). The streaming of the received data can be controlled either by enabling the continuous transmission or by polling for data each time it is necessary. Most applications will operate with the 3DM-GX3-45 sending a continuous data stream since polling for data is less efficient than processing a continuous data stream. Moreover, the vehicle dynamics mode setting can be changed in order to adjust the GPS Kalman filter expectation of the vehicle motion. The choice between three types of applications is possible: low acceleration applications, low vertical acceleration, wheeled - vehicle dynamics or typical airborne applications. The data is transmitted between the 3DM-GX3-45 GPS/INS sensor and the CPU through a serial interface.

Figure 5-2: Microstrain 3DM-GX3-45.

5.1.3 Airspeed sensor

An Eagle Tree Airspeed MicroSensor V3 has been installed on the aircraft to measure its velocity with respect to the atmosphere. The MicroSensor uses a Prandtl style pitot-static tube and it can display the maximum speed on the built-in 7 segment LED display when used in standalone mode. Turning the power off and on makes the maximum speed from the last flight to be displayed. Additionally, the MicroSensor can be connected to a eLogger to provide airspeed data for the entire flight [48].

The sensor contains an aluminum Prandtl style pitot-static tube and a Standalone Cable of silicon hose. The pitot tube has been mounted at the front of the fuselage aligned with the airplane longitudinal axis. This is to ensure that the static holes and pitot pickup are in undisturbed air. In order to make the sensor accessible with the Rabbit microprocessor, the switch from "Eagle Tree" mode to "Third Party" mode (actual airspeed returned via I2C) ir required.

Figure 5-3: Eagle Tree Airspeed MicroSensor V3.

5.1.4 Actuators

An actuator is a mechanical device that converts an input signal (energy, electricity, hydraulics, etc.) into motion in order to move or control a system. Generally, the actuation system on aircraft is hydraulic but, for small fixed-wing UAV models, it rather consists of electric actuators. They transform the CPU electrical signals into desired motion of the airplane by adjusting the thrust force and the deflection of the control surfaces. In the case of our flight platforms, the actuators are the propulsion system composed of an electronic speed controller (ESC), brushless motor and propeller and several servomotors to actuate the control surfaces deflection.

Servomotors

Servomotors are commonly designed to provide precise control of angular position and velocity. Therefore, they can be employed in R/C aircraft models to actuate the control surfaces deflection. They consists of an electric motor, a potentiometer and a control board linked together. These actuators are controlled using pulse width modulation signals (PWM) sent by the CPU based on the computed controller. Figure $5-4$ shows the Futaba S3003 Servomotor, which has been employed within the developed flight platforms.

Figure 5-4: Futaba S3003 Servomotor.

Propulsion system

The propulsion system of the platform consists of one or two brushless DC motors and the appropriate number of ESCs and propellers. A brushless motor is a rotating electric machine with a classic three phase stator and a surface-mounted permanent magnets rotor. The electronic speed controller is required in order to vary the speed and the direction of rotation of the motor while the propellers are airfoils producing the thrust force. The motors can be driven by either PWM signals or I^2C communication protocol. The propulsion system is represented in Figure $5-5$.

Figure 5-5: Airplane propulsion system.

5.1.5 Data transmission

For the UAV to perform effectively, a data link with a ground station is required. First, the communication between the aerial vehicle and a ground station is employed for control purposes (in order to manually fly the device or to update the flight path online). Secondly, real-time navigation data can be received from the UAV, such as actual position, flown trajectory, etc. The communication may be achieved through different ways.

Radio Control

The aircraft can be remotely controlled by the use of an ordinary RC transmitter/receiver. The receiver, installed on board the aircraft, links the microprocessor to the pulse train coming from the transmitter. The CPU processes the information and converts it into control signals which are sent to the actuation system. The communication with the receiver is made through the input capture port of the microprocessor. Figure $5-6$ shows the receiver/transmitter devices used in our setup.

Figure 5-6: RC receiver Futaba R617FS and transmitter Futaba 6EX 2.4GHz.

Radio Modem

Radio modems provide the possibility to create private radio networks between the vehicle and the ground station. The modem is connected to the microprocessor through a serial port and it allows large amounts of real-time data communication. Two modules RF XBee Pro, illustrated in Figure $5-7$, have been used in our implementation to monitor the status of the vehicle during the flight.

Figure 5-7: Xbee Pro 2.4 GHz.

5.1.6 Electronics diagram

An overview of the complete avionics suite of our experimental setup is illustrated in Figure $5-8$ along with the corresponding communication interfaces employed to collect data from sensors and to send control signals to actuators.

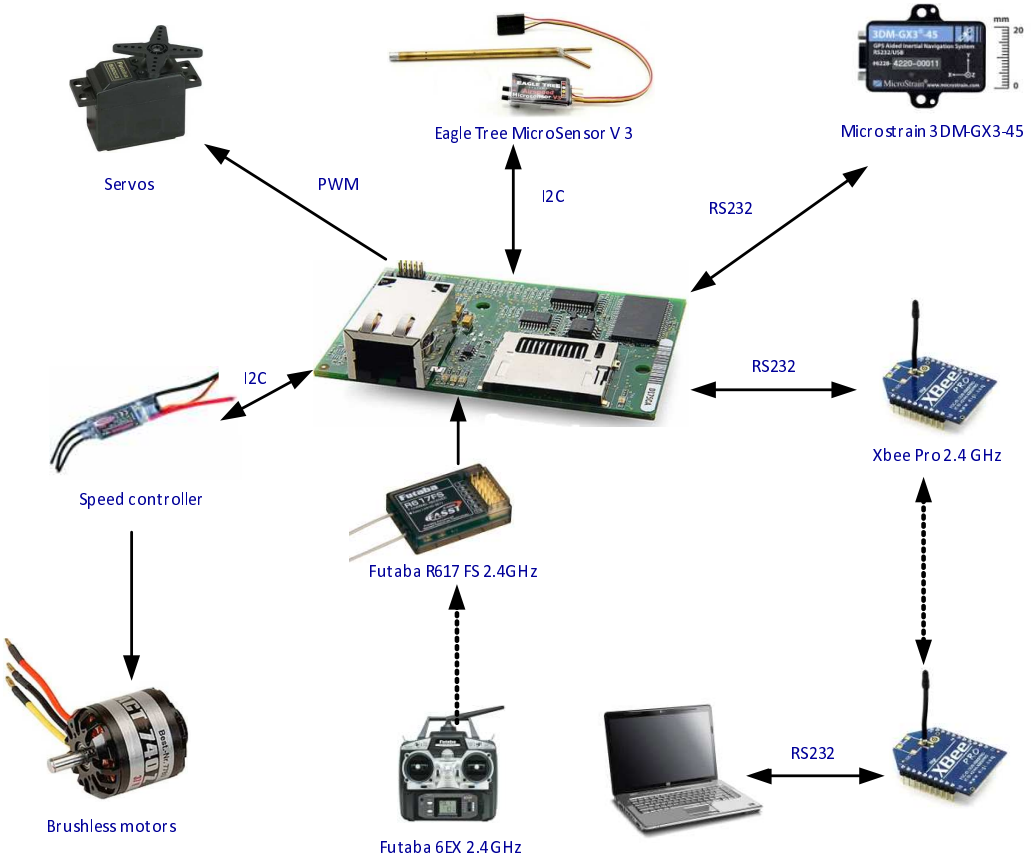

Figure 5-8: Synoptic view of the avionics along with the employed communication interfaces.

5.2 Ground station

A ground station is an information and a control terminal located at ground level which is capable to establish a radio communication link with a moving device. In terms of lightweight miniature UAVs, it is typically a software application providing a friendly graphical interface that shows cockpit displays of real-time data on the vehicle performance. It can also be used for control purposes to update the objectives of the ongoing mission or to adjust the flight controller settings. According to the needs encountered during the development of the experimental platform, we have designed two ground station applications whose main features will be highlighted further.

5.2.1 Graphical interface for monitoring purposes

First, a graphical interface using the LabView software has been designed in order to visualize the performance of the developed flying prototype during real-time flight tests. By means of this interface, we are able to monitor data measured by the onboard sensors, such as airspeed and aircraft orientation, in a graphical manner at the ground level. Also, the control signals sent by a human pilot, who handles the platform remotely, can be displayed on a computer screen running this application. Moreover, it allows the storage of the data which can then be analyzed offline. Figure $5-9$ shows the developed graphical interface along with the flying airframe during a manual flight.

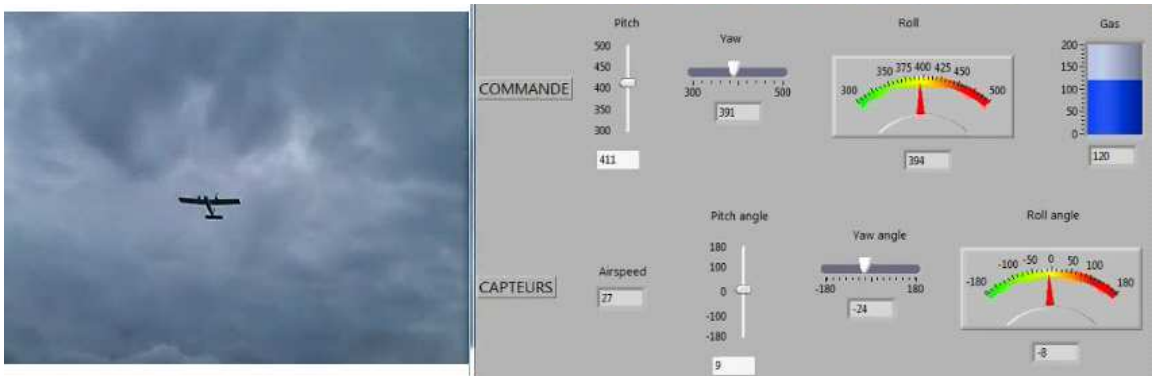

Figure 5-9: The graphical interface of the monitoring ground station.

5.2.2 Software application for monitor and control purposes

In addition to the LabView graphical interface, we have developed an application in *Visual Studio .NET* using the programming language *C #* which provides extended capabilities of real-time control, monitoring and navigation. To this end, an open source "virtual cockpit" showing many of the instruments contained on board of a real plane, such as attitude, airspeed or height indicators, was incorporated. An additional display panel allows the visualization of a complete set of inertial data. In addition, an open source *.NET* control which enables the use of the *Google Maps* tool, was included in order to illustrate the Earth relative traveled path.

Further, the developed application was suited for real time parameter adjustment of the flight controller. For example, the airspeed of the aircraft is held constant through a PID controller whose parameters were tuned in real time flights using the developed application. The software is continuously under development in order to adapt its features to the requirements of the aircraft mission. Several improvements are planned in order to offer real-time wind estimates visualization or to be able to define the trajectories to be flown graphically. Figure $5-10$ illustrates the software application displaying the virtual flight instruments and the map of the flight site.

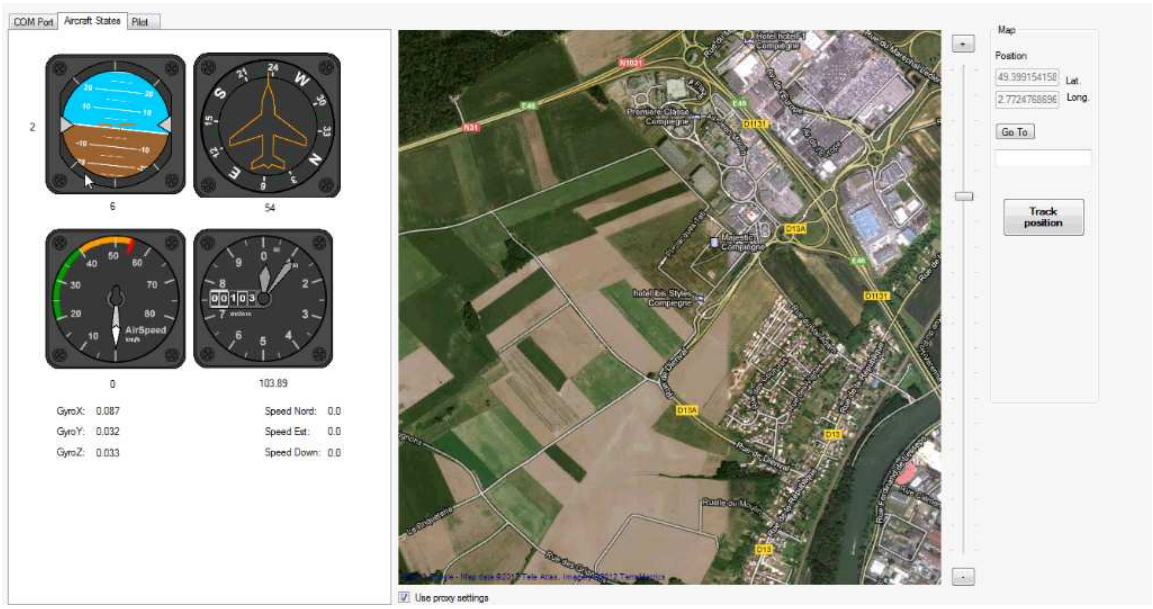

Figure 5-10: Visual C# Ground Station.

5.3 Flight platform

Not only the choice of the avionics equipment requires increased attention but also the considered airframe which is the typical location of all the electronics involved in the development of a flight platform. A robust airframe possessing reliable flight characteristics is essential for real flight tests. At the same time, sufficient payload capacity to carry the weight of sensors and batteries is a feature of great interest. For this reason, the airfoil must be chosen so that it produces adequate lift for the requirements of various missions. This section discusses the main characteristics of the experimental platforms which have been developed in our laboratory.

5.3.1 Prototype used for training purposes

A first experimental platform was developed for training purposes. Its configuration is based on the classic aerodynamic layout and it is built of polystyrene foam sheet and carbon fiber tubes. The airplane is powered by a brushless motor placed in front of the body and it has a main flat sheet foam wing fixed to the body, a couple of ailerons, an elevator and a rudder. Servomotors are attached to ailerons, the elevator and the rudder as control surface actuators. The prototype is illustrated in Figure 5-11 and its parameters are given in Table 5.1.

The airplane is able to take off from a short distance runway and to land on the ground. The control surfaces are connected to a Futaba system representing the servo signal generator/receiver unit. All servomotors are controlled manually via radio signals from a ground position.

Parameter	Value
Airfoil	Flat sheet
Wing span (b)	1.4 m
Aspect ratio (AR)	6.49
Wing Area (s)	0.302 m^2
Mass Vehicle	0.70 kg
Length	1 m

Table 5.1: Parameters of the first developed prototype.

Figure 5-11: First prototype.

5.3.2 Airfoil-shaped wing aircraft

The first prototype provides a good maneuverability due to its large wing area and large control surfaces. Nevertheless, it does not possesses the capacity to carry large payloads because the flat foam sheet airfoil does not produce sufficient lift. Therefore, an analysis of different airfoils was conducted and a $NACA$ 2609 airfoil shape for the aircraft wings, illustrated in Figure 5-12, was built of polystyrene foam. In addition, a dihedral design was considered in order to increase the stability of the vehicle. The first flight tests collecting real-time data were conducted using this prototype. However, its space for avionic systems is limited so another airframe had to be considered in order to install the required equipment.

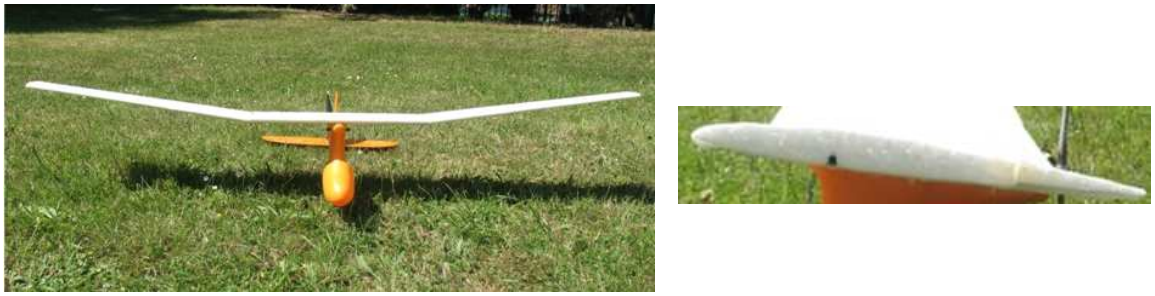

Figure 5-12: Illustration of the developed airfoil-shaped wing aircraft.

5.3.3 Multiplex Twinstar II airframe

The third developed flying platform uses the commercially available Multiplex Twinstar II model which is shown in Figure 5-13. Its configuration is based on the classic aerodynamic layout and it is made of molded Elapor foam. Two brushless motors were mounted on the airfoil-shaped wings to power the airplane. A couple of ailerons, an elevator and a rudder are used as control surfaces and are actuated by servo motors.

The technical characteristics of the Multiplex Twinstar II are given in Table 5.2. A payload of approximately 300 g, consisting of sensors and a central processing unit, was added to the airframe as the embedded electronics. The central processing unit collects the measurements of the IMU (employed to estimate the airplane attitude and angular rates), of the airspeed sensor and of the GPS system, to compute the control law. The control responses are sent to the servo signal generator/receiver unit and also to the two electric speed controllers to activate the brushless motors. Besides, a modem is added to exchange data with the ground station.

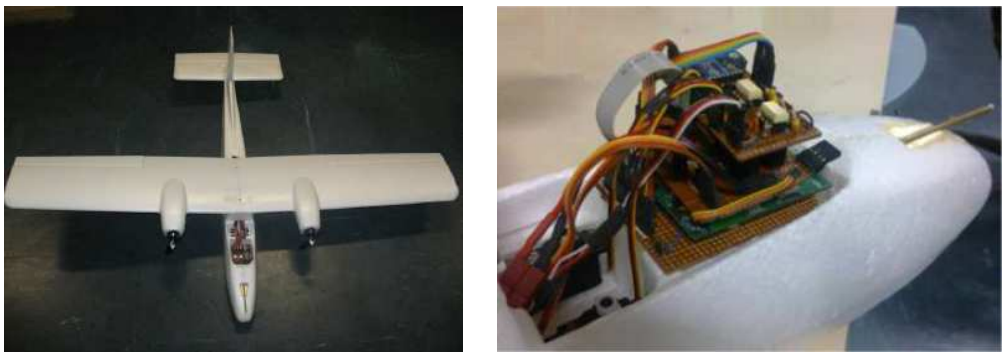

Figure 5-13: Multiplex Twinstar II airframe.

Parameter	Value
Wingspan	1420 mm / 55.9 in
Fuselage length	1085 mm / 42.7 in
Wing area	43 dm^2 / 666.5 $inch^2$
Weight approx.	1340 g / 47.3 oz
Wing loading	31.2 g/dm^2 / 10.3 oz/sq.ft
RC functions	Aileron, elevator, rudder, throttle

Table 5.2: Parameters of the Multiplex Twinstar II airplane.

5.4 Manual flight tests

Several flight tests have been conducted in manual mode and data collected in real-time are shown in the following figures. For example, Figure 5-16 plots the path of the aircraft in three dimensions. Data was provided by the GPS sensor and transmitted to the ground station through the radio link created by the transimter/receiver devices.

Besides, the developed ground station software application allows plotting the aircraft path in real-time as shown in Figure 5-14. As it was shown in the previous section, this application was designed for control purposes also and this is illustrated in Figure 5-15 in which the airspeed controller parameters are adjusted online for an improved performance.

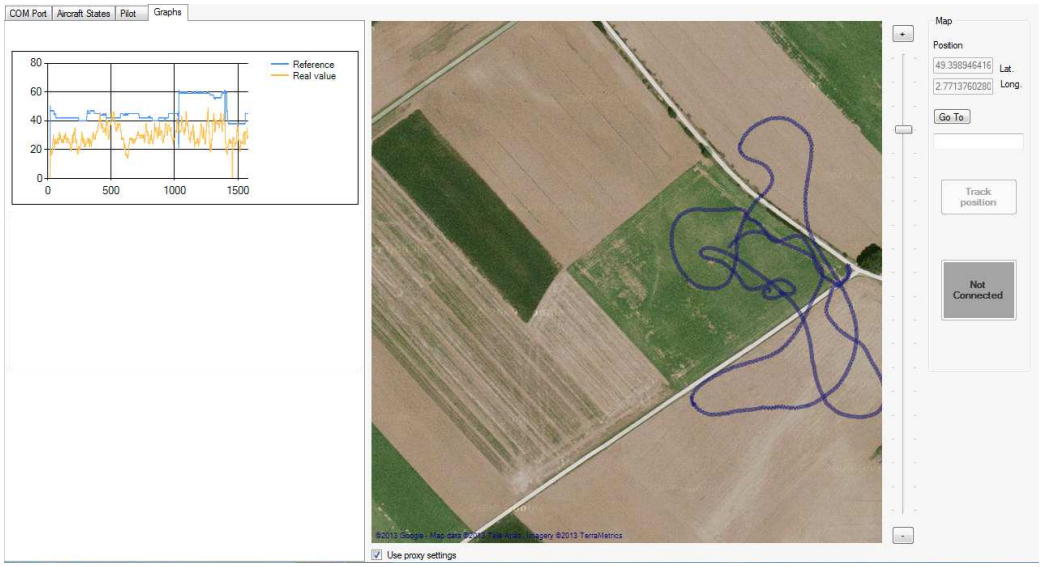

Figure 5-14: Manual flight traveled path.

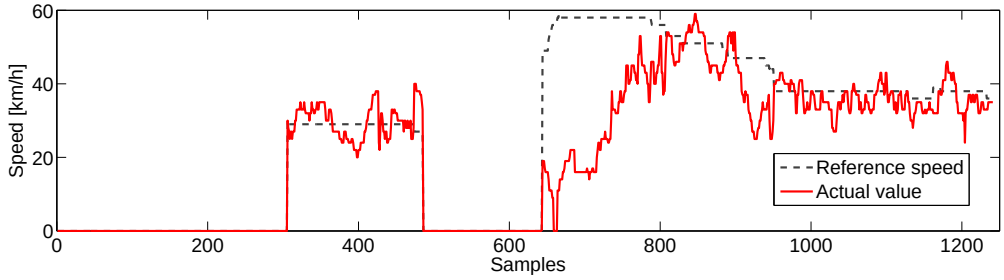

Figure 5-15: Manual flight airspeed.

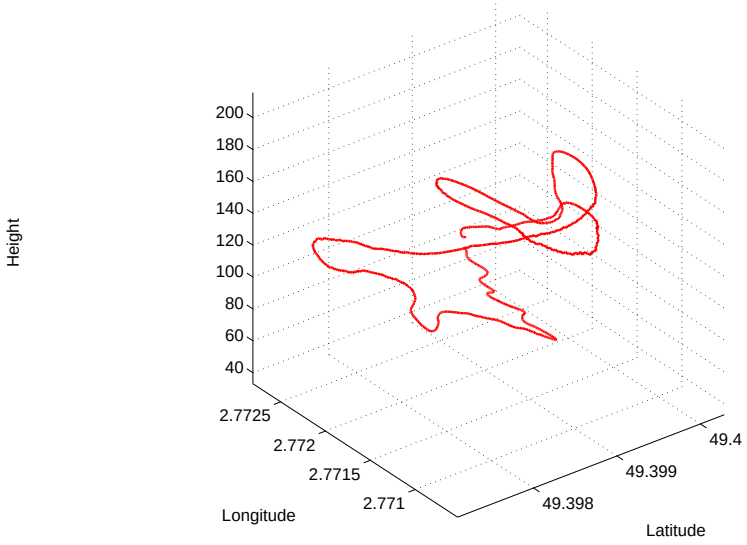

Figure 5-16: Manual flight 3D path.

Chapter 6

Conclusions

In this thesis we have developed a navigation strategy for lightweight UAVs flying in windy conditions. Sensors providing high-resolution measurements at high-frequency update rates are not typically available for UAVs. This fact affects the uncertainty of the computed wind which is noisy. Successful path following and accurate wind estimation can be obtained by exploiting fully the potential of these sensors that are readily available.

6.1 Results

In order to clearly identify and analyze relevant issues related to this project, we have conducted a literature review on the fundamental principles that govern the flight of the aircraft. Initially, we addressed a comprehensive study on the aerodynamic aspect of the plane, including the forces acting on the aircraft in flight. As a result, we have obtained the nonlinear aerodynamic model and we have used the Matlab software to simulate the behavior of the aircraft in undisturbed flight. Since the object of the work is a lightweight miniature UAV flying at low speed, which makes it very vulnerable to environmental disturbances, we studied the influence of the wind on the airplane navigation and we incorporated the resulting forces into the mathematical model.

The complete structure of the nonlinear model is complex and problematic for control purposes since it depends on uncertain aerodynamic forces. For this reason,

we have analyzed models that reproduce the essential behavior of the system in a simplified context. We have considered the dynamics of the different phases of flight such as coordinated turn flight. Then, we have presented nonlinear reduced complexity models that are easier to analyze and simulate and more adapted to the design of control strategies.

Once the equations of motion obtained, we have formulated the problem of trajectory following for a plane. It has been considered that all the missions outlined in the thesis objectives can be accomplished by providing a solution to this basic problem. To this end, we have developed a navigation strategy for the plane that minimizes the deviation from a straight line and we have proposed a control algorithm for a simplified model of the aircraft. Specifically, we hypothesized a stabilized level flight in the presence of constant and measurable wind, and we opted for a flight controller of the vehicle in the horizontal plane. It has been shown that the proposed strategy offers a linear behavior of the aircraft along the desired trajectory and results, validated by simulations, have been published in an international conference.

In the same context, we have used a nonlinear controller based on backstepping approach to obtain improved response of the aircraft response. In order to eliminate the error between the wind measured by the ground station and the wind actually experienced by the device, estimation of the wind parameters (intensity and direction) are required. Therefore, we have proposed a strategy of adaptive navigation based on the theory of Lyapunov and the results were presented in an international conference and published in a journal. Finally, we have worked on the optimization of the estimation algorithm using control technology based on the control functions (tuning functions). We have presented these results together with a comparison between the proposed methodology and other wind identification methods from literature in an international conference.

In order to validate the theoretical results, we have developed several airplane models that served as a tool for learning and testing. Subsequently, we developed a hardware platform for real-time validation of the control techniques presented above. The aircraft has been developed based on a classic aerodynamic configuration powered

by two brushless motors. The platform is equipped with a central control unit, a GPS-Aided Inertial Navigation system, a Pitot tube and a communication modem for exchanging data with the ground station. The first experiments were carried out in open loop and we continued with closed-loop tests. To facilitate testing, we have designed a graphical interface using the LabView software that allows real-time visualization of the state of the aircraft. We have used an application developed in Visual Studio .NET using C # language in order to exchange commands in real time between the aircraft and the ground station.

6.2 Future work

Several aspects are critical to the successful flight of lightweight fixed-wing UAVs in wind. First, all aerodynamic forces and moments depend on the velocity vector of the aircraft relative to the surrounding air mass which is defined in terms of angle of attack and sideslip. These angles are extremely difficult to measure precisely for small UAVs. Therefore, sensors capable to compute them or methods to estimate their values are required. Furthermore, autonomous flight is the highest control objective to be accomplished in this work. However, the absence of a stable complete aircraft platform has required additional work. Therefore, autonomous flight has not been achieved and it is, consequently, a mandatory step in further work for which current test flights are in advanced stages.

For this reason, a suitable model of an airplane needs to be developed and the pertinent parameters must be determined by means of parameter identification methods. Also, the developed ground station requires several improvements in order to offer real-time wind estimates visualization or to be able to define the trajectories to be flown graphically.

Appendix A

Standard backstepping design

Let us rewrite the nonlinear system described by (3.21)

$$\begin{aligned} \dot{d} &= V \sin(\psi - \psi_s) + W \sin(\psi_w - \psi_s) \\ \dot{\psi} &= r \\ \dot{r} &= cN \end{aligned}$$

We intend to achieve regulation of $d(t)$ designing backstepping control, for this purpose we define the following error variable

$$e_1 = d - d_{min}$$

where d_{min} is the minimum constant distance from the desired trajectory. The dynamics of e_1 yields

$$\dot{e}_1 = V \sin(\psi - \psi_s) + W \sin(\psi_w - \psi_s) \tag{A.1}$$

Let us consider the following positive function

$$V_{L_1} = \frac{1}{2} e_1^2$$

thus

$$\dot{V}_{L_1} = e_1 \left[V \sin(\psi - \psi_s) + W \sin(\psi_w - \psi_s) \right]$$

The e_1 term can be stabilized if we introduce ψ^v as virtual control in the form

$$V \sin(\psi^v - \psi_s) = -e_1 - W \sin(\psi_w - \psi_s)$$

Evaluating $\dot{V}_{L_1}$ when $\psi \to \psi^v$ it follows that

$$\dot{V}_{L_1}|_{\psi=\psi^v} = -e_1^2$$

Since ψ is not the real control, let us define the deviation from its desired value

$$e_2 = V \sin(\psi - \psi_s) - V \sin(\psi^v - \psi_s) = V \sin(\psi - \psi_s) + e_1 + W \sin(\psi_w - \psi_s) \quad \text{(A.2)}$$

and rewrite $(A.1)$ in terms of e_1 and e_2

$$\dot{e}_1 = e_2 - e_1$$

This implies that

$$\dot{e}_2 = Vr \cos(\psi - \psi_s) + e_2 - e_1 \quad \text{(A.3)}$$

Notice that $\cos(\psi - \psi_s) = \sqrt{1 - \sin^2(\psi - \psi_s)}$. From $(A.2)$

$$\sin(\psi - \psi_s) = \frac{e_2 - e_1 - W \sin(\psi_w - \psi_s)}{V}$$

and assuming that $-\frac{\pi}{2} < \psi - \psi_s < \frac{\pi}{2}$ it follows that (A.3) becomes

$$\dot{e}_2 = rR + e_2 - e_1 \quad \text{(A.4)}$$

with $R = \sqrt{V^2 - [e_2 - e_1 - W \sin(\psi_w - \psi_s)]^2}$. Let us consider the positive definite function

$$V_{L_2} = \frac{1}{2}\left(e_1^2 + e_2^2\right)$$

whose derivative is

$$\dot{V}_{L_2} = -e_1^2 + e_2(e_2 + rR)$$

Using the virtual control r^v in the form

$$r^v R = -2e_2$$

$\dot{V}_{L_2}$ becomes when $r \to r^v$

$$\dot{V}_{L_2}|_{r=r^v} = -e_1^2 - e_2^2$$

Let e_3 be the deviation of r from its desired value

$$e_3 = rR - r^v R = rR + 2e_2 \tag{A.5}$$

This implies

$$r = \frac{e_3 - 2e_2}{R}$$

It is more convenient to write the error system representation

$$\begin{aligned}
\dot{e}_1 &= -e_1 + e_2 \\
\dot{e}_2 &= -e_1 - e_2 + e_3 \\
\dot{e}_3 &= cNR - \frac{(e_3 - 2e_2)^2[e_2 - e_1 - W\sin(\psi_w - \psi_s)]}{V^2 - [e_2 - e_1 - W\sin(\psi_w - \psi_s)]^2} - 2e_2 - 2e_1 + 2e_3
\end{aligned}$$

Introducing $V_L = \frac{1}{2}{e_1}^2 + \frac{1}{2}e_2^2 + \frac{1}{2}e_3^2$ as the Lyapunov function, then

$$\dot{V}_L = -e_1^2 - e_2^2 + e_3(e_2 + \dot{e}_3) \tag{A.6}$$

Let us propose the control input as

$$cN = \frac{(e_3 - 2e_2)^2[e_2 - e_1 - W\sin(\psi_w - \psi_s)]}{[V^2 - (e_2 - e_1 - W\sin(\psi_w - \psi_s))^2]R} + \frac{e_2 - 3e_3 + 2e_1}{R} \tag{A.7}$$

Using (A.5), the control law takes the form

$$cN = -3r - \frac{5e_2 - 2e_1 - r^2[e_2 - e_1 - W\sin(\psi_w - \psi_s)]}{R} \tag{A.8}$$

Thus, $(A.6)$ becomes

$$\dot{V}_L = -e_1^2 - e_2^2 - e_3^2 \tag{A.9}$$

which proves that in the (d, e_1, e_2) coordinates the equilibrium $(0, 0, 0)$ is GAS. In view of (d, ψ, r), the resulting control is

$$cN = -3r + \tan(\psi - \psi_s)(r^2 - 5) - \frac{3d + 5W\sin(\psi_w - \psi_s)}{V\cos(\psi - \psi_s)}$$

Appendix B

Path following with on-line parameter estimation

Let us rewrite the nonlinear system described by (3.21)

$$\dot{d} = V \sin(\psi - \psi_s) + k_\omega \tag{B.1}$$

$$\dot{\psi} = r \tag{B.2}$$

$$\dot{r} = c\tau_\psi \tag{B.3}$$

where $k_\omega = W \sin(\psi_w - \psi_s)$ is considered constant for control design and and it is due to the wind perturbation

Define the following error variable

$$e_1 = d - d_{min} \tag{B.4}$$

where d_{min} is the minimum constant distance from the desired trajectory. Thus,

$$\dot{e}_1 = V \sin\psi + k_\omega \tag{B.5}$$

Convergence of e_1 to zero

Propose the following positive function

$$V_{L_1} = \frac{1}{2} e_1^2$$

thus

$$\dot{V}_{L_1} = e_1 \left(V \sin \psi + k_\omega \right)$$

To stabilize e_1 we introduce ψ^v as a virtual control in the following form

$$V \sin \psi^v = -c_1 e_1 - \hat{k}_{\omega_1}$$

where $\hat{k}_{\omega_1}$ is the estimate of k_ω and $c_1 > 0$ is a constant. Evaluating $\dot{V}_{L_1}$ when $\psi \to \psi^v$ it follows that

$$\dot{V}_{L_1}|_{\psi=\psi^v} = -c_1 e_1^2 + e_1 \tilde{k}_{\omega_1}$$

where $\tilde{k}_{\omega_1} = k_\omega - \hat{k}_{\omega_1}$. Notice from the above equation that if $\hat{k}_{\omega_1} \to k_\omega$ then $\dot{V}_{L_1} \leq 0$. Thus, rewriting V_{L_1}, it yields

$$V_{L_1} = \frac{1}{2} \left(e_1^2 + \frac{1}{\gamma_1} \tilde{k}_{\omega_1}^2 \right)$$

where $\gamma_1 > 0$ denotes a constant adaptation gain. Then

$$\dot{V}_{L_1}|_{\psi=\psi^v} = -c_1 e_1^2 + \left(e_1 - \frac{\dot{\hat{k}}_{\omega_1}}{\gamma_1} \right) \tilde{k}_{\omega_1}$$

Choosing the update law as

$$\dot{\hat{k}}_{\omega_1} = \gamma_1 e_1 \tag{B.6}$$

It follows that

$$\dot{V}_{L_1}|_{\psi=\psi^v} = -c_1 e_1^2$$

Convergence of ψ to ψ^v

Define the error

$$e_2 = V \sin\psi - V \sin\psi^v = V \sin\psi + c_1 e_1 + \hat{k}_{\omega_1} \tag{B.7}$$

and rewrite (B.5) in terms of e_1 and e_2

$$\dot{e}_1 = e_2 - c_1 e_1 + \tilde{k}_{\omega_1} \tag{B.8}$$

This implies that

$$\dot{e}_2 = Vr\cos\psi + \left(\gamma_1 - c_1^2\right) e_1 + c_1 e_2 + c_1 \tilde{k}_{\omega_1} \tag{B.9}$$

Notice that $\cos\psi = \sqrt{1-(\sin\psi)^2}$. From $(B.7)$

$$\sin\psi = \frac{e_2 - c_1 e_1 - \hat{k}_{\omega_1}}{V}$$

and assuming that $-\frac{\pi}{2} < \psi < \frac{\pi}{2}$ it follows that (B.9) becomes

$$\dot{e}_2 = rR + \left(\gamma_1 - c_1^2\right) e_1 + c_1 e_2 + c_1 \tilde{k}_{\omega_1} \tag{B.10}$$

with $R = \sqrt{V^2 - \left(e_2 - c_1 e_1 - \hat{k}_{\omega_1}\right)^2}$.

Introduce the following positive function

$$V_{L_2} = V_{L_1} + \frac{1}{2} e_2^2 = \frac{1}{2}\left(e_1^2 + \frac{1}{\gamma_1}\tilde{k}_{\omega_1}^2 + e_2^2\right)$$

From $(B.6)$, $(B.8)$ and $(B.10)$ the derivative reads

$$\dot{V}_{L_2} = -c_1 e_1^2 + e_2\left[c_1 e_2 + e_1(\gamma_1 + 1 - c_1^2) + c_1\tilde{k}_{\omega_1} + rR\right]$$

By selecting the virtual control as

$$r^v R = -e_2(c_1 + c_2) - e_1(\gamma_1 + 1 - c_1^2) - c_1(\hat{k}_{\omega_2} + \hat{k}_{\omega_1})$$

$\dot{V}_{L_2}$ becomes when $r \to r^v$

$$\dot{V}_{L_2}|_{r=r^v} = -c_1 e_1^2 - c_2 e_2^2 + c_1 e_2 \tilde{k}_{\omega_2}$$

where $\tilde{k}_{\omega_2} = k_\omega - \hat{k}_{\omega_2}$, $\hat{k}_{\omega_2}$ represents a new estimate for k_ω and c_2 denotes a positive constant gain. Notice that if we had employed the existing estimate $\hat{k}_{\omega_1}$, we would have had no design freedom left to cancel the unknown parameter from $\dot{V}_{L_2}$. Additionally, $\hat{k}_{\omega_2}$ could be seen as a factor correction for $\hat{k}_{\omega_1}$.

Notice from the above equation that if $\hat{k}_{\omega_2} \to k_\omega$ then $\dot{V}_{L_2} \leq 0$. Thus, rewriting V_{L_2}, it yields

$$V_{L_2} = V_{L_1} + \frac{1}{2}\left(e_2^2 + \frac{1}{\gamma_2}\tilde{k}_{\omega_2}^2\right)$$

with $\gamma_2 > 0$ and constant. Hence $\dot{V}_{L_2}$ becomes

$$\dot{V}_{L_2}|_{r=r^v} = c_1 e_1^2 - c_2 e_2^2 + \tilde{k}_{\omega_2}\left(c_1 e_2 - \frac{\dot{\hat{k}}_{\omega_2}}{\gamma_2}\right)$$

Proposing the update law

$$\dot{\hat{k}}_{\omega_2} = \gamma_2 c_1 e_2$$

then, it follows

$$\dot{V}_{L_2}|_{r=r^v} = c_1 e_1^2 - c_2 e_2^2$$

Convergence of r to r^v

Let us define the third error variable

$$\begin{aligned} e_3 &= rR - r^v R \\ &= rR + L_2 e_2 + L_1 e_1 + c_1(\hat{k}_{\omega_2} - \hat{k}_{\omega_1}) \end{aligned} \tag{B.11}$$

where $L_1 = 1 - c_1^2 + \gamma_1$, $L_2 = c_1 + c_2$. Rewriting the error system representation, we obtain

$$\begin{bmatrix} \dot{e}_1 \\ \dot{e}_2 \end{bmatrix} = \begin{bmatrix} -c_1 & 1 \\ -1 & -c_2 \end{bmatrix} \begin{bmatrix} e_1 \\ e_2 \end{bmatrix} + \begin{bmatrix} \tilde{k}_{\omega_1} \\ e_3 + c_1 \tilde{k}_{\omega_2} \end{bmatrix}$$

thus, the derivative of e_3 yields

$$\begin{aligned}\dot{e}_3 =& c\tau_\psi R - \frac{r(e_2 - c_1 e_1 - \hat{k}_{\omega_1})(e_3 - L_2 e_2 - L_1 e_1 + c_1\hat{k}_{\omega_1} - c_1\hat{k}_{\omega_2})}{R} \\ &+ L_2 e_3 + L_3 e_2 + L_4 e_1 + c_1 L_2 \tilde{k}_{\omega_2} + L_1 \tilde{k}_{\omega_1}\end{aligned}$$

with $L_3 = -c_1 c_2 - c_1^2 - c_2^2 + 1 + \gamma_1 + c_1^2\gamma_2$ and $L_4 = -2c_1 - c_2 + c_1^3 - 2c_1\gamma_1$.

Finally, introduce the following Lyapunov function

$$V_L = \frac{1}{2}\left(e_1^2 + \frac{1}{\gamma_1}\tilde{k}_{\omega_1}^2 + e_2^2 + \frac{1}{\gamma_2}\tilde{k}_{\omega_2}^2 + e_3^2\right)$$

then

$$\dot{V}_L = -c_1 e_1^2 - c_2 e_2^2 + e_3\left(\dot{e}_3 + e_2\right) \tag{B.12}$$

Propose the control input as

$$\begin{aligned}c\tau_\psi =& -\frac{e_3(L_2 + c_3) + e_2(L_3 + 1 - r^2) + e_1(L_4 + c_1 r^2)}{R} \\ &- \frac{\hat{k}_{\omega_3}(L_1 + c_1 L_2) - \hat{k}_{\omega_2} c_1 L_2 - \hat{k}_{\omega_1}(L_1 - r^2)}{R}\end{aligned}$$

where $\tilde{k}_{\omega_3} = k_\omega - \hat{k}_{\omega_3}$ and c_3 is a positive constant gain. Notice that the unknown term k_ω appears again in $\dot{V}_L$, thus we propose a correction factor in order to realize the convergence of the states.

Introducing the above into (B.12), we have

$$\dot{V}_L = -c_1 e_1^2 - c_2 e_2^2 - c_3 e_3^2 + e_3\left(L_1 + c_1 L_2\right)\tilde{k}_{\omega_3}$$

Observe that $\dot{V}_L \leq 0$ if $\hat{k}_{\omega_3} \to k_\omega$. Therefore augmenting V_L, it yields

$$V_L = \frac{1}{2}\left(e_1^2 + \frac{1}{\gamma_1}\tilde{k}_{\omega_1}^2 + e_2^2 + \frac{1}{\gamma_2}\tilde{k}_{\omega_2}^2 + e_3^2 + \frac{1}{\gamma_3}\tilde{k}_{\omega_3}^2\right)$$

and

$$\dot{V}_L = -c_1 e_1^2 - c_2 e_2^2 - c_3 e_3^2 + \tilde{k}_{\omega_3} \left[e_3 \left(L_1 + c_1 L_2 \right) - \frac{\dot{\hat{k}}_{\omega_3}}{\gamma_3} \right]$$

Choosing

$$\dot{\hat{k}}_{\omega_3} = \gamma_3 (L_1 + c_1 L_2) e_3$$

$\dot{V}_L$ becomes

$$\dot{V}_L = -c_1 e_1^2 - c_2 e_2^2 - c_3 e_3^2 \tag{B.13}$$

The error representation of the closed-loop adaptive system is summarized below

$$\begin{bmatrix} \dot{e}_1 \\ \dot{e}_2 \\ \dot{e}_3 \end{bmatrix} = \begin{bmatrix} -c_1 & 1 & 0 \\ -1 & -c_2 & 1 \\ 0 & -1 & -c_3 \end{bmatrix} \begin{bmatrix} e_1 \\ e_2 \\ e_3 \end{bmatrix} + \begin{bmatrix} \tilde{k}_{\omega_1} \\ c_1 \tilde{k}_{\omega_2} \\ L_5 \tilde{k}_{\omega_3} \end{bmatrix}$$

$$\begin{bmatrix} \dot{\hat{k}}_{\omega_1} \\ \dot{\hat{k}}_{\omega_2} \\ \dot{\hat{k}}_{\omega_3} \end{bmatrix} = \begin{bmatrix} \gamma_1 & 0 & 0 \\ 0 & c_1 \gamma_2 & 0 \\ 0 & 0 & L_5 \gamma_3 \end{bmatrix} \begin{bmatrix} e_1 \\ e_2 \\ e_3 \end{bmatrix} \tag{B.14}$$

where $L_5 = c_1 c_2 + \gamma_1 + 1$.

Rewriting the control input $c\tau_\psi$ in terms of d, ψ, r we have

$$c\tau_\psi = \tan\psi (r^2 - L_6) - L_7 r - \frac{L_8 d + L_9 \hat{k}_{\omega_1} + L_{10} \hat{k}_{\omega_2} + L_{11} \hat{k}_{\omega_3}}{V \cos\psi} \tag{B.15}$$

with the updated parameters

$$\begin{aligned} \dot{\hat{k}}_{\omega_1} &= \gamma_1 d \\ \dot{\hat{k}}_{\omega_2} &= \gamma_2 c_1 \left(V \sin\psi + c_1 d + \hat{k}_{\omega_1} \right) \\ \dot{\hat{k}}_{\omega_3} &= \gamma_3 L_{11} V \left[r \cos\psi + L_2 \sin\psi \right] + \gamma_3 L_{11} \left[d L_{11} + c_1 \hat{k}_{\omega_2} + c_2 \hat{k}_{\omega_1} \right] \end{aligned}$$

where

$$\begin{aligned} L_6 &= 1 + L_2 c_3 + L_2^2 + L_3 \\ L_7 &= L_2 + c_3 \\ L_8 &= L_7(L_1 + c_1 L_2) + c_1(L_3 + 1) + L_4 \\ L_9 &= 1 - c_1 L_7 + L_3 - L_1 + L_2 L_7 \\ L_{10} &= c_1 L_7 - c_1 L_2 \\ L_{11} &= L_1 + c_1 L_2 \end{aligned}$$

Notice from (B.13) that $\dot{V}_L \leq 0$ and it estates the global stability of the equilibrium $(e_i, \tilde{k}_{\omega_i}) = (0, 0)$. From the LaSalle-Yoshizawa theorem, we have that e_i and $\tilde{k}_{\omega_i}; i = 1, 2, 3;$ are bounded and go to zero as $t \to \infty$. From (B.4) it follows that $d \to d_{min}$. $(B.4)$ implies that $\hat{k}_{\omega_1}$ is also bounded and

$$\lim_{t\to\infty} \psi = \arcsin\left(-\frac{\hat{k}_{\omega_1}}{V}\right)$$

Observe that from $(B.11)$ r is bounded and $r \to 0$. On the other hand, from $(B.15)$ it follows that $c\tau_\psi$ is bounded.

LaSalle's invariance principle assures that the state $(e_i, \tilde{k}_{\omega_i})$ converges to the largest invariant set M contained in $\{(e_1, e_2, e_3, \tilde{k}_{\omega_1}, \tilde{k}_{\omega_2}, \tilde{k}_{\omega_3}) \in \mathbb{R}^6 | \dot{V}_L = 0\}$. On this invariant set, we have $e_i \equiv 0$ and $\dot{e}_i \equiv 0$. From $(B.14)$ it yields $\dot{\tilde{k}}_{\omega_i} = 0$ and $\tilde{k}_{\omega_i} = 0$. Thus, the largest invariant set M is

$$\begin{aligned} M =& \{(e_i, \tilde{k}_{\omega_i}) \in \mathbb{R}^6 | e_i = 0, \tilde{k}_{\omega_i} = 0\} \\ =& \{(d, \psi, r, \hat{k}_{\omega_1}, \hat{k}_{\omega_2}, \hat{k}_{\omega_3}) \in \mathbb{R}^6 | (d, \psi, r, \hat{k}_{\omega_1}, \hat{k}_{\omega_2}, \hat{k}_{\omega_3}) \\ & = (0, \arcsin(-\frac{\hat{k}_{\omega_1}}{V}), 0, k_\omega, k_\omega, k_\omega)\} \end{aligned}$$

The manifold M is the single point $d = 0$, $\psi = \arcsin(-\frac{\hat{k}_{\omega_1}}{V})$, $r = 0$, $\hat{k}_{\omega_i} = k_\omega$ for

$i = 1$, 2 and 3, which is globally asymptotically stable.

Appendix C

Parameter estimation with minimum-order design

Let us rewrite the nonlinear system described by (3.21)

$$\begin{aligned} \dot{d} \equiv \dot{p}_{e\_s} &= V \sin(\psi - \psi_d) + k_\omega \\ \dot{\psi} &= r \\ \dot{r} &= c\tau_\psi \end{aligned}$$

where $k_\omega = \omega \sin(\psi_\omega - \psi_d)$ is considered constant and due to the wind, and d is the cross track error from the desired trajectory.
In the following, a step by step adaptive backstepping control algorithm is developed in order to stabilize the above system system.

Let us define the following error variable

$$e_1 = d - d_{min} \tag{C.2}$$

where $d_{min} \neq 0$ when needed to stabilize the aircraft to fly at a constant distance from the desired segment line. Thus,

$$\dot{e}_1 = V \sin(\psi - \psi_d) + k_\omega \tag{C.3}$$

Regulation of e_1

Propose the following positive function

$$V_{L_1} = \frac{1}{2}e_1^2$$

thus

$$\dot{V}_{L_1} = e_1 \left[V \sin\left(\psi - \psi_d\right) + k_\omega \right]$$

Define the second error as

$$e_2 = V \sin\left(\psi - \psi_d\right) - V \sin\left(\psi^v - \psi_d\right) \tag{C.4}$$

where ψ^v defines the virtual control with the form

$$V \sin\left(\psi^v - \psi_d\right) = -c_1 e_1 - \hat{k}_\omega$$

In the above, $\hat{k}_\omega$ is an estimate of k_ω and $c_1 > 0$ is a constant. Then, (C.4) becomes

$$e_2 = V \sin\left(\psi - \psi_d\right) + c_1 e_1 + \hat{k}_\omega \tag{C.5}$$

Rewriting (C.3)

$$\dot{e}_1 = e_2 - c_1 e_1 + \tilde{k}_\omega$$

where $\tilde{k}_\omega = k_\omega - \hat{k}_\omega$. Hence, (C) yields

$$\dot{V}_{L_1} = -c_1 e_1^2 + e_1 e_2 + e_1 \tilde{k}_\omega$$

Notice from the above equation that if $\hat{k}_\omega \to k_\omega$ and $e_2 \to 0$ then $\dot{V}_{L_1} \leq 0$ and this implies that $e_1 \to 0$.

In order to converge $\tilde{k}_\omega \to 0$, propose the following positive function

$$V_{L_2} = \frac{1}{2\gamma}\tilde{k}_\omega^2$$

where $\gamma > 0$ is a constant adaptation gain. Then

$$\dot{V}_{L_2} = -\frac{\dot{\hat{k}}_\omega}{\gamma}\tilde{k}_\omega$$

Define the following tuning function

$$\tau_1 = \gamma e_1 \tag{C.6}$$

Thus

$$\dot{V}_{L_1} + \dot{V}_{L_2} = -c_1 e_1^2 + e_1 e_2 + \left(\tau_1 - \dot{\hat{k}}_\omega\right)\frac{\tilde{k}_\omega}{\gamma}$$

Regulation of e_2

From $(C.5)$, it follows that

$$\dot{e}_2 = Vr\cos(\psi - \psi_d) + c_1 e_2 - c_1^2 e_1 + c_1\tilde{k}_\omega + \dot{\hat{k}}_\omega \tag{C.7}$$

Consider the following positive function

$$V_{L_3} = \frac{1}{2}e_2^2$$

Taking the time derivative leads to

$$\dot{V}_{L_3} = e_2\left[Vr\cos(\psi - \psi_d) + c_1 e_2 - c_1^2 e_1 + c_1\tilde{k}_\omega + \dot{\hat{k}}_\omega\right)$$

Observe in the above equation the term $\tilde{k}_\omega$. To reduce the adaptive error, we introduce the second tuning function of the form

$$\tau_2 = \tau_1 + \gamma c_1 e_2 \tag{C.8}$$

Define now, the third error as

$$e_3 = Vr\cos(\psi - \psi_d) - Vr^v\cos(\psi - \psi_d)$$

The r^v term represents a virtual control and it is given by

$$Vr^v \cos(\psi - \psi_d) = -e_2(c_1 + c_2) - e_1(1 - c_1^2) - \tau_2$$

then, e_3 yields

$$e_3 = Vr \cos(\psi - \psi_d) + e_2(c_1 + c_2) + e_1(1 - c_1^2) + \tau_2 \tag{C.9}$$

Rewriting $(C.7)$ in terms of e_3

$$\dot{e}_2 = e_3 - c_2 e_2 - e_1 + c_1 \tilde{k}_\omega + \dot{\hat{k}}_\omega - \tau_2$$

Thus, $\dot{V}_{L_3}$ becomes

$$\dot{V}_{L_3} = -c_2 e_2^2 - e_1 e_2 + e_2 e_3 + e_2 \left(c_1 \tilde{k}_\omega + \dot{\hat{k}}_\omega - \tau_2 \right)$$

and

$$\dot{V}_{L_1} + \dot{V}_{L_2} + \dot{V}_{L_3} = -c_1 e_1^2 - c_2 e_2^2 + e_2 e_3 + e_2 \left(-\tau_2 + \dot{\hat{k}}_\omega \right) + \frac{\tilde{k}_\omega}{\gamma} \left(\tau_2 - \dot{\hat{k}}_\omega \right)$$

Regulation of e_3

The derivative of e_3 yields

$$\dot{e}_3 = Vc\tau_\psi \cos(\psi - \psi_d) - Vr^2 \sin(\psi - \psi_d) + L_1 e_1 + L_2 e_2 + L_3 e_3 + L_4 \tilde{k}_\omega + L_3 \dot{\hat{k}}_\omega$$

where

$$\begin{aligned}
L_1 &= -c_1(3\gamma + 2 + \gamma^2 - c_1^2) - c_2(1 + \gamma), \\
L_2 &= -c_1 \left[c_1(1 + \gamma + \gamma^2) + c_2(1 + 2\gamma) \right] + 1 + \gamma - c_2^2, \\
L_3 &= c_1 + c_2 + \gamma c_1 \\
L_4 &= c_1(\gamma c_1 + c_2) + 1 + \gamma.
\end{aligned}$$

Propose

$$V_{L_4} = \frac{1}{2}e_3^2$$

The derivative reads

$$\dot{V}_{L_4} = e_3 \left(Vc\tau_\psi \cos(\psi - \psi_d) - Vr^2 \sin(\psi - \psi_d) + L_1 e_1 + L_2 e_2 + L_3 e_3 + L_4 \tilde{k}_\omega + L_3 \dot{\hat{k}}_\omega \right)$$

Finally, define the Lyapunov function

$$V_L = V_{L_1} + V_{L_2} + V_{L_3} + V_{L_4} = \frac{1}{2}\left(e_1^2 + \frac{1}{\gamma}\tilde{k}_\omega^2 + e_2^2 + e_3^2 \right) \tag{C.10}$$

thus

$$\begin{aligned} \dot{V}_L = & - c_1 e_1^2 - c_2 e_2^2 + \frac{\tilde{k}_\omega}{\gamma}(\tau_2 + \gamma L_4 e_3 - \dot{\hat{k}}_\omega) + e_2(\dot{\hat{k}}_\omega - \tau_2) \\ & + e_3 \left[Vc\tau_\psi \cos(\psi - \psi_d) - Vr^2 \sin(\psi - \psi_d) + L_1 e_1 + (1 + L_2) e_2 + L_3 e_3 + L_3 \dot{\hat{k}}_\omega \right] \end{aligned} \tag{C.11}$$

Notice that the term $\tilde{k}_\omega$ yields in V_{L_4}, to reduce the adaptive error, we introduce the third tuning function as

$$\tau_3 = \tau_2 + \gamma L_4 e_3 \tag{C.12}$$

Observe that

$$\dot{\hat{k}}_\omega - \tau_2 = \dot{\hat{k}}_\omega - \tau_3 + \tau_3 - \tau_2 = \dot{\hat{k}}_\omega - \tau_3 + \gamma L_4 e_3$$

Then, (C.11) becomes

$$\begin{aligned} \dot{V}_L = & - c_1 e_1^2 - c_2 e_2^2 + e_2(\dot{\hat{k}}_\omega - \tau_3) + \frac{\tilde{k}_\omega}{\gamma}(\tau_3 - \dot{\hat{k}}_\omega) \\ & + e_3 \left[Vc\tau_\psi \cos(\psi - \psi_d) - Vr^2 \sin(\psi - \psi_d) + L_1 e_1 + (1 + L_2 + \gamma L_4) e_2 + L_3 e_3 + L_3 \dot{\hat{k}}_\omega \right] \end{aligned}$$

Proposing the controller

$$c\tau_\psi = r^2 \tan(\psi - \psi_d) - \frac{L_5 e_1 + L_6 e_2 + L_7 e_3}{V \cos(\psi - \psi_d)} \tag{C.13}$$

and the update law

$$\dot{\hat{k}}_\omega = \tau_3 \tag{C.14}$$

consequently, it follows that

$$\dot{V}_L = -c_1 e_1^2 - c_2 e_2^2 - c_3 e_3^2 \tag{C.15}$$

where

$$\begin{aligned} L_5 &= L_1 + \gamma L_3 \\ L_6 &= 1 + L_2 + \gamma c_1 L_3 + \gamma L_4 \\ L_7 &= c_3 + L_3 + \gamma L_3 L_4. \end{aligned}$$

The error system representation of the resulting closed-loop adaptive system is summarized below

$$\begin{aligned} \dot{e}_1 &= -c_1 e_1 + e_2 + \tilde{k}_\omega \\ \dot{e}_2 &= -e_1 - c_2 e_2 + (1 + \gamma L_4) e_3 + c_1 \tilde{k}_\omega \\ \dot{e}_3 &= -(1 + \gamma L_4) e_2 - c_3 e_3 + L_4 \tilde{k}_\omega \\ \dot{\tilde{k}}_\omega &= -\gamma e_1 - \gamma c_1 e_2 - \gamma L_4 e_3 \end{aligned} \tag{C.16}$$

Rewriting (C.13) and (C.14) in terms of d, ψ, r we have

$$c\tau_\psi = \tan(\psi - \psi_d)(r^2 - L_8) - L_7 r - \frac{L_9 d + L_8 \hat{k}_\omega}{V \cos(\psi - \psi_d)} \tag{C.17}$$

and

$$\dot{\hat{k}}_\omega = \gamma \left(L_{10} d + L_{11} \hat{k}_\omega + L_{11} V \sin(\psi - \psi_d) + L_4 V r \cos(\psi - \psi_d) \right)$$

with

$$\begin{aligned} L_8 &= L_6 + L_7 L_3 \\ L_9 &= L_5 + c_1 L_6 + L_7(1 + \gamma + c_1 c_2 + c_1^2 \gamma) \\ L_{10} &= 1 + L_4(1 - c_1^2 + \gamma) + c_1 L_{11} \\ L_{11} &= c_1 + L_3 L_4 \end{aligned}$$

Stability analysis

Notice that, the global stability of the equilibrium $(e_i, \tilde{k}_\omega) = 0$ follows from (C.10) and (C.15). (C.15) implies that $V_L \leq 0$ and from the LaSalle-Yoshizawa theorem [4] we have that e_i and $\hat{k}_\omega$ are bounded and $e_i,\ \tilde{k}_\omega \to 0$ as $t \to \infty$; $i = 1, 2, 3$. From (C.2), it follows that $d \to d_{min}$. The boundedness of ψ follows from the boundedness of e_1, $\hat{k}_\omega$ and e_2 defined in $(C.5)$. Observe that the convergence to zero of e_i does not imply the convergence to zero of ψ. From $(C.5)$ it can be noted that ψ is bounded, i.e.

$$\lim_{t\to\infty} \psi = \arcsin\left(-\frac{\hat{k}_\omega}{V}\right) + \psi_d$$

Observe that from (C.16), (C.14), (C.12), (C.8) and (C.6) it follows that $\dot{\hat{k}}_\omega, \tau_i \to 0$; $i = 1, 2, 3$. (C.9) implies that $r \to 0$ as $t \to \infty$. Finally from (C.13), we conclude that the control τ_ψ is also bounded.

LaSalle's invariance principle [4] assures that the state $(e_i, \tilde{k}_\omega)$ converges to the largest invariant set M contained in $\{(e_1, e_2, e_3, \tilde{k}_\omega) \in \mathbb{R}^4 | \dot{V}_L = 0\}$. On this invariant set, we have $e \equiv 0$ and $\dot{e} \equiv 0$. From $(C.14)$ it yields $\dot{\tilde{k}}_\omega = 0$ and $\tilde{k}_\omega = 0$. Thus, the largest invariant set M is

$$\begin{aligned} M &= \{(e, \tilde{k}_\omega) \in \mathbb{R}^4 | e = 0, \tilde{k}_\omega = 0\} \\ &= \{(d, \psi, r, \hat{k}_\omega) \in \mathbb{R}^4 | (d, \psi, r, \hat{k}_\omega) = (0, \arcsin(-\frac{k_\omega}{V}) + \psi_d, 0, k_\omega)\} \end{aligned}$$

The manifold M is the single point $d = 0, \psi = \arcsin(-\frac{k_\omega}{V}), r = 0, \hat{k}_\omega = k_\omega$ which is globally asymptotically stable.

For a perturbed system is very important to estimate if not delimitate the region of attraction of its equilibrium points. Equation $(C.5)$ can be rewritten as

$$e_2 = V \sin(\psi - \psi_d) + e_1 + \left(\hat{k}_\omega - k_\omega\right) + k_\omega$$

Thus

$$|V \sin(\psi - \psi_d)| \leq |e_2| + |e_1| + |\tilde{k}_\omega| + |k_\omega| \tag{C.18}$$

From the proposed Lyapunov function we can write the inequalities

$$\begin{aligned}
\frac{1}{2}e_1^2 &\leq V_L \leq V(0) \Rightarrow |e_1| \leq \sqrt{2V(0)} \\
\frac{1}{2}e_2^2 &\leq V_L \leq V(0) \Rightarrow |e_2| \leq \sqrt{2V(0)} \\
\frac{1}{2}\tilde{k}_\omega^2 &\leq V_L \leq V(0) \Rightarrow |\tilde{k}_\omega| \leq \sqrt{2V(0)}
\end{aligned}$$

Using the above and $(C.18)$ we can write

$$|\sin(\psi - \psi_d)| \leq \frac{3\sqrt{2V(0)}}{V} + \frac{|k_\omega|}{V}$$

To remove the singularities we impose $|\sin(\psi - \psi_d)| < 1$. Therefore, the region of attraction is $\frac{|k_\omega|}{V} \leq 1 - \varepsilon$, where $\varepsilon = 3\sqrt{2V(0)}$.

Bibliography

[1] Derek R. Nelson, Blake Barber, Timothy W. McLain, Randal W. Beard, Vector Field Path Following for Miniature Air Vehicles, IEEE Transactions on Robotics, vol. 23, no. 3, June, 2007, $519 - 529$.

[2] Liu, C., McAree, O. and Chen, W.-H., (2012) Path-following control for small fixed-wing unmanned aerial vehicles under wind disturbances, International Journal of Robust Nonlinear Control. doi: 10.1002/rnc.2938

[3] M. Krstic, I. Kanellakopoulos and P. V. Kokotovic, Nonlinear and Adaptive Control Design, John Wiley and Sons, Inc., New York, 1995.

[4] H.Khalil, Nonlinear Systems, Macmillan Publishing Company, New York, 1992.

[5] D. Lawrence and W. Rugh, Gain Scheduling Dynamic Linear Controllers Nonlinear Plant, Automatica, Vol. 31, No. 3, pp. 381-390, 1995.

[6] W. J. Rugh and J. S. Shamma, Research on Gain Scheduling, Automatica 36, pg. 1401-1425, 2000.

[7] C. Silvestre, A. Pascoal and I. Kaminer, On the design of gain-scheduled trajectory tracking controllers, International Journal of Robust and Nonlinear Control 12, 797-839, 2002.

[8] Nicholas, R. A., Reichert, R. T., Rugh, W. J., Gain Scheduling for H-infinity Controllers: A Flight Control Example, IEEE Transactions on Control Systems Technology, Vol. 1, No. 2, June 1993.

[9] O. Harkergard, Backstepping and Control Allocation with Applications to Flight Control, Ph.D. thesis, Linkoping University, 2003.

[10] J. J. E. Slotline, W. Li, Applied Nonlinear Control, 1991.

[11] Niculescu, Marius. Lateral track control law for Aerosonde UAV. In : 39th AIAA Aerospace Sciences Meeting and Exhibit. 2001

[12] S. Park, J. Deyst, and J. How, A new nonlinear guidance logic for trajectory tracking, In Proceedings of the AIAA Guidance, Navigation and Control Conference, AIAA-2004-4900, August 2004.

[13] G. Ducard, K. Kulling, and H. P. Geering, A simple and adaptive online path planning system for a UAV, in Proc. 15th Mediterranean Conf. Control and Automation, pp. 1-6, 2007.

[14] Kaminer I, Pascoal A, Xargay E, Hovakimyan N, Dobrokhodov V., Path following for unmanned aerial vehicles using L1 adaptive augmentation of commercial autopilots. Journal of Guidance, Control, and Dynamics, Vol. 33, No. 2, 2010.

[15] E. Frew and D. Lawrence, Cooperative standoff tracking of moving targets using lyapunov guidance vector fields, AIAA Journal of Guidance, Control, and Dynamics 31(2), pp. 290-306, 2008.

[16] R. Rysdyk, Unmanned aerial vehicle path following for target observation in wind, Journal of Guidance, Control, and Dynamics 29(5), pp. 1092-1100, 2006.

[17] Bernard Etkin, Dynamics of Atmospheric Flight, 1972.

[18] Z. Artstein, Stabilization with relaxed controls. Nonlinear Analysis, TMA, 1983, vol. 7, p. 1163-1173.

[19] S. Watkins, J. Milbank and B. J. Loxton, Atmospheric Winds and the Implications for Microair Vehicles, AIAA Journal, Vol. 44, No. 11, pp. 2591-2600, November 2006.

[20] A. van den Kroonenberg, T. Martin, M. Buschmann, J. Bange and P. Vorsmann, Measuring the Wind Vector Using the Autonomous Mini Aerial Vehicle M^2AV, J. Atmos. Ocean. Tech., 25, 1969-1982, 2008.

[21] S. Martin, J. Bange and F. Beyrich, Meteorological profiling of the lower troposphere using the research UAV "M^2AV Carolo", Atmos. Meas. Tech., 4, 705-716, doi:10.5194/amt-4-705-2011, 2011.

[22] E. A. Haering Jr., Airdata Measurement and Calibration, NASA TM-104316, 1995, AGARD-AG-300 Vol. 14, Sept. 1995.

[23] W Frost and R. L. Bowels, Windshear Terms in the Equations of Aircraft Motion, Journal of Aircraft, Vol. 21, No. 11, pp. 866-872, 1984.

[24] C. Liu, O. McAree, W. H. Chen, Path-following control for small fixed-wing unmanned aerial vehicles under wind disturbances, International Journal of Robust and Nonlinear Control, doi: 10.1002/rnc.2938, 2012.

[25] J. W. Langelaan, N. Alley, and J. Neidhoefer, Wind field estimation for small unmanned aerial vehicles, AIAA Journal of Guidance, Control and Dynamics. vol. 34, no. 4, pp. 1016-1030, 2011.

[26] N. Lawrance and S. Sukkarieh, A guidance and control strategy for dynamic soaring with a gliding UAV, in Proceddings of the International Conference on Robotics and Automation, Japan, 2009.

[27] M. Pachter, N. Ceccarelli and P. R. Chandler, Estiamting MAV's Heading and the wind Speed and Direction using GPS, Inertial and Air Speed Measurements, AIAA Guidance, Navigation and Control Conference, Aug. 2008.

[28] D. H. Lenschow, Aircraft Measurements in the Boundary Layer. A chapter in Probing the Atmospheric Boundary Layer, American Meteorological Society, Boston, MA, 1986.

[29] S. M. Meenakshisundaram, K. G. Venkatanarayana and B. Sashi Kanth. Vector field guidance for path following of MAVs in three dimensions for variable altitude maneuvers. International Journal of Micro Air Vehicles, vol. 2, no 4, p. 255-265, 2010.

[30] Mulgund, Sandeep S. and Stengel, Robert F. Optimal recovery from microburst wind shear. Journal of guidance, control, and dynamics, vol. 16, no 6, p. 1010-1017, 1993.

[31] National Aeronautics and Space Administration ($NASA$), http://www.grc.nasa.gov/WWW/k-12/airplane/cp.html.

[32] National Aeronautics and Space Administration ($NASA$), http://www.grc.nasa.gov/WWW/K-12/airplane/lift1.html.

[33] National Aeronautics and Space Administration ($NASA$), http://www.grc.nasa.gov/WWW/K-12/airplane/wrong1.html

[34] National Aeronautics and Space Administration ($NASA$), http://www.grc.nasa.gov/WWW/K-12/airplane/wrong2.html

[35] National Aeronautics and Space Administration ($NASA$), http://www.grc.nasa.gov/WWW/K-12/airplane/right2.html

[36] National Aeronautics and Space Administration ($NASA$), http://www.grc.nasa.gov/WWW/K-12/airplane/drag1.html.

[37] G. M. Craig, Stop Abusing Bernoulli! - How Airplanes Really Fly, Regenerative Press, 1998.

[38] K. Chang, Staying Aloft; What Does Keep Them Up There?, New York Times, Dec 9, 2003.

[39] D. Anderson and S. Eberhardt, A physical description of flight. Fermi National Accelerator Laboratory Seattle, WA, 2004.

[40] R. W. Beard and T. W. McLain, Small Unmanned Aircraft: Theory and Practice. Princeton: Princeton University Press, http://public.j.eblib.com/EBLPublic/PublicView.do?ptiID=832065, 2012.

[41] http://www.mathworks.fr/fr/help/aeroblks/drydenwindturbulencemodelcontinuous.html

[42] Wikipedia, Wind shear, http://en.wikipedia.org/wiki/Wind_shear (as of Aug. 25, 2013, 12:13 GMT).

[43] http://www.wind-power-program.com/windestimates.htm.

[44] Wikipedia, Wind gradient, http://en.wikipedia.org/wiki/Wind_gradient (as of Aug. 25, 2013, 13:09 GMT).

[45] L. Loftin,"Quest for Performance", NASA SP-468, 1985.

[46] http://www.digi.com/products/wireless-wired-embedded-solutions/solutions-on-module/rabbitcore/rcm4300.

[47] http://www.microstrain.com/inertial/3dm-gx3-45.

[48] http://www.eagletreesystems.com/support/manuals/airspeed-v3.pdf.

[49] Brian L. Stevens and Frank L. Lewis, Aircraft Control and Simulation, 2003.

[50] How, Jonathan. 16.333 Aircraft Stability and Control, Fall 2004. (MIT OpenCourseWare: Massachusetts Institute of Technology), http://ocw.mit.edu/courses/aeronautics-and-astronautics/16-333-aircraft-stability-and-control-fall-2004 (Accessed 28 Aug, 2013). License: Creative Commons BY-NC-SA

[51] M. J. Abzug and E. E. Larrabee, Airplane Stability and Control: A History of the Technologies that Made Aviation Possible, Cambridge University Press, 2002.

[52] Robert F. Stengel, Lecture Slides for "Aircraft Flight Dynamics", MAE 331, http://www.princeton.edu/ stengel/MAE331Lectures.html, Fall 2012.